DETERMINATION OF INTERLAMINAR TOUGHNESS OF GFRP LAMINATES AT VERY HIGH CRACK VELOCITY

By
MALLIKHARJUNA RAO RAVIPATI

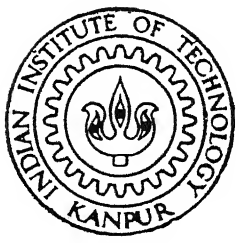

DEPARTMENT OF MECHANICAL ENGINEERING
INDIAN INSTITUTE OF TECHNOLOGY, KANPUR
JULY, 1998

DETERMINATION OF INTERLAMINAR TOUGHNESS OF GFRP LAMINATES AT VERY HIGH CRACK VELOCITY

A Thesis Submitted
in Partial Fulfilment of the Requirements
for the Degree of

MASTER OF TECHNOLOGY

By

MALLIKHARJUNA RAO RAVIPATI

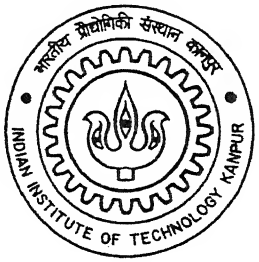

to the
Department of Mechanical Engineering

INDIAN INSTITUTE OF TECHNOLOGY KANPUR

July, 1998

ME-1998-M-RAV-DET

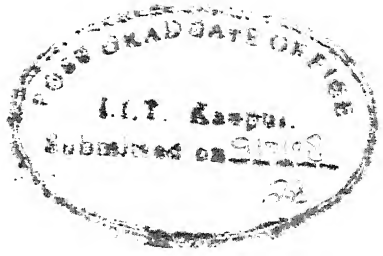

CERTIFICATE

This is to certify that the work entitled " ***Determination of Interlaminar Toughness of GFRP Laminates at Very High Crack velocity*** " by " ***Mallikharjuna Rao Ravipati*** " has been carried out under my supervision and this work has not been submitted else where for a degree.

P Kumar

(Prof. Prashant Kumar)

Dept. of Mechanical Engineering

I I T Kanpur

July 1998.

ABSTRACT

In experimental-numerical technique of the present study, the aim is to find the initiation and propagation toughness of fast moving interlaminar cracks in GFRP laminates. Experimental technique consists of a specimen, the front face of which is bonded to a rigid block and the cantilever plate on the rear is screwed to a load bar. A striker bar impacts the load bar, which in turn impacts the specimen and causes the crack propagation. Strain gauges mounted on the load bar monitor the end displacement of the load bar. Since the specimen is screwed to the load bar, the end displacement of the load bar is same as the deflection of the cantilever end. Two strain gauges bonded ahead of the crack tip on the specimen monitors the crack velocity. Thus the experimentation provides the deflection of the cantilever end, the crack velocity and the crack initiation time.

This data along with the material properties are used as input to the FE code to simulate the crack propagation. Gradual nodal release method is used to model the crack propagation. The variation of $\hat{J}$ integral with time is obtained from the program. It's value steadily increases till the initiation time. Value of $\hat{J}$ integral at the initiation time is treated as the initiation toughness (J_{ini}). At the initiation time the crack propagation algorithm is called. The $\hat{J}$ integral suddenly drops at that point and stabilizes after some time. This stabilized of $\hat{J}$ is treated as propagation toughness J_{prop}. The initiation and propagation toughness of a crack moving at a speed of 550-950 m/s were found to be 140-350 J/m^2 and 30-95 J/m^2 respectively. These values are very much lower than the quasistatic interlaminar toughness (1050 J/m^2).

ACKNOWLEDGEMENTS

I am grateful to Prof. Prashant Kumar for his invaluable guidance throughout the present work. Without his constant encouragement and constructive suggestions I could not have surmounted the difficulties in this work.

My sincere thanks are due to Mr. Anurag Goel for his cooperation in timely preparing the laminates. A word of appreciation is due to Mr. Tiwari for his help in preparing the specimens. I am also thankful to Mr. Pankaj Mr. Diwakar, Mr Ashutosh, and Mr Pandey for their help in one way or the other. I am thankful to Narendra for his help in learning stage.

I do not have any words to express my gratitude to KV and Madhu, with out whose encouragement and support I could not have been what I am today.

It gives me immense pleasure to recall my association with Ramana, JP, Phani, Kalyan, Siva, Sreedhar, Vissu, RajKumar who made my stay here at IIT K a pleasent memory.

Last, but not least I am grateful to Aeronautical Research and Development Board (Structure Panel) for providing the financial assistance for this project.

dedicated

to

MY PARENTS

Contents

List of Figures

List of Tables

Chapter 1

Introduction

1.1 Introduction

The word "composite" in composite material signifies that two or more materials are combined on a macroscopic scale to form a useful material. The key is the macroscopic examination of a material. Different materials can be combined on a microscopic scale, such as in alloying, but the resulting material is macroscopically homogeneous. The advantage of composites is that they usually exhibit the best qualities of their constituents and often some qualities that neither constituent possesses. The properties that can be improved by forming a composite material include

- Strength
- Stiffness
- Weight
- Fatigue life, etc.

Therefore the fibre reinforced composite materials have seen extensive application especially in aerospace industry, where the weight saving is most essential. They have good strength, stiffness and fatigue life but are suceptible to delamination when a foreign object impacts it at high velocity. On a metallic sheet (e.g. steel, aluminium) only a dent is formed when it is impacted by a foreign object with low or intermediate velocity; the

damage is local. Where as in case of composite materials it causes delamination. Several such impacts leads to extensive delamination and then the material integrity is in question. Therefore it is of our interest to study the dynamic fracture behaviour of the composite under impact loading.

Dynamic fracture phenomenon has several important features. The mathematical models are complex than the static models. The boundaries of the body changes with time. From experimental point of view, many parameters have to be measured accurately with in a very short period.

1.2 Literature Survey

A large number of investigations have been carried out on dynamic crack propagation employing through the thickness crack in a large plate. Stress waves are continuously generated at the crack tip of a fast moving crack. As these stress waves reach the boundary of the specimen, they are reflected. Some of these reflected stress wave come back to the region just in front of crack tip. Experiments with large size plate are controlled such that the monitoring of important parameters is complete before the reflected waves arrive. In other words, the experiments are controlled to isolate the effect of specimen edges. In case of an interlaminar crack in a FRP laminate, which is usually not thicker than 6 mm, the free surfaces are always close to the crack tip and there is no way one can isolate the region of interest from the reflected waves. Therefore a new approach is required to find dynamic toughness of interlaminar cracks.In this section, investigations on the large plates with through the thickness are briefly reviewed.

Initial and extensive investigations on crack propagation of through the thickness crack in a large plate were done by several groups. Ravi Chandar and Knauss (1982, 1984a, 1984b, 1984c, 1984d) have done an exhaustive study of dynamic crack propagation phenomena

using the method of caustics for Homalite-100. This included study of crack initiation and arrest, microstructural aspects, crack branching and interaction of stress waves with the crack tip. Rosakis, Duffy and Fruend (1984) performed dynamic crack propagation experiments on double cantilever beam specimen using wedge loading. Zehnder and Rosakis (1990) used optical method of reflected caustics combined with high speed photography to investigate the dynamic fracture initiation and propagation in 4340 steel specimen. These investigations, based on caustic have been very effectively used to study the fracture phenomena in a large plate with through the thickness crack. The method is not likely to be effective for the interlaminar crack in a slender sheet because the strength of the interlaminar bond is very weak and it will introduce very little strain in the bonded sheet making the size of the caustic negligibly small.

Ravichandran and Clifton (1989) developed a special technique to study the initiation and propagation of crack in the steel under dynamic impact loading. They presented a plate impact experiment and an associated finite difference model to study the fracture process that occurs in sub-micron loading. A disc containing a prefatigued edge crack on the midplane up to half way across the diameter is impacted by a thin flyer plate of same material. A compressive pulse propagates through the specimen and reflects from the rear surface as a tensile pulse of $1\mu s$ duration. The motion of the rear surface is monitored by using the laser interferometer.

Sun and Grandy (1988) investigated dynamic delamination fracture toughness in a $[90/0]_{5s}$ T900/934 graphite/epoxy laminate using impact loading. Delamination cracks of different sizes were embedded at the midplane of the composite specimen. The threshold impact velocity that causes propagation of delamination crack was used in the dynamic analysis with the finite element method. From the finite element solution, the time-history of the strain energy release rate was calculated. The critical strain energy release

rate was taken equal to that of maximum value of the response history.

Berger and Dally (1990a) used a series of strain gauges ahead of the crack tip to monitor the strain and crack propagation. Berger, Dally and Sanford (1990b) also used strain gauges ahead of the crack tip to determine dynamic stress intensity factor associated with a propagating crack.

Takeda et.al., (1982) used high speed photography to measure the speed of interlaminar in composite laminates. They observed that the interlaminar crack in composite laminates moves at 200-500 m/s, when impacted by foreign bodies. Freund (1990) found that the crack velocity is subsonic i.e. less than Rayleigh wave speed.

Nishioka and Atluri (1983) studied the use of path independent $\hat{J}$-integral for dynamic crack propagation by the finite element method. Other path integrals were also investigated along with $\hat{J}$-integral. Numerical results showed that combined use of $\hat{J}$-integral and the finite element method is a useful tool to obtain the fracture parameters such as stress intensity factors and energy release rates.

Kolednik (1991) presented his theoretical study for physical interpretation of the J-a curves for elastic-plastic fracture. He derived the difference between the exact initiation toughness and crack growth toughness for a very low velocity crack using energy balance under quasi-static conditions. He considered three point bend specimens each of which consists of two parts glued together along the ligament. The analysis was made on large specimens.

Verma et al. (1995) investigated SIF in a DCB specimen made of thin cantilevers of steel bonded with epoxy through a combined scheme of measuring the strain near the crack

tip and analyzing the experimental data using FEM. In the finite element programme he developed a relationship between stress intensity factor and strain near the crack tip. The strain measured near crack tip with a strain gauge is used in the FEM programme to obtain the SIF of the DCB specimen. Lovi (1993) improved this method by using two strain gauges on each cantilever to neutralize the possibility of recording the bending strains in the cantilevers which might develop during the specimen preparation.

Verma (1995) developed a combined experimental and numerical technique to determine interlaminar dynamic fracture toughness under impact loading. An interlaminar crack is propagated at very high speed in DCB specimen made of two steel plates which are bonded together by epoxy with a precrack. Strain gauges are bonded ahead of crack tip to monitor the crack velocity. The experimentally obtained data such as the end deflection of the cantilever, crack velocity and crack initiation time are used as input to the FE code to simulate the crack propagation, and to find the initiation and propagation toughness.

Ramakrishna (1997) applied the technique developed by Verma to composite laminates. He obtained initiation and propagation toughness of GFRP laminates which are of relatively poor quality. Babu(1998) further exploited the same technique to find the initiation and propagation toughness of GFRP laminates of relatively superior quality.

Raman P. singh et al. (1996) described various experimental observations for dynamic intersonic decohesion of bimaterial interfaces. Two separate but complementary optical methods are used in conjunction with high speed photography to explore the nature of the large scale contact and shock wave formation at the vicinity of running cracks in two different bimaterial systems.

R.W.Truss et al. (1997) had attempted to find interlaminar and intralaminar fracture toughness of uniaxial continuous and discontinuous carbon fiber/epoxy composites, using compact tension and double cantilever beam test geometries. The discontinuous carbon fiber/epoxy composites have been found to have a slightly misalignment of the fibers from the average fiber direction and this misalignment was found to increase both initiation fracture toughness and to greater extent the propagation fracture toughness. The increase in fracture toughness in discontinuous carbon fibers/epoxy samples was due to fibers bridging the crack and this has been modelled as if the the bridging fibers provide an increase in compressive stress across the crack.

A.Pegoretti et al. (1998) investigated effects of the temperature and fiber surface finishing on dynamic interfacial fracture toughness of nylon-6/E glass fibers composites. They have conducted experiments on embedded single fiber micro composites. For the unsized E-glass fibers an interfacial toughness of 165 J/m^2, while for the polyamide and epoxy compatible E-glass fibers debonding energy value was found as 340 J/m^2. Both types of E-glass fiber micro composites showed a strong decrease of interfacial toughness as the temperature increased.

John Lambros and Rosakis A.J (1997a) investigated dynamic delamination of thick fiber reinforced polymeric matrix composite laminates using optical techniques and high speed photography. They had used 65% fiber volume fraction of Graphite/epoxy laminates consisting of 48 plies. Square plates of $152mm \times 152mm$ dimensions were impacted in an out-of-plane configuration using high speed gas gun. Real time imaging of the laminate out-of-plane displacement was performed using lateral shearing of interferometer of Coherent Gradient Sensing in conjunction with high speed photography. Delamination speeds up to 1800 m/s were observed.

John Lambros and Rosakis A.J (1997b) investigated dynamic crack initiation and growth in unidirectional graphite/epoxy plates with high speed photography. Edge notch plates are impact loaded in one point bend configuration using drop weight tower. Initiation fracture toughness data were reported and significant dynamic effects are observed through emission of stress waves from the propagating crack tip.

1.3 Present Work

Verma(1995) developed a technique to determine the interlaminar toughness of two steel specimens bonded with epoxy. The technique employs a combined experimental and numerical work. Ramakrishna (1997) , Babu(1998) developed the same technique to GFRP laminates. In this work the technique has been further exploited to determine the dynamic initiation toughness and propagation toughness.

The technique consists of applying an impact load on a specimen with a precrack (Fig 1.1). The portion that is on the front side of the precrack remains straight during experimentation because it is bonded to a solid block. The rear rear portion of the specimen works as a cantilever plate. When an impact load is applied on the cantilever plate, the crack propagates. Strain gauges are mounted ahead of the crack tip to monitor the response. The experimental work determines the end deflection of the catilevr, crack velocity and the crack initiation time. These are used as input to the FE code developed by Verma (1995) to simulate the crack propagation.

Chapter 2 of the thesis describes the experimental setup and the details of the specimen. Chapter 3 describes the brief outline of the FE code developed by Verma (1995). Results are discussed in chapter 4 and finally the conclusions and the scope for further work are stated in chapter 5.

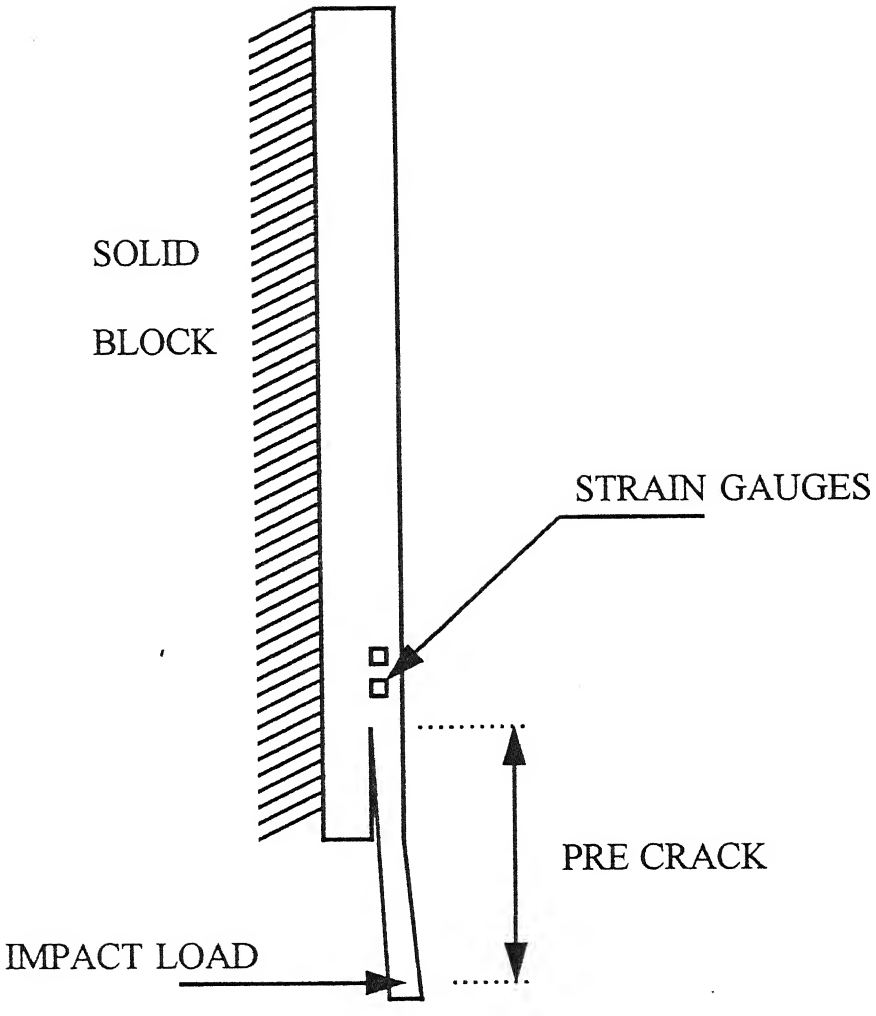

Figure 1.1: Specimen under impact loading

Chapter 2

Experimental Technique

2.1 Introduction

In the experimental - numerical technique of the present study, the experiments are conducted to determine the deflection of the cantilever end, crack propagation velocity and initiation time under impact load on the specimen. (Fig 1.1). This chapter deals with the specimen details and its preparation, experimental setup, experimental measurements and data analysis.

The technique developed by Verma(1995) is adopted to the present work. In this technique a stress pulse is generated in a cylindrical load bar (Fig. 2.1) by impacting it with a striker bar, accelerated in an air-gun. This load bar impacts the cantilever end of the specimen, whose other end is bonded to a very high inertia solid block. Two strain gauges are mounted in symmetrically opposite direction, on the surface of the load bar to monitor the stress pulses that is acting on the specimen. Two strain gauges are mounted ahead of the crack tip, to measure the crack velocity. Oscilloscope is used to record the data from the strain gauges. All the strain gauges are connected to the oscilloscope through the bridge circuits. The details of the experimental setup would be presented in Sec 2.3.

2.2 Specimen Details

The specimen used in the present work is unidirectional glass fibre reinforced epoxy composite. This section describes the basic raw materials used for the specimen, preparation of the laminate, geometry of the specimen, and preparation of the specimen.

2.2.1 Preparation of the Laminate

The basic raw materials for the preparation of the laminate are glass fibre and epoxy resin mixture. The composition of the epoxy resin is as follows:

Araldite	LY556	100 parts by weight
Hardener	HT976	35 parts by weight
Accelerator	XY73	1 part by weight
Coupling agent (γ -Amino propyl triethoxy silane)		0.5 parts by weight

Unidirectional glass fibres (of diameter 5-20 μm) reinforce the epoxy resin matrix. The glass fibre unidirectional prepegs are obtained in the semicured state from the unidirectional prepeg machine available in the laboratory. Number of lamina can be stacked together to get the laminate of required size. In the present work 52 of such lamina (of length 200 mm) are stacked with a precrack (thin teflon insert, 0.02 mm thick) placed exactly at the mid plane and to one end of the laminate. This laminate is then cured in a hydraulic press. The laminate is placed between the two platens of the press and is heated to 120 ^{0} C. Then the pressure is gradually raised to 0.7 Mpa ($\approx$ 7 ata) in half an hour. At the same pressure and temperature it is allowed to cure for four hours. Then keeping the pressure same,the temperature is increased to 150^0 C and is maintained for 3 hours. It is then allowed to cool to room temperature. The cured laminate is taken out of the press and is cut to required sized specimens by a diamond cutter.

2.2.2 Specimen Geometry

The geometry of the specimen is as shown in Fig.2.2. Figure 2.3 shows the isometric view of the same. It is 25 mm wide and 180-200 mm long with an edge precrack on the mid plane of the specimen. The portion that is on the front side of the precrack remains straight during experimentation because it is bonded to the solid block. The rear portion of the specimen works as a cantilever plate. The thickness of the cantilever is about 4 mm. A hole of ϕ $6mm$ is drilled on the cantilever end in order to fix it to the load bar. The center of this hole is the loading point on the cantilever.

2.2.3 Crack Sharpening

The as-cast precrack in the specimen is not very sharp due to the finite thickness of the teflon insert. So further extension of the crack is needed to sharpen the tip. It is done with the help of a fixture and pressure plates as shown in Fig 2.4. Two pressure plates are cut to 2 mm depth leaving a width of 8 mm at each end, to ensure that high compressive stress exists at a few millimeters away from the as-cast tip. Before the pressure plates are tightened between the two jaws of a vice, they are placed on their side face over the third base plate whose top surface is also grounded flat. This ensures that the edges of the pressure plates are parallel to the crack front. The specimen is placed between the pressure plates in such a way that the tip of the pre crack is out by 2-3 mm beyond the edges of the pressure plates. The specimen between the pressure plates is pressed properly between the jaws of the vice. Now with a cautious pressing of a sharp chisel at the mouth of the precrack the crack is extended up to the edges of the pressure plates. The tip of the extended crack is sharp.

2.3 Experimental Setup

Figure 2.5 shows the photograph of the overall experimental setup, the schematic diagram of which is as shown in Fig.2.1. The front plate of the specimen is bonded to a rigid block,

which in turn is clamped to the rigid base using C-clamps. The cantilever plate of the specimen is screwed to the load bar. Two strain gauges are bonded at diametrically opposite locations of the load bar. These are connected to an oscilloscope through a bridge circuit. Each one of the velocity strain gauges which are located ahead of the crack tip on the specimen is also connected to the same oscilloscope through another bridge circuit.

The striker bar accelerated in the barrel of the air-gun impacts the load bar. This produces a compressive stress pulse in the load bar which propagates towards the specimen. When the load bar impacts the specimen some part of its energy is transmitted to the specimen and the rest is reflected back as tensile pulse. The energy that is transmitted to the specimen causes the deflection of the cantilever plate and in turn propagates the crack. The strain gauges mounted on the load bar records the incident and reflected pulses through the oscilloscope. The velocity strain gauges on the specimen, which are connected to the oscilloscope, record the crack propagation history.

2.3.1 Solid Block

As shown in Fig.2.1 the front plate of the specimen is bonded to a rigid block of Mild steel of dimensions $75mm \times 75mm \times 150mm$. The block is placed on a rigid base plate; after aligning the specimen to the load bar, the block is firmly clamped to the base plate with the help of C-clamps. Care is to be taken to make sure that the crack plane is exactly perpendicular to the load bar; otherwise, the specimen will be preloaded and the numerical simulation would be inaccurate.

2.3.2 Striker and the Load bar

Applying an impact load on the specimen includes an air-gun, a striker bar and a load bar. The striker and load bar are made of cold rolled mild steel of diameter 19 mm. The load bar is aligned properly with the center line of the barrel of the air-gun. The striker bar is accelerated in the air-gun and its impacting face is made spherical (radius $\simeq$90 mm). It

impacts the load bar, which in turn impacts the specimen. When the striker bar hits the load bar, a compressive stress pulse is produced in the load bar which travels towards the specimen. A part of this compressive stress pulse is transmitted to the specimen and the rest is reflected back as a tensile pulse. Two strain gauges ($120\Omega, 6mm$ gauge) mounted at diametrically opposite locations on the load bar are used to monitor the stress pulses. These strain gauges, connected to the oscilloscope through a bridge circuit monitors the incident and reflected stress pulses.

2.3.3 Bridge Circuit

The purpose of bridge circuit is to convert the resistance change in strain gauges into a voltage difference. This voltage difference can be recorded in the oscilloscope. Figure 2.6 shows the details of the bridge circuit used. There are four arms in each bridge. One strain gauges is connected to each of these arms. They are named R_1, R_2, R_3, R_4. In an half bridge circuit two strain gauges are active gauges, (i.e R_1 and R_3) and in a quarter bridge circuit only one gauge (i.e R_1) is active. The remaining gauges are dummy gauges. These dummy gauges are provided by mounting them on a plate of the same material as that of the load bar, which acts as a heat sink for the heat generated in the gauges when current passes through the gauges. The half bridge circuit is used to monitor the stress pulses in the load bar. In this case the two active gauges are the two gauges mounted on the load bar at diametrically opposite locations.

The quarter bridge circuits are used to monitor the crack propagation history through velocity strain gauges. Since there are two velocity strain gauges bonded on the specimen two quarter bridges are needed to monitor the crack propagation history.

The bridge circuit is balanced to zero volatage output by connecting 1 Ω resistance for coarse adjustment and 1 M Ω resistance for fine adjustment, as shown in the circuit. To

calibrate the circuit a calibration resistance ($R_c = 47.0\ K\Omega$) is connected in parallel to any active gauge through a switch. The equations involving the calibration of the bridge circuit are as follows.

For a balanced bridge circuit the output voltage Δe is given by

$$\frac{\Delta e}{E} = \frac{R_1.R_2}{(R_1+R_2)^2}\left(\frac{\Delta R_1}{R_1} - \frac{\Delta R_2}{R_2} + \frac{\Delta R_3}{R_3} - \frac{\Delta R_4}{R_4}\right) \tag{2.1}$$

where E is the input voltage. It can be seen from the equation that similar (both positive or both negative) changes in resistance of opposite arms of the bridge circuit are added and dissimilar (one positive and other negative) changes are cancelled. Thus by taking the active strain gauges at the opposite arms, only compressive pulse is recorded in the load bar and bending effect is nullified, if there is any.

The relation between the strain in the strain gauge and corresponding change in its resistance is governed by the following equation

$$S_g = \frac{\Delta R/R}{\Delta L/L} \tag{2.2}$$

where S_g is the gauge factor and $\Delta R/R$ is the strain recorded by the strain gauge. Rearranging the above equation,

$$\frac{\Delta L}{L} = \frac{\Delta R/R}{S_g}\ . \tag{2.3}$$

For Half Bridge

The change in resistance of the arm AB after connecting R_c is given by

$$\Delta R_1 = R_1 - (\frac{R_1.R_c}{R_1 + R_c}) \ . \tag{2.4}$$

This implies

$$\Delta R_1/R_1 = \frac{R_1}{R_1 + R_c} \ . \tag{2.5}$$

Corresponding to this change in resistance a voltage difference (Calibration Voltage, V_c) develops between terminals A and C. Similar resistance change will also occur in R_1 and R_3, when the load bar experiences the load pulses. From Eqs. 2.3 and 2.5 the calibration voltage corresponds to the strain

$$\epsilon_c = \Delta L/L = \frac{R_1}{2(R_1 + R_c)S_g} \ . \tag{2.6}$$

The strain value, ϵ_c will thus correspond to the calibration voltage, V_c. A factor of 1/2 is introduced to take the average of the strains recorded by the strain gauges R_1 and R_3 which are at the opposite arms of the bridge circuit. By the linear relationship between the voltage drop across AC and strain in the strain gauges bonded on the load bar, the strain in the load bar corresponding to a voltage V recorded on the oscilloscope can be given as

$$\epsilon = \frac{\epsilon_c}{V_c}.V = \frac{R_1 \ V}{2 \ (R_1 + R_c) \ S_g \ V_c} \tag{2.7}$$

For Quarter Bridge

The analysis for this circuit is also same as that of the the half-bridge circuit except that there is only one active strain gauge (R_1), R_3 acting as a dummy gauge in this case. Since

there is only one active gauge ϵ_c is

$$\epsilon_c = \Delta L/L = \frac{R_1}{(R_1 + R_c)S_g} \tag{2.8}$$

and strain at the crack velocity strain gauge is

$$\epsilon = \frac{\epsilon_c}{V_c}.V = \frac{R_1\ V}{(R_1\ + R_c)\ S_g\ V_c}\ . \tag{2.9}$$

The strain gauges are connected to the Wheatstone bridge through a specially designed cap and stud arrangements to have press contact at the terminals (Verma (1995)). Coaxial wires are used to connect the circuit to all the gauges to shield the fast changing signals. A bridge is enclosed within a conducting box of aluminium to have shielding from spurious signals. The grounds of all coaxial cables and the oscilloscope are connected to the aluminium enclosures to have the same common ground of the entire measuring system.

2.3.4 Oscilloscope

Each one of the strain gauges is connected to the oscilloscope through the bridge circuits. The oscilloscope records the resistance change in the strain gauges as the potential difference. The oscilloscope used in the present work is a 4-channel Digital Storage Oscilloscope (Model 1624, Gould Inc., U.K). It has 8-bit resolution in vertical direction and 16-bit resolution in horizontal direction. The sensitivity of the Oscilloscope is 0.025 mV on vertical axis and 0.25 μs on horizontal axis. It is integrated with a personal computer. A PC compatible software is used to transfer the data from the oscilloscope to the PC for further analysis.

2.3.5 Deflection of Cantilever end

Figure 2.7 shows a typical record of the incident and reflected pulses in the load bar. From this experimental record the deflection of the cantilever end can be obtained using one

dimensional wave propagation theory. Figure 2.8 shows the time-distance(t-x) diagram for the propagation of stress pulses in the load bar. When the striker bar impacts the load bar, the compressive incident stress pulse (σ_1) propagates towards the specimen and is recorded at the location 1. The reflected tensile stress pulse (σ_3) is recorded at the same location but at a diferent time and is depicted by point 3 in the t-x diagram. The aim is to express particle velocity v_2, at point 2 in terms of experimentally recorded σ_1 and σ_3. One dimensional wave equation along the characteristic with the acoustic impedance ρ c is expressed as

$$\mathrm{d}\,\sigma - \rho\,\mathrm{c}\,\mathrm{dv} = 0 \qquad (\text{along +ve characterstic})$$

$$\mathrm{d}\,\sigma + \rho\,\mathrm{c}\,\mathrm{dv} = 0 \qquad (\text{along -ve characterstic})$$

where σ is stress, v the particle velocity, c the longitudinal wave velocity, and ρ the density of the load bar material.

Using the above concept the relation along characteristic 1-2 can be obtained as

$$\sigma_2 - \rho\,c\,v_2 = \sigma_1 - \rho\,c\,v_1 \quad . \tag{2.10}$$

Along the characteristic 1-5 the relation is

$$\sigma_1 + \rho c v_1 = \sigma_5 + \rho c v_5 \quad . \tag{2.11}$$

But σ_5=0 and v_5=0, because the load bar is initially at rest and stress wave never reaches point 5. Then the above equation becomes

$$\sigma_1 = -\rho\,c\,v_1 \quad . \tag{2.12}$$

Substituting Eq.2.12 in Eq.2.10,

$$\sigma_2 - \rho\,c\,v_2 = 2\sigma_1 \quad . \tag{2.13}$$

Relations along the characteristics 2-3 and 3-4 are

$$\sigma_2 + \rho\, c\, v_2 = \sigma_3 + \rho\, c\, v_3 \tag{2.14}$$

and

$$\sigma_3 - \rho\, c\, v_3 = \sigma_4 - \rho\, c\, v_4 \ . \tag{2.15}$$

It is worth noting that $\sigma_4 = 0$ and $v_4 = 0$ at point 4, because the striker bar and the load bar are made of the same material and diameter and the striker comes to rest. Then the above two equations yield

$$\sigma_2 + \rho\, c\, v_2 = 2\sigma_3 \tag{2.16}$$

Adding equation 2.13 and Eq.2.16, one obtains

$$\sigma_2 = \sigma_1 + \sigma_3 \tag{2.17}$$

By substituting σ_2 from the above equation in Eq. 2.13,

$$v_2 = \frac{\sigma_3 - \sigma_1}{\rho\, c} \tag{2.18}$$

Since σ_1 is compressive and σ_3 is tensile in nature the particle velocity of cantilever end is found by taking the sum of the absolute value of the incident and the reflected pulses. The displacement u_2 of the load bar end can be found by integrating the velocity. It is given by

$$u_2(t) = \int_0^t v_2\ dt = \int_0^t \left(\frac{\sigma_3 - \sigma_1}{\rho\, c}\right) \tag{2.19}$$

Since the specimen is screwed to the load bar the displacement of the load bar end becomes the defelction of the cantilever end. Figure 2.9 shows a typical variation of the deflection of the cantilever end with time.

2.3.6 Crack Velocity

Verma(1995) developed a technique to find the dynamic interlaminar toughness of steel DCB specimen bonded with epoxy; under impact loading. He used strain gauges bonded ahead of the crack tip to monitor the crack propagation history. The strain gauges used in his work were supplied by Tokyo Sokki Kenkyujo Co. Ltd, Japan. They have a gauge length of 0.2 mm and a gauge factor of 2.05. The resistance of the gauges is 120 $\pm 0.3\Omega$. He placed the strain gauges at $+45^0$and at the mid plane of the cantilever. The technique worked quite reliably.

Ramakrishna (1997) applied the same technique on GFRP laminates. It also worked reliably. However the interlaminar toughness of the GFRP of Ramakrishna's work was poor due to the poor quality of the laminate. When Babu (1998) applied the same technique to GFRP laminates of substantially higher interlaminar toughness the technique based on more than 25 experiments, was found to be unreliable. Thus it was concluded that the technique developed by Verma, works only with specimen having low interlaminar toughness.

Thus to overcome the problem a modified technique has been developed. In this technique same strain gauges (0.2 mm gauge length, supplied by Tokyo Sokki Kenkyujo Co. Ltd, Japan) were used but they were bonded much closer to the crack plane and with a different orientation. The unnecessary portion of the strain gauge is cut and thrown away. (Fig 2.10 shows the blown of views of the strain gauge prior to and after cutting). The strain gauge is then placed very close to the crack plane (Fig 2.11). Since the strain gauges are very close to the crack plane, the singular strain field gives a strain peak when the crack tip passes close to the strain gauge. There are two such velocity strain gauges the distance between the two strain gauges is measured accurately through travelling microscope; the velocity can be found (Fig 2.12) using the formula

$$Velocity = \frac{a_2 - a_1}{t_2 - t_1}$$

where a_i is the location of strain gauge from the cantilever end and t_i the time of the strain peak, monitored by the velocity strain gauge.

Verma (1995), using three velocity strain gauges, found that the crack velocity does not very much with time. Therefore in this study the crack velocity is assumed to be constant and only two strain gauges are employed.

Bonding the strain gauges

Initially the surface of the specimen is polished and degreased. Then the strain gauges are placed in their marked locations taking the help of a cello tape. Fewi-quick (Supplied by Pedilite industries) is used to bond the strain gauges. The strain gauges are placed very close to the crack plane and perpendicular to the crack plane.

2.3.7 Initiation time

The two strain gauges mounted ahead of the crack tip feels the response of the crack thereby giving the crack velocity. The initiation time can be found by extrapolating these data. Figure 2.13 shows the details of the extrapolation. Extrapolation of the crack velocity to determine the initiation time can be justified as follows.

John Lambros and Ares J. Rosakis (1997a) conducted an impact loading test on a one point bend (edge-notched unidirectional specimen with fibers parallel to the crack plane) configuration on unidirectional graphite/epoxy composite plates. For obtaining crack initiation and monitoring crack growth, an experimental technique with high speed photography was used. The measured crack velocity, shown in Fig. 2.14, is in microsecond

domain; the crack, after initiation acquires high velocity immediately with rise time much less than 1 μs. It is infered from the experimental result that the extrapolation invoked in this study in finding initiation time is not too bad. Further more it is clear from Fig 2.14 that crack velocity does not change drastically after initiation time. It increases from 500-600 m/s in first 5 μs (20%). Thus if there is an error of 30% (chosen higher to account for unknown factors), in estimating the time taken by the tip of the precrack to the first strain gauge, the error in estimating the initiation time is only 1.10 μs, for the crack to reach the first strain gauge at a distance of 3 mm with a crack velocity of 800 m/s.

2.4 Closure

The specimen details such as the basic raw materials, laminate preparation, crack sharpening and the overall experimental setup, which include rigid block, the stress pulses, the bridge circuit and the oscilloscope were discussed in this chapter. The experimentation provides

- The deflection of the cantilever end
- Crack velocity
- Initiation time

These are used as the input to the FE code (developed by Verma (1995)). A brief outline of its formulation is presented in the next chapter.

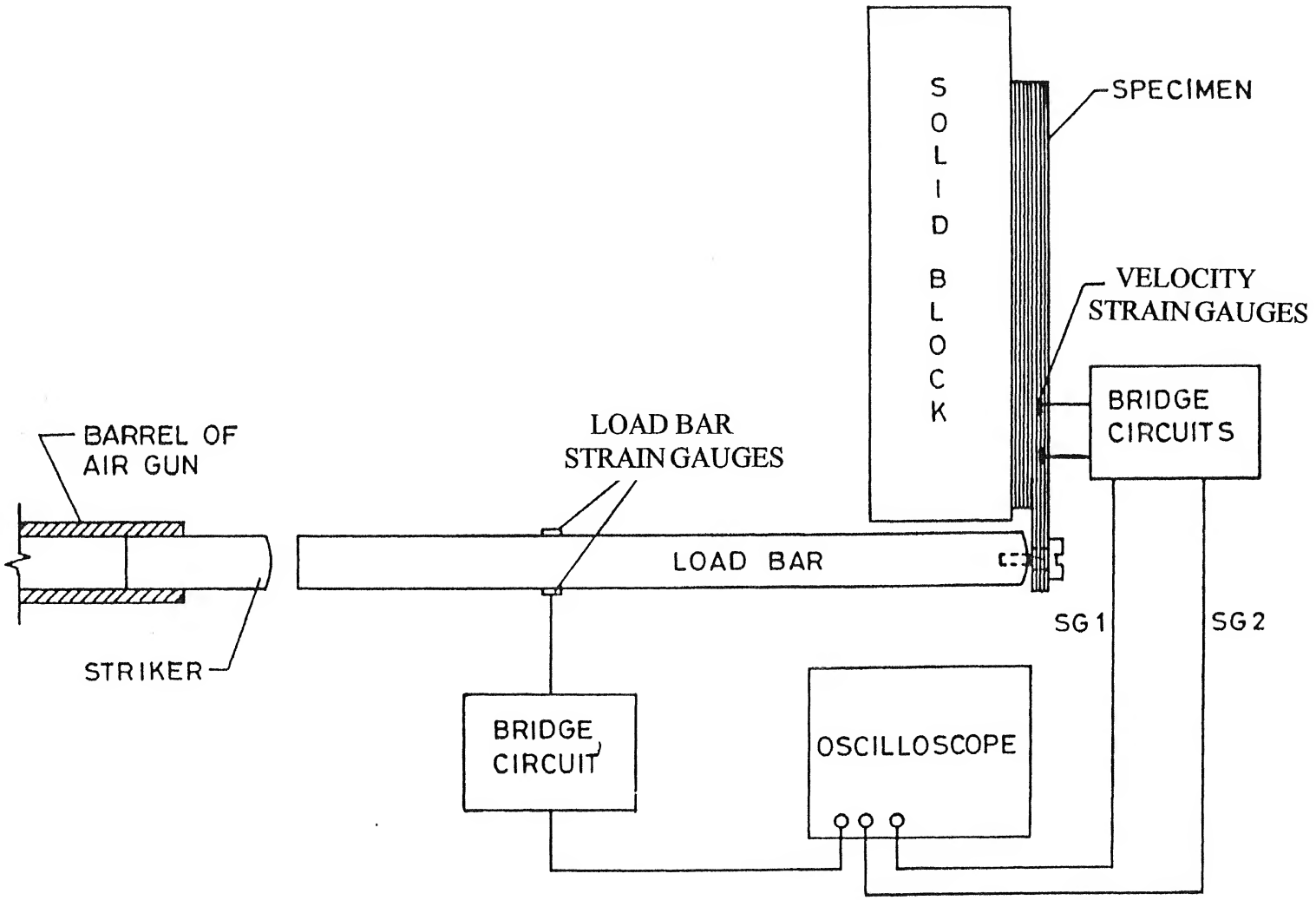

Figure 2.1: Schematic diagram of the experimental Setup

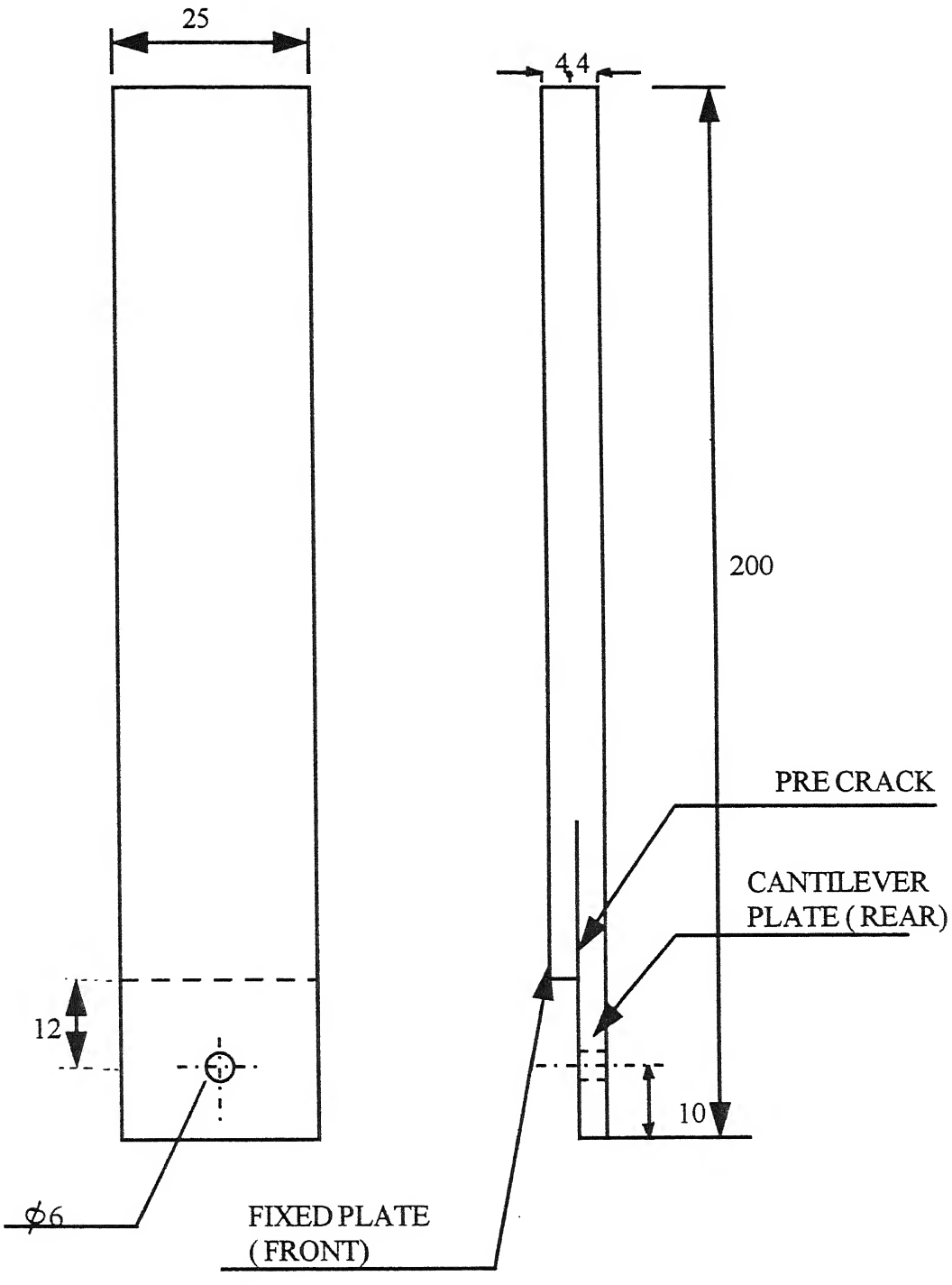

All Dimensions in mm

Fig 2.2 : Specimen Geometry

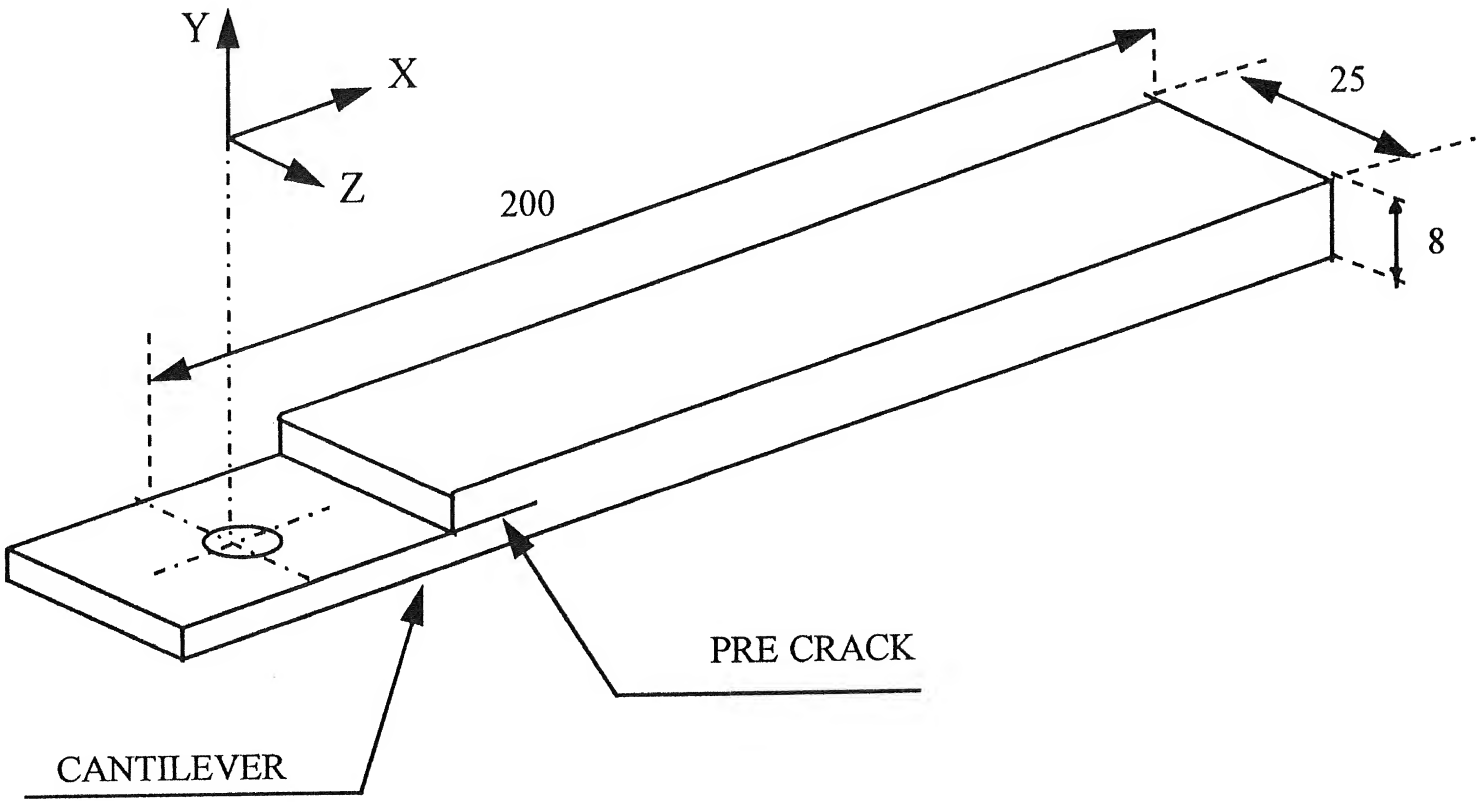

Fig 2.3 : Isometric view of the specimen

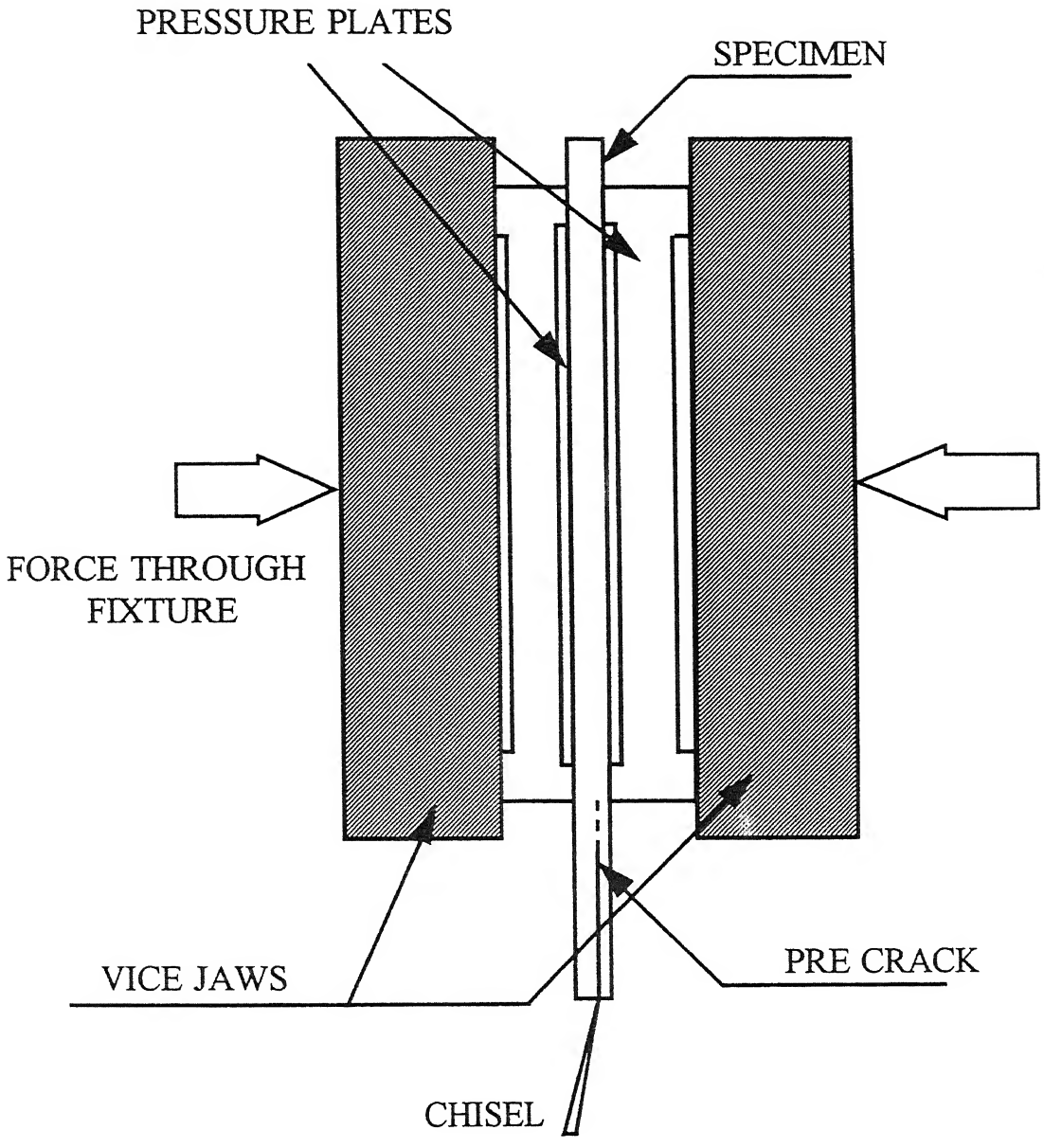

Figure 2.4: Crack sharpening fixture

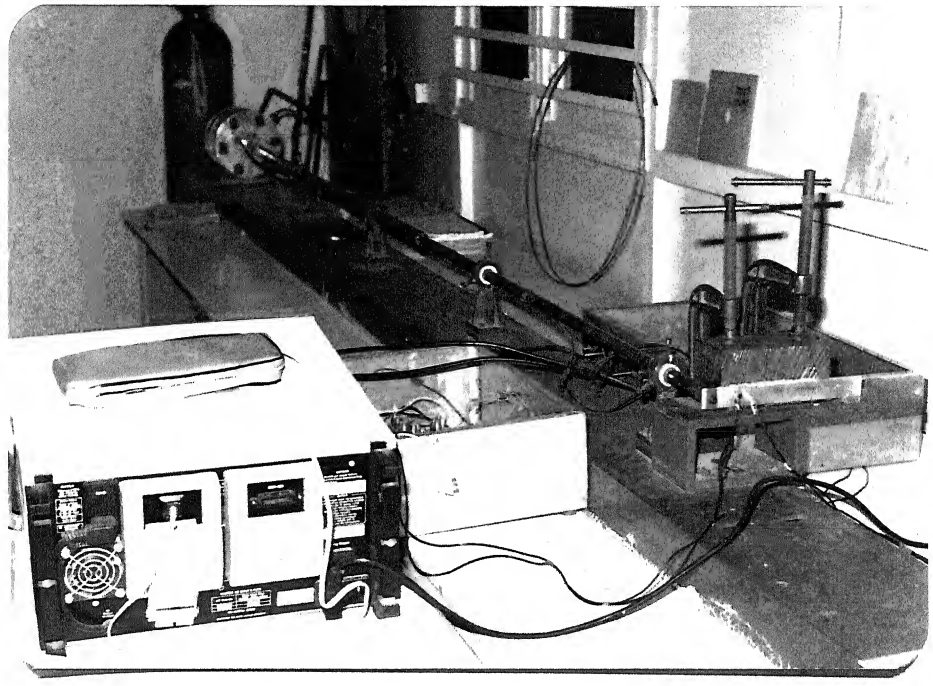

Figure 2.5: Photograph of overall experimental setup

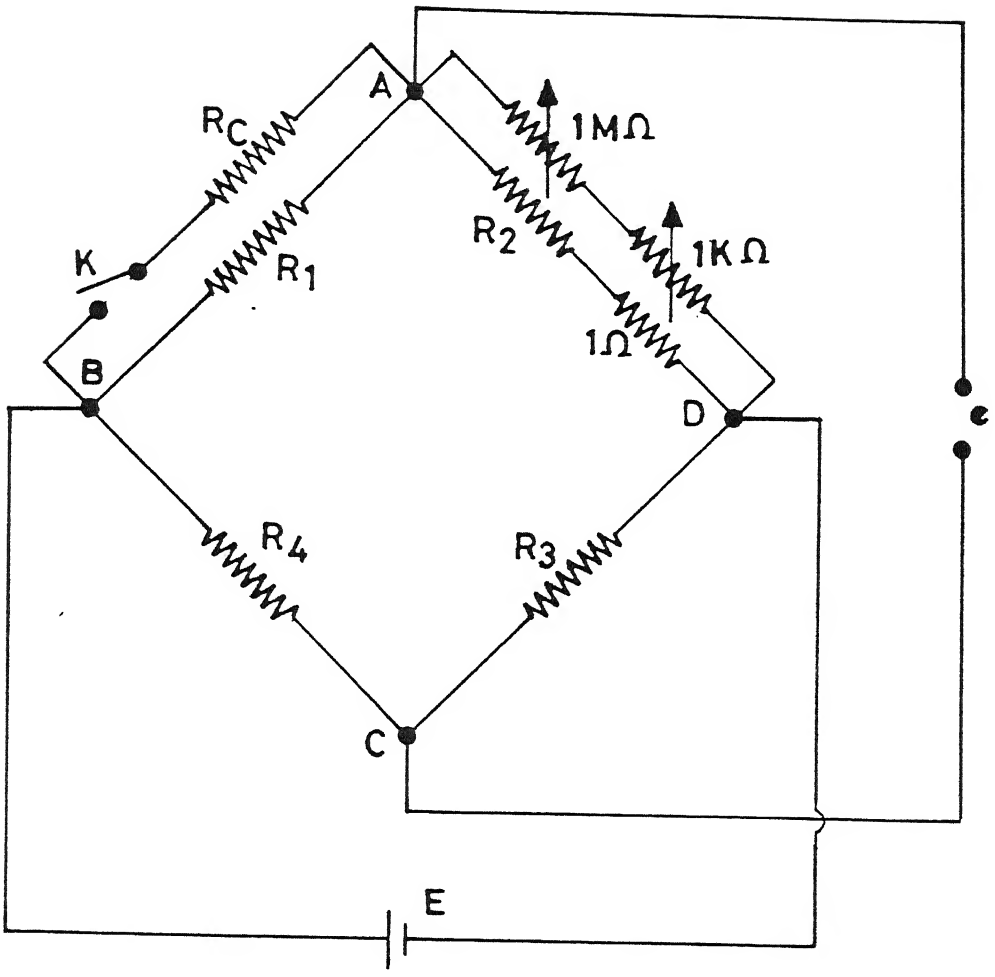

Figure 2.6: Details of the bridge circuit

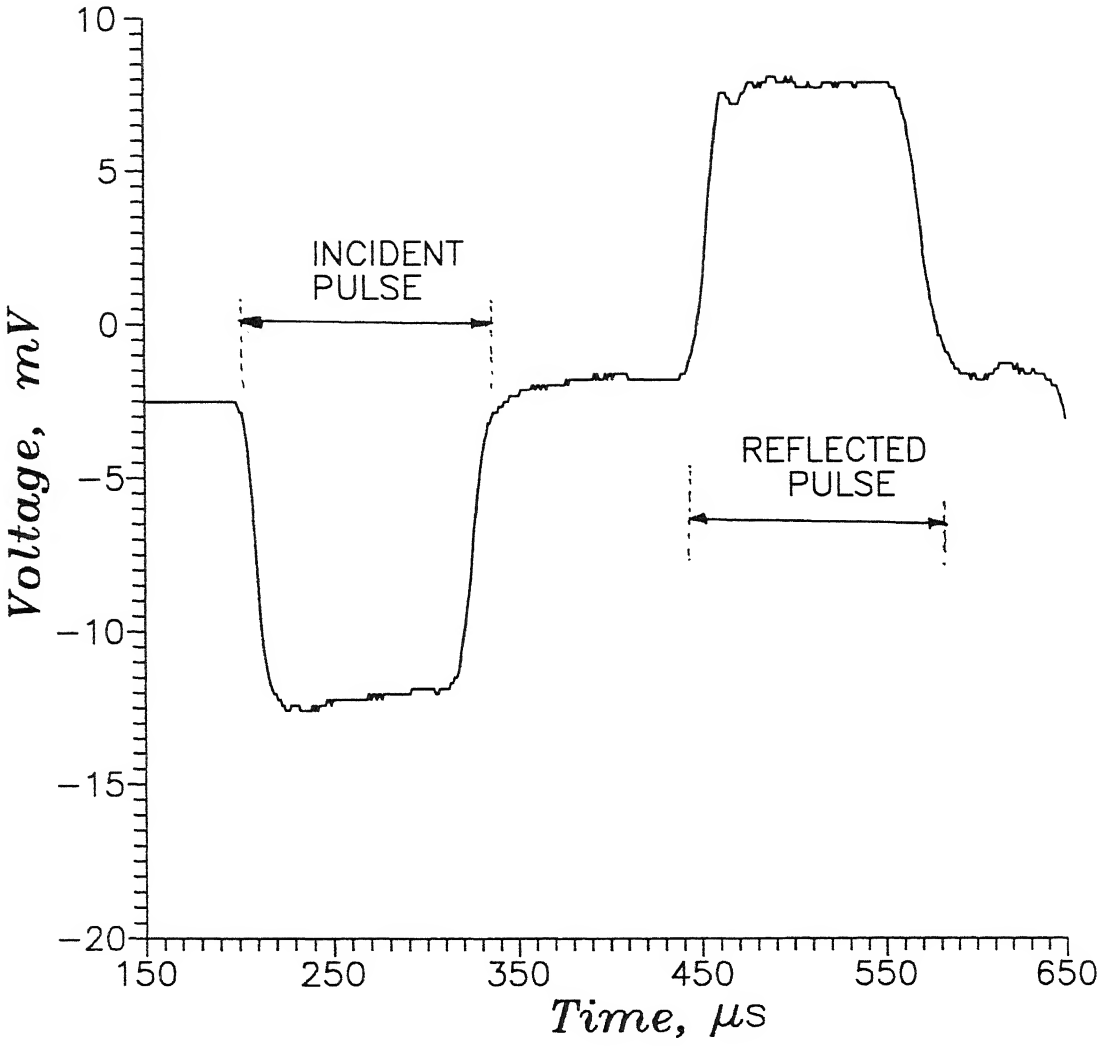

Figure 2.7: Typical record of incident and reflected pulses in the load bar (Expt.1)

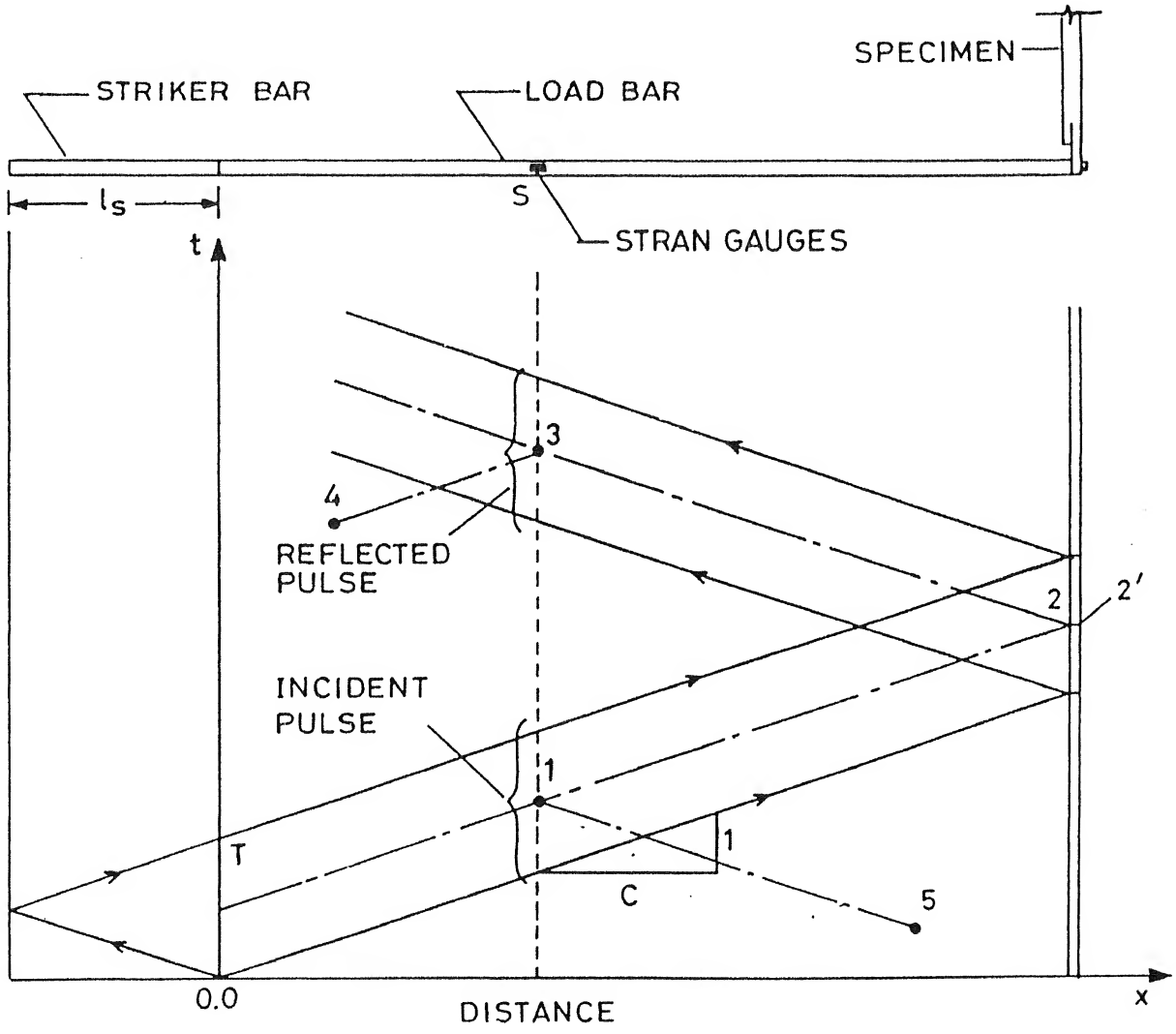

Figure 2.8: Time - distance (t-x) diagram

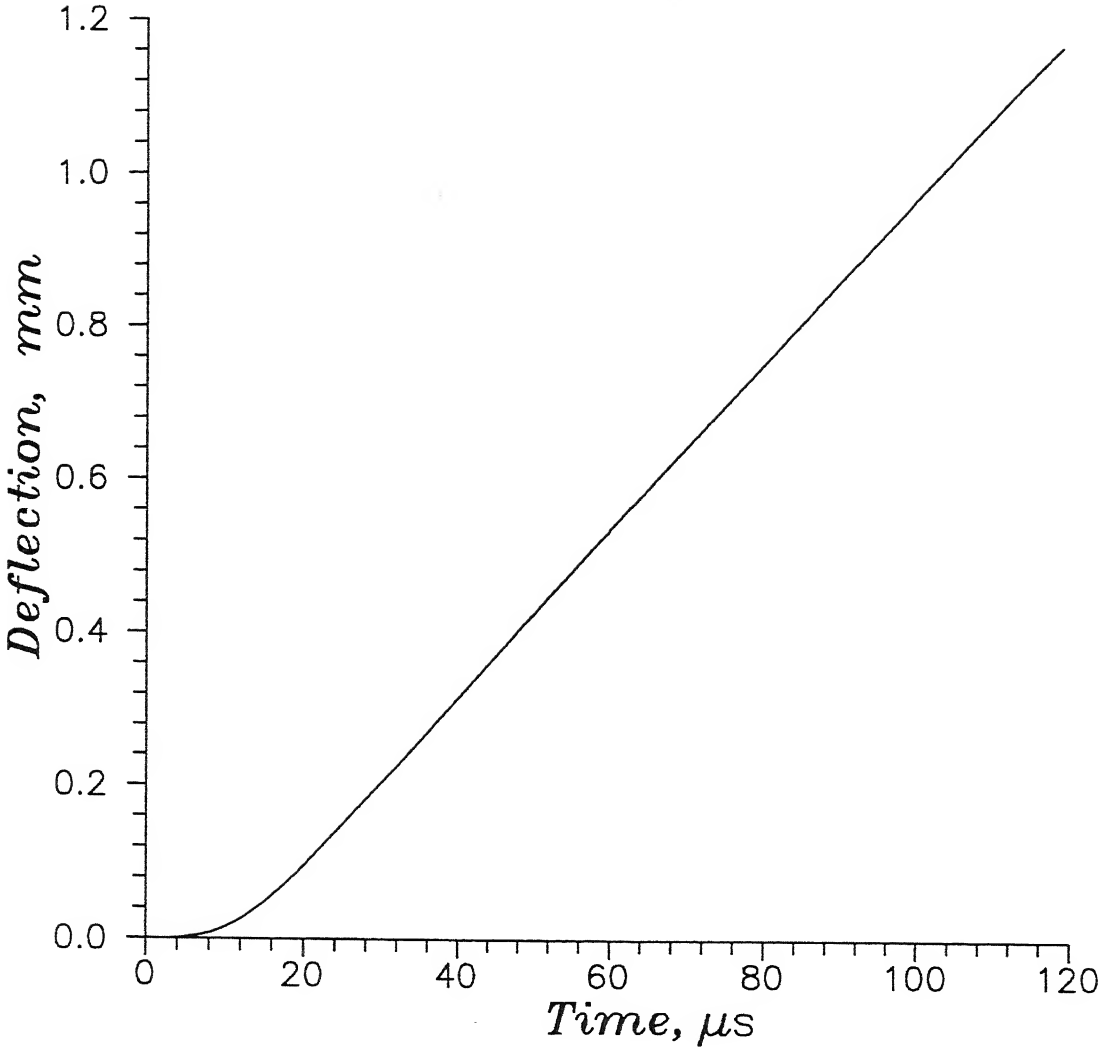

Figure 2.9: Variation of deflection of cantilever end with time (Expt.1)

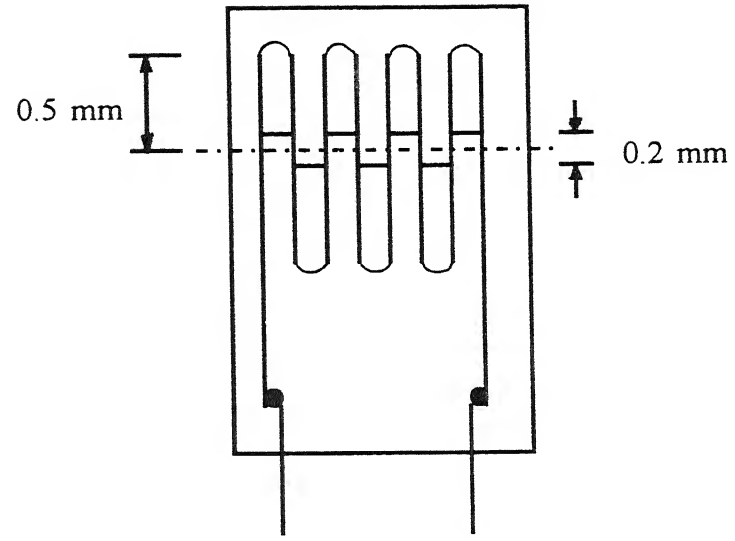

(a)

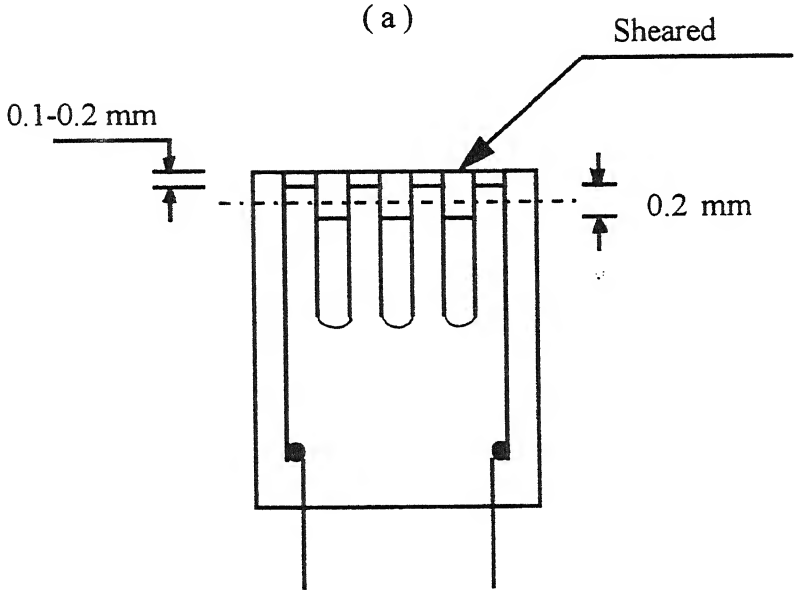

(b)

Figure 2.10: Blown up view of the strain gauges (a) before cutting , (b) after cutting

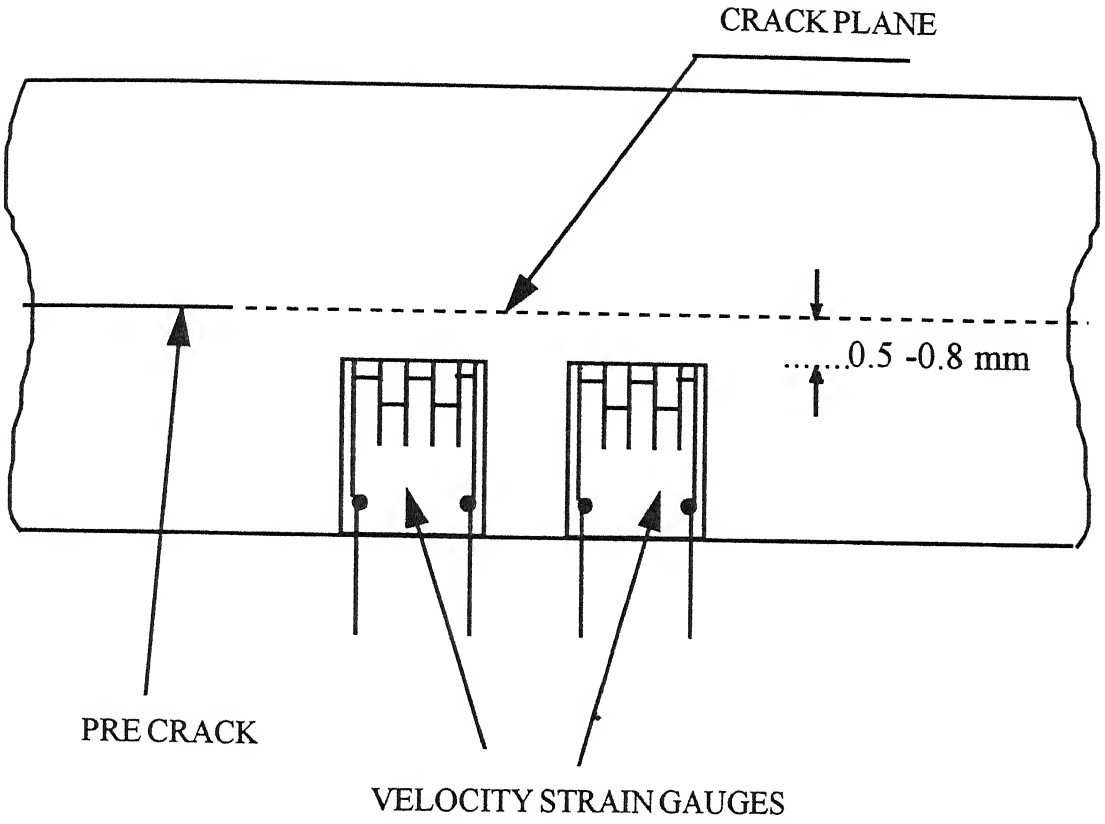

Figure 2.11: Position of the strain gauges with reference to the crack plane

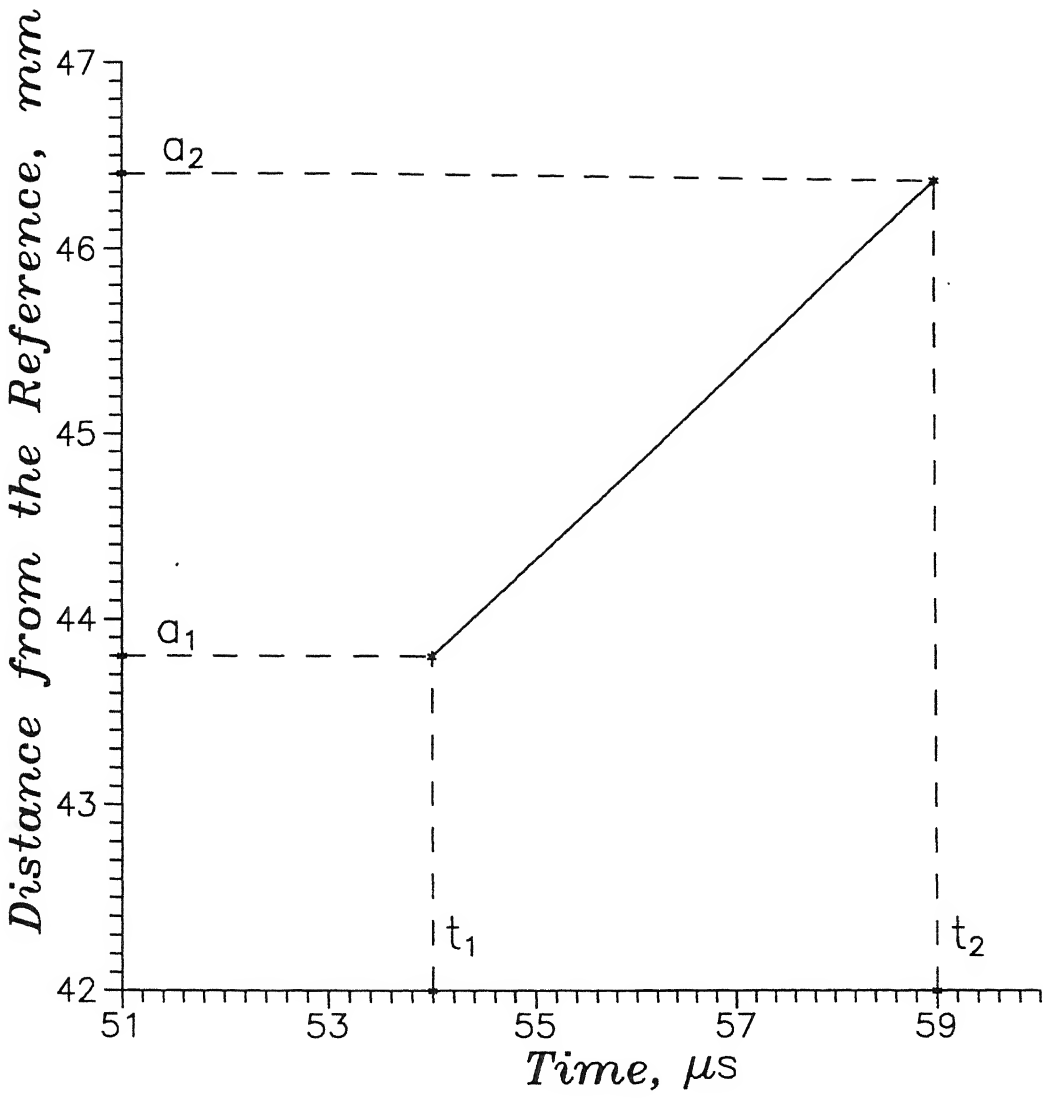

Figure 2.12: Determination of crack velocity from the response times

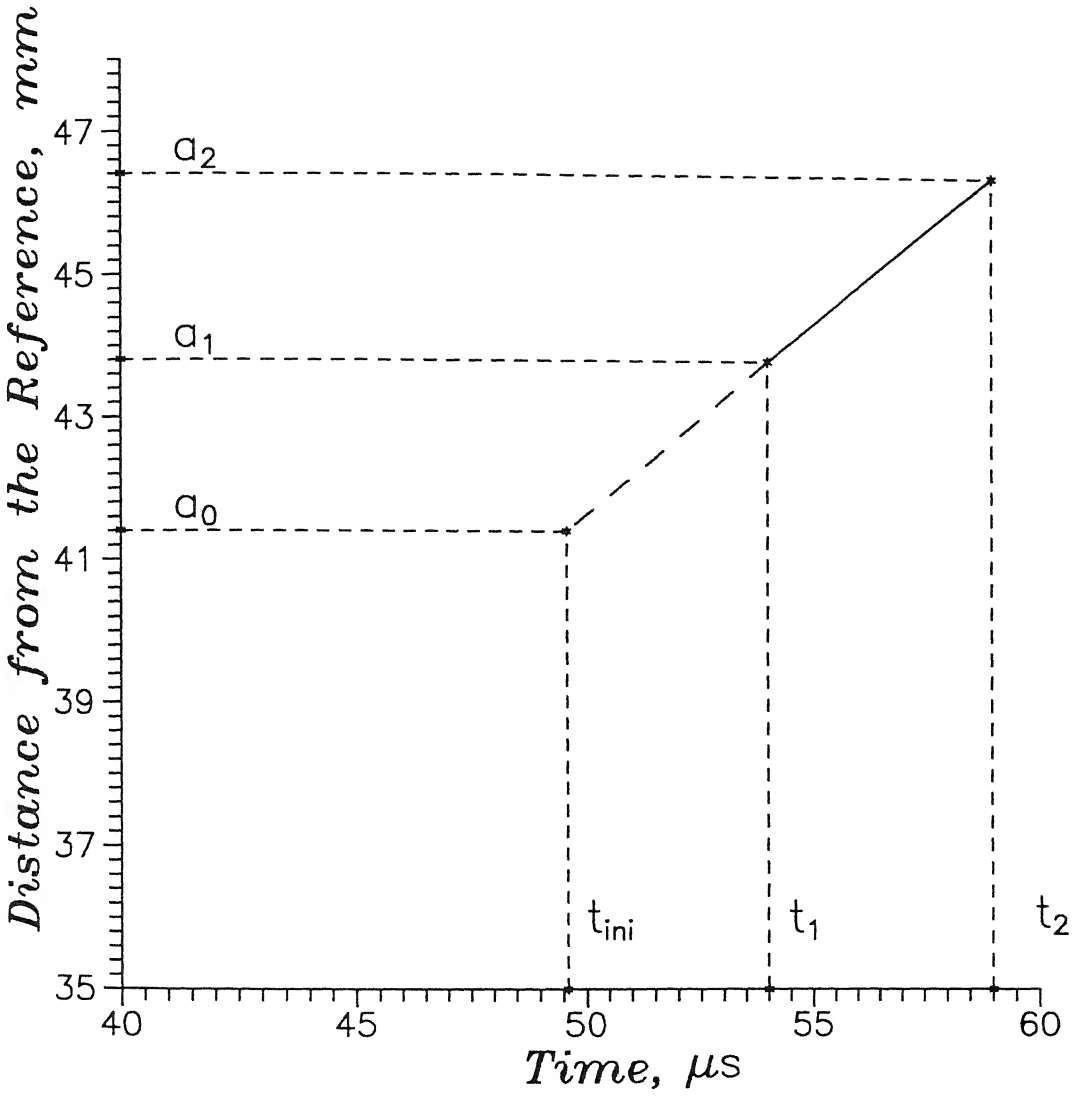

Figure 2.13: Details of extrapolation to find initiation time corresponding to the length of the precrack (a_o).

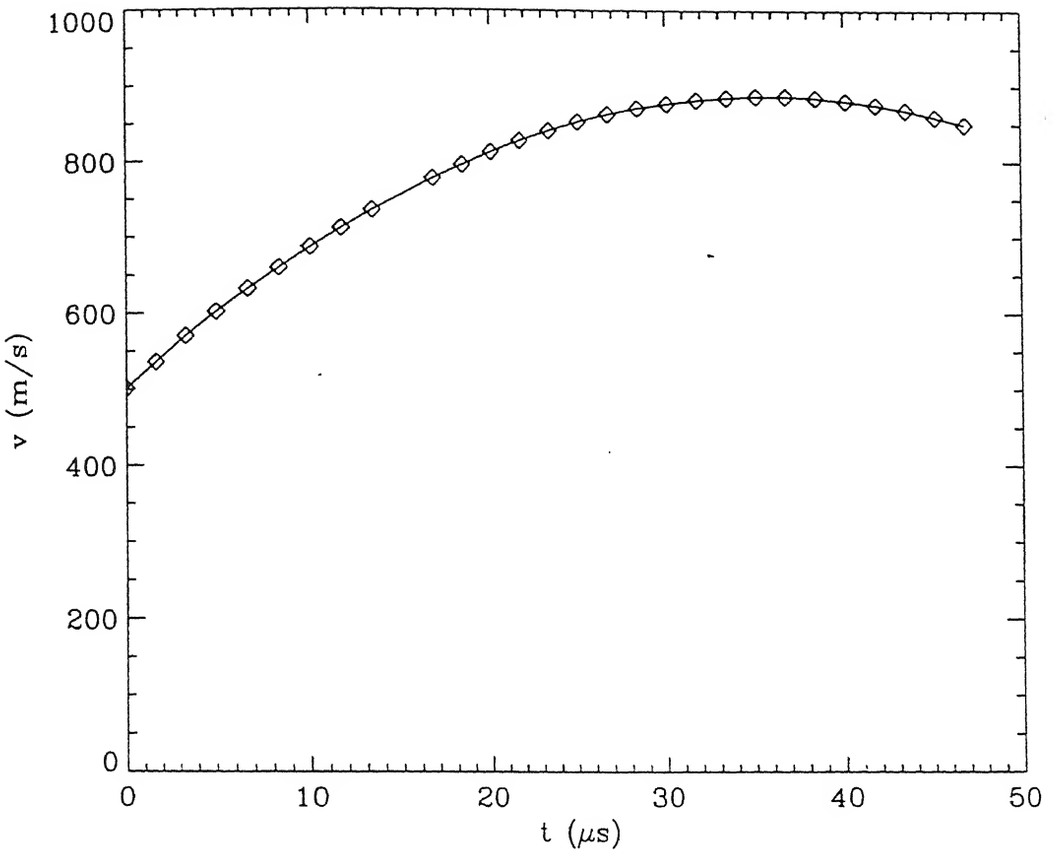

Figure 2.14: Crack tip speed history in a 4×6 inch unidirectional graphite/epoxy composite plate containing a sharp starter crack. (Ref: Rosakis et al.(1996)).

Chapter 3

Numerical Analysis

3.1 Introduction

The data obtained from the experiments such as the initiation time, crack velocity and the cantilever end deflection are taken as input to the FE Code developed by Verma(1995) to simulate the crack under dynamic conditions. Verma developed the technique to find the interlaminar dynamic toughness of steel specimens under impact loading. Ramakrishna(1997) and Babu(1998) extended the same technique to the GFRP laminates.

This chapter briefly describes the finite element formulation, the path independent integral, the crack opening scheme and the flow chart of the code.

3.2 Formulation

The governing system of finite element equations for the linear dynamic response of an elastic body is given in the matrix form as

$$[M]\{\ddot{U}\} + [C]\{\dot{U}\} + [K]\{U\} = \{R\} \tag{3.1}$$

where [M],[C] and [K] are the mass,damping and stiffness matrices respectively and {R} is the external load vector; {U},$\{\dot{U}\}$and $\{\ddot{U}\}$ are the displacement, velocity and acceleration vectors respectively. In the above equation

$$[M] = \Sigma[M]^e$$

$$[K] = \Sigma[K]^e$$

$$\{R\} = \Sigma\{R\}^e$$

where the elemental matrices are defined as

$$[M]^e = \int_V \rho\, [N]^T\, [N]\, dV$$

$$[K]^e = \int_V [B]^T\, [D]\, [B]\, dV$$

$$\{R\}^e = \int_S [N]\{T\}\, dS$$

In these equations $[N]$ is shape function matrix, $[B]$ the derivative of shape functions, $[D]$ the elastic constitutive relation matrices, and $\{T\}$ the traction vector.

In the analysis the damping forces were neglected and therefore the governing equation becomes

$$[M]\{\ddot{U}\} + [K]\{U\} = \{R\} \ . \tag{3.2}$$

The above equation can be solved either by time integration or by mode superposition, of which the the former is preferred for simulating wave propagation problems of the present kind. In this integration scheme, there are many different methods. In the present work Newmark integration method for time variable is used. Since the specimen width is large in comparison to its thickness (Fig 2.3) plane strain relations are used. Furthermore the front face of the specimen remains fixed to the rigid block and its effect on the $\hat{J}$-integral is negligible(Verma (1995)). The analysis is therefore carried out only on the cantilever plate to avoid unnecessary computation.

3.2.1 Constitutive relation for Composites

Verma (1995) developed the program for isotropic materials. It has been modified by Ramakrishna(1997) and Babu(1998) to apply it to the composite materials. In the isotropic materials there are only two independent elastic constants, where as in case of the composite materials there are four independent elastic constants. The elastic constants are longitudinal modulus E_L, transverse modulus E_T, rigidity modulus G_{LT}, the major Poisson ratio ν_{LT} and the minor Poisson ratio ν_{TL}; only four of them are independent. The principal material directions of the composite materials are as shown in Fig 3.1. Tests are conducted to find E_L, E_T, G_{LT} and ν_{LT}. E_L and E_T can be directly obtained from the tension tests on 0^o and 90^o ply laminates respectively. And one more tension test is conducted on a 45^o ply laminate to get the modulus in that direction. G_{LT} is obtained from the expression

$$\frac{1}{E_{45^o}} = \frac{1}{4}\{\frac{1}{E_L} + \frac{1}{E_T} + \frac{1}{G_{LT}} - \frac{2\nu_{LT}}{E_L}\} \tag{3.3}$$

The details of the specimen used and the related results are discussed in detail in Appndix A. The obtained values from the experiments are as follows

$$\begin{aligned} E_L &= 40.53 \text{ GPa}, \\ E_T &= 6.98 \text{ GPa}, \\ G_{LT} &= 2.84 \text{ GPa and} \\ \nu_{LT} &= 0.277 \, . \end{aligned}$$

The constitutive relation for the composite materials is given by

$$\{\sigma\} = [Q] \{\epsilon\}$$

where

$$[Q] = \begin{bmatrix} Q_{11} & Q_{12} & 0 \\ Q_{12} & Q_{22} & 0 \\ 0 & 0 & Q_{66} \end{bmatrix}.$$

Q_{ij} are the stiffness coefficients of the composite. They can be expressed as

$$Q_{11} = \frac{E_L}{1 - \nu_{LT}\,\nu_{TL}}$$

$$Q_{22} = \frac{E_T}{1 - \nu_{LT}\,\nu_{TL}} \tag{3.4}$$

$$Q_{12} = \frac{\nu_{TL}\,E_L}{1 - \nu_{LT}\,\nu_{TL}} = \frac{\nu_{LT}\,E_T}{1 - \nu_{LT}\,\nu_{TL}}$$

$$Q_{66} = G_{LT}$$

3.2.2 Path independent integral

Under appropriate assumptions of material homogeneity, the strength of the crack tip field is governed by an integral evaluated over a path that is far removed from the crack tip. Since the stress and displacement data are evaluated far away from the crack tip, these are relatively insensitive to the finer details of modelling of crack tip region. Therefore a path independent integral,($\hat{J}$ integral) is used in the analysis. In this analysis the $\hat{J}$ integral given by Kishimoto, Aoki and Sakata (1980) is used. It is defined as

$$\hat{J} = lim_{\epsilon \rightarrow 0} \int_{\Gamma_c^- + \Gamma + \Gamma_c^+} [\, W\, n_1 - T_i\, u_{i,1} \,]\, ds + \int_{V - V_\epsilon} \rho\, \ddot{u}_i\, u_{i,1}\, dV$$

where W is the strain energy density, u_i is displacement, n_1 is the direction cosine of the unit outward normal in x_1 direction, T_i is the traction, Γ_c^-, Γ, Γ_c^+ are defined paths (Fig 3.2) and V, V_ϵ are volumes.

The value of $\hat{J}$ is independent of the choice of the path only under ideal conditions such as steady state crack growth. In many cases though these conditions are not met, the path independence of the $\hat{J}$ integral can still be established within an allowable error. The path was held stationary as the crack tip is extended in a self similar manner.

3.2.3 Parameters in the Program

The choice of certain parameters will infleuence the outcome of the program. Such parameters in this problem are time step, mesh size, etc. The choice of time step (Δt) for time integration is important for an accurate solution. An optimum choice of time step is $\Delta t = d/c$, where d is the smallest mesh size and c is the fastest wave velocity. However it has been observed that the the value of $\hat{J}$ integral does not vary much with time before opening the crack. Therefore in the present study, a coarse time step of $0.2\mu s$ is selected prior to the growth of the crack and fine time step of 0.02 μs is used after the crack growth in initiated.

Mesh size

As discussed by Seron et al. (1990) higher order elements are not required in the analysis of dynamic problems. Thus four noded isoparametric elements are used in this work. To take into the consideration of bending as well, fine mesh is used. At the same time to avoid non uniformity of mass distribution which leads to reflection of waves, uniform mesh is used throughout the specimen. Figure 3.3 shows mesh generated in the present work.

3.3 Crack opening scheme

As the crack propagation velocity is lower than the wave velocity, the crack tip occupies positions in between the nodes at various time steps of the numerical integration. Thus if a simple node shifting procedure is used, then the crack tip either stay at one node or

jump from one node to the next node in time Δt in the computational simulation. When the crack tip movement is irregular spurious fluctuations are superposed on the value of $\hat{J}$ determined through simulation.

Thus to overcome this difficulty Verma (1995) adopted a technique where the nodes are released gradually. The holding force at any node is linearly reduced to zero as the crack reaches the end of the next element. If the actual crack tip is located at C in between the element nodes B and D as shown in Fig 3.4. The holding back force F at node B is gradually reduced to zero as the crack tip reaches the node E. When the crack tip is in between nodes B and D, the holding force is given by,

$$\frac{F_B}{F_{BC}} = [\, 1 - \frac{b_1}{2\,d}\,] \tag{3.5}$$

where F_{BC} is the force at node B when the node was not opened and the crack tip was located at point B, b_1 is the crack extension beyond node B and d is the element length as shown in Fig. 3.4. When crack propagates beyond the node D to a point D_1

$$\frac{F_B}{F_{BC}} = [\, 1 - \frac{d + b_2}{2\,d}\,] \tag{3.6}$$

3.4 Initiation and Propagation toughness

Initiation fracture toughness is the fracture resistance of the material under dynamic loading conditions for a specific crack length and specified boundary conditions. Initiation fracture toughness represents the toughness of the material just before the initiation of crack. Figure 3.5 shows the variation of $\hat{J}$ integral with time for the stationary crack.

At the initiation time, determined experimentally, the crack opening scheme is is invoked (Eqs. 3.5,3.6) in the numerical simulation. Figure 3.6 shows rise of $\hat{J}$ for stationary crack upto the initiation time and $hatJ$ for the propagating crack. The toughness at the initiation time is called the initiation toughness (J_{ini}). As shown in Fig 3.6, once the

crack is initiated, $\hat{J}$ drops suddenly to lower values and after some time it stabilizes. This stabilized value of the $\hat{J}$ integral is treated as the propagation toughness ($\hat{J}_{prop}$). The results are discussed in detail in Chapter 4.

3.5 Summary of the program

Figure 3.7 shows the flow chart of the program developed by Verma(1995). The input for the program is end deflection of the cantilever $u(t)$, determined experimentally. At the initiation time, crack length as function of time is provided to the computer simulation and crack initiation through node release is invoked.

3.6 Closure

The aim of this chapter was to describe the finite element formulation, the path independent integral, the crack opening scheme, the initiation and propagation toughness, and the summary of the program.

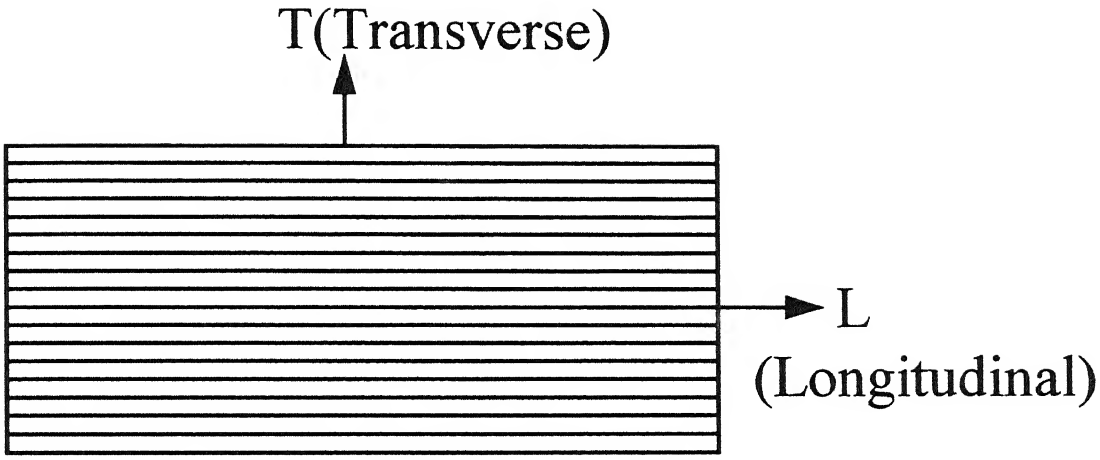

Figure 3.1: Principal directions of composite material

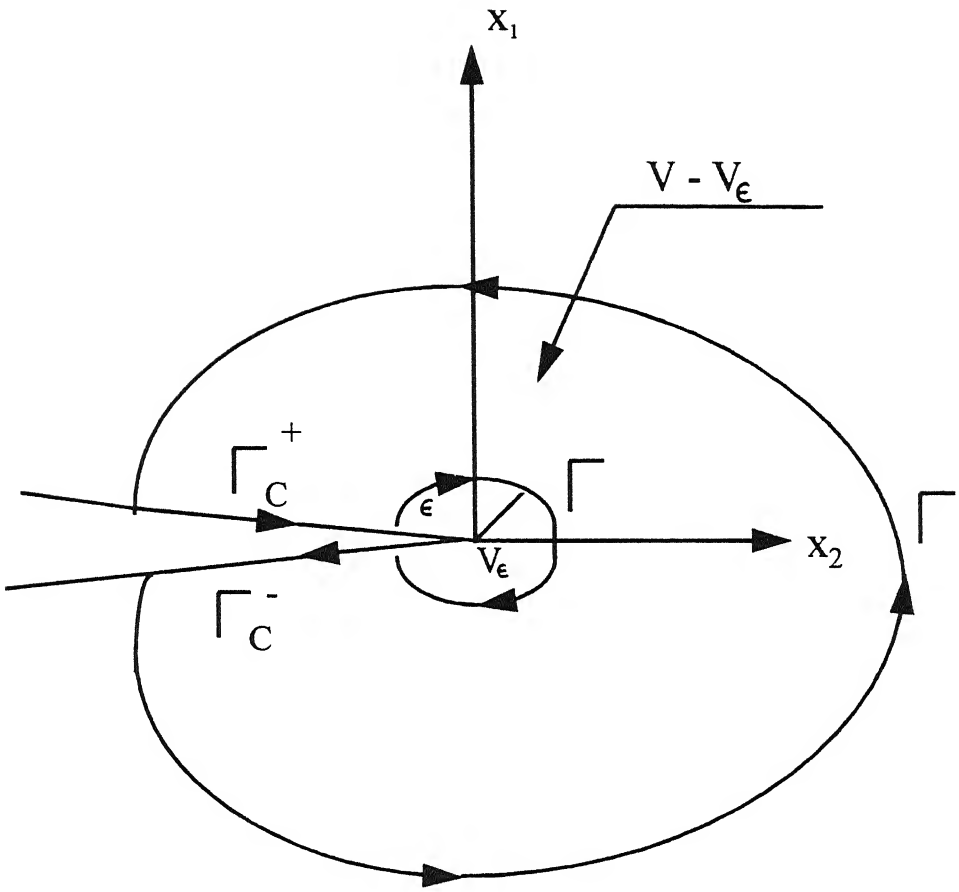

Figure 3.2: Contour for $\hat{J}$-integral

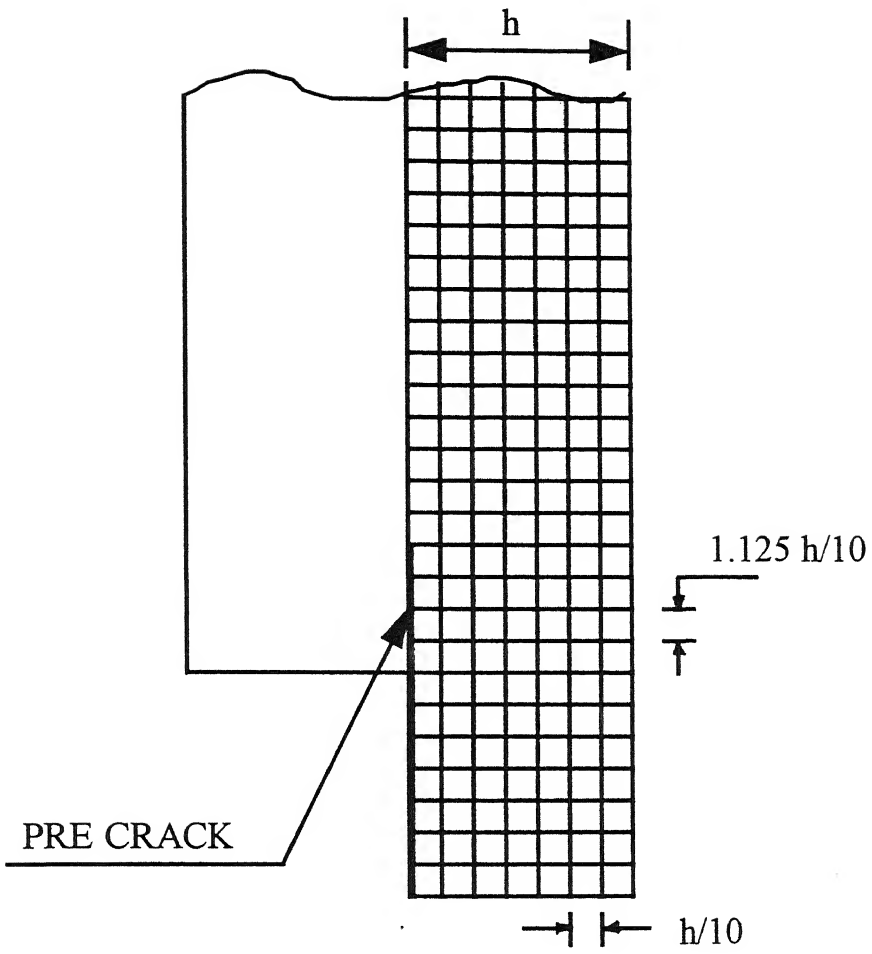

Figure 3.3: Mesh generated for the simulation

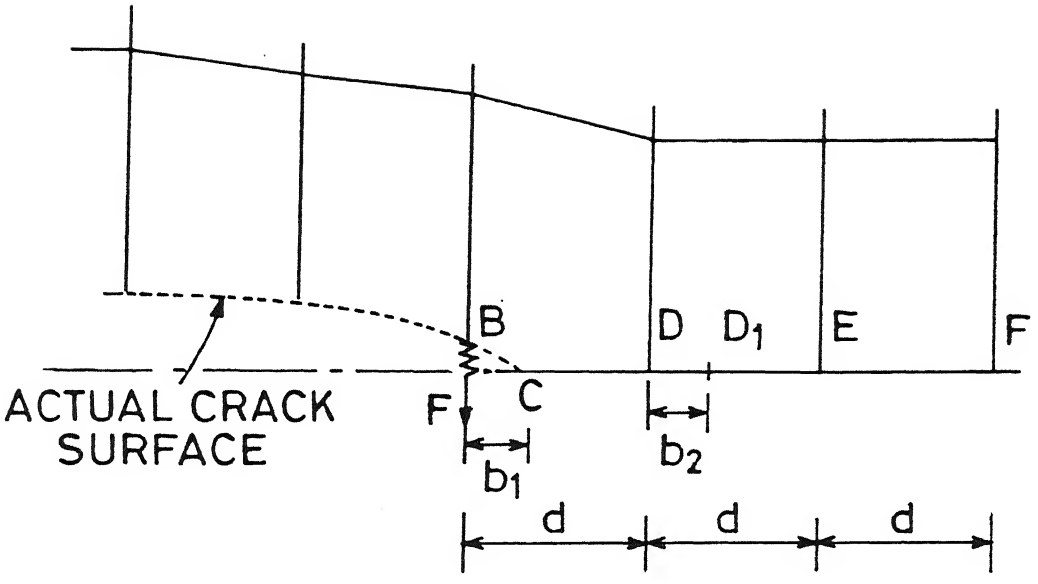

Figure 3.4: Crack opening scheme

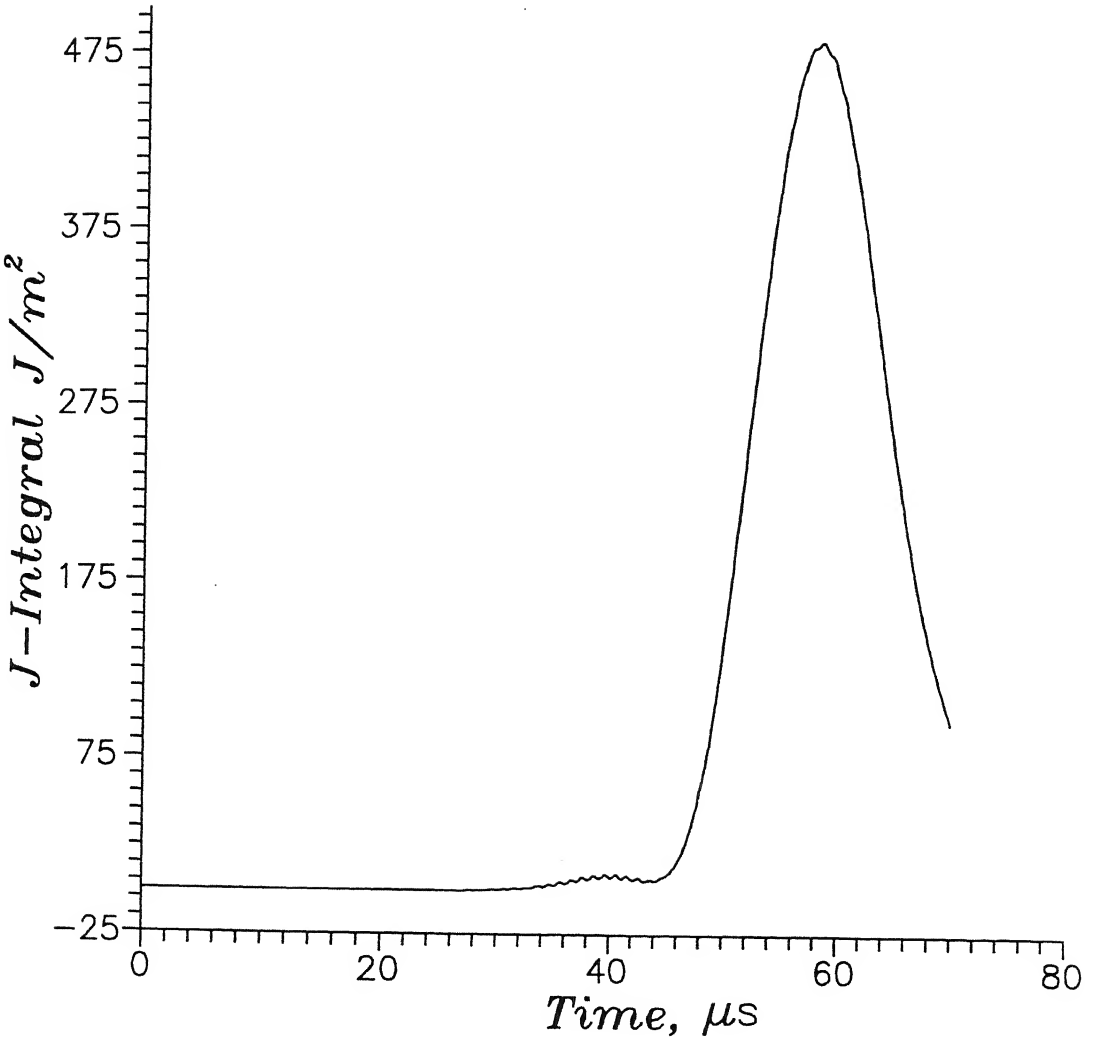

Figure 3.5: Variation of $\hat{J}$ for stationary crack (Expt.1)

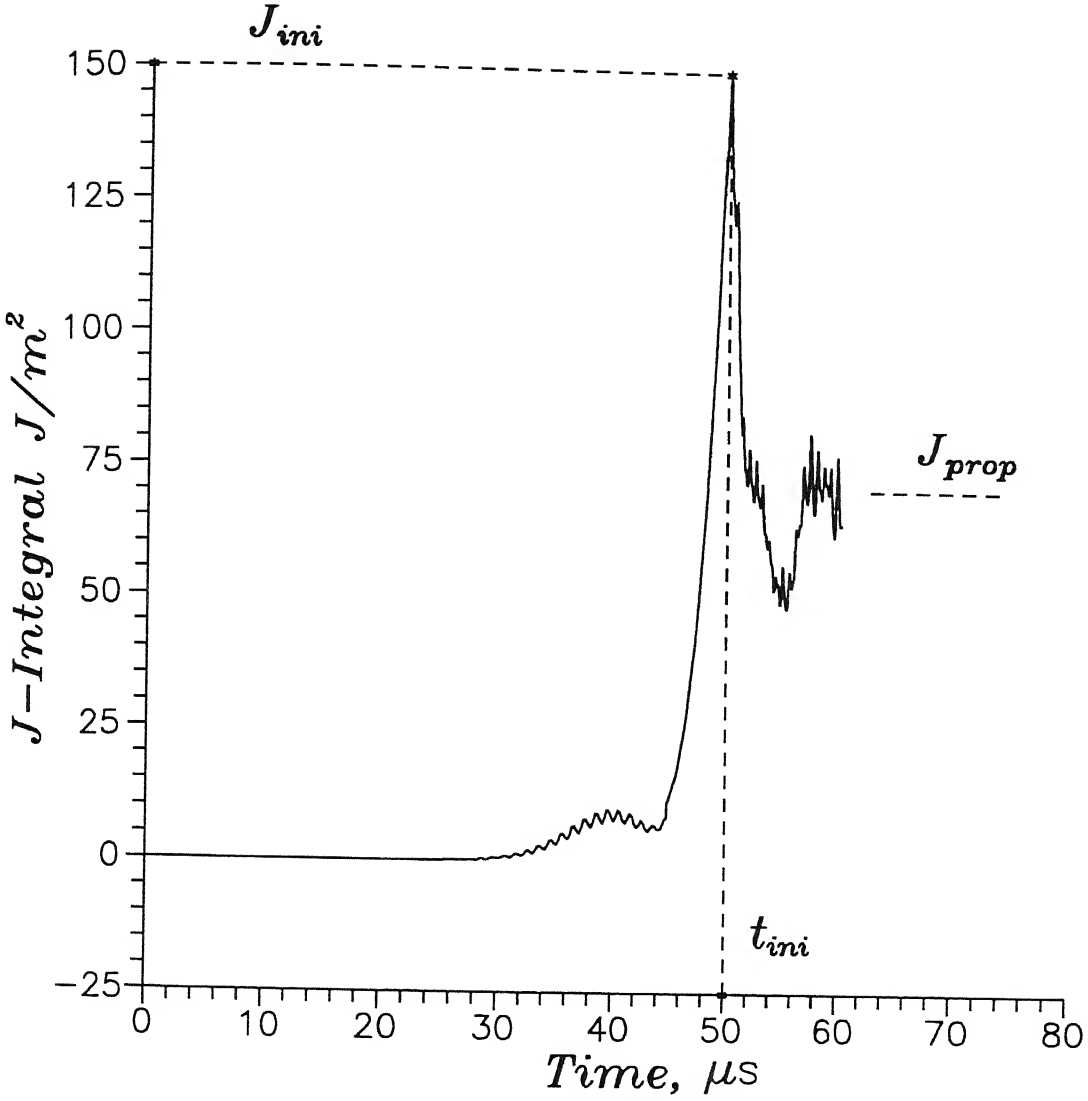

Figure 3.6: Variation of $\hat{J}$ for propagating crack (Expt.1)

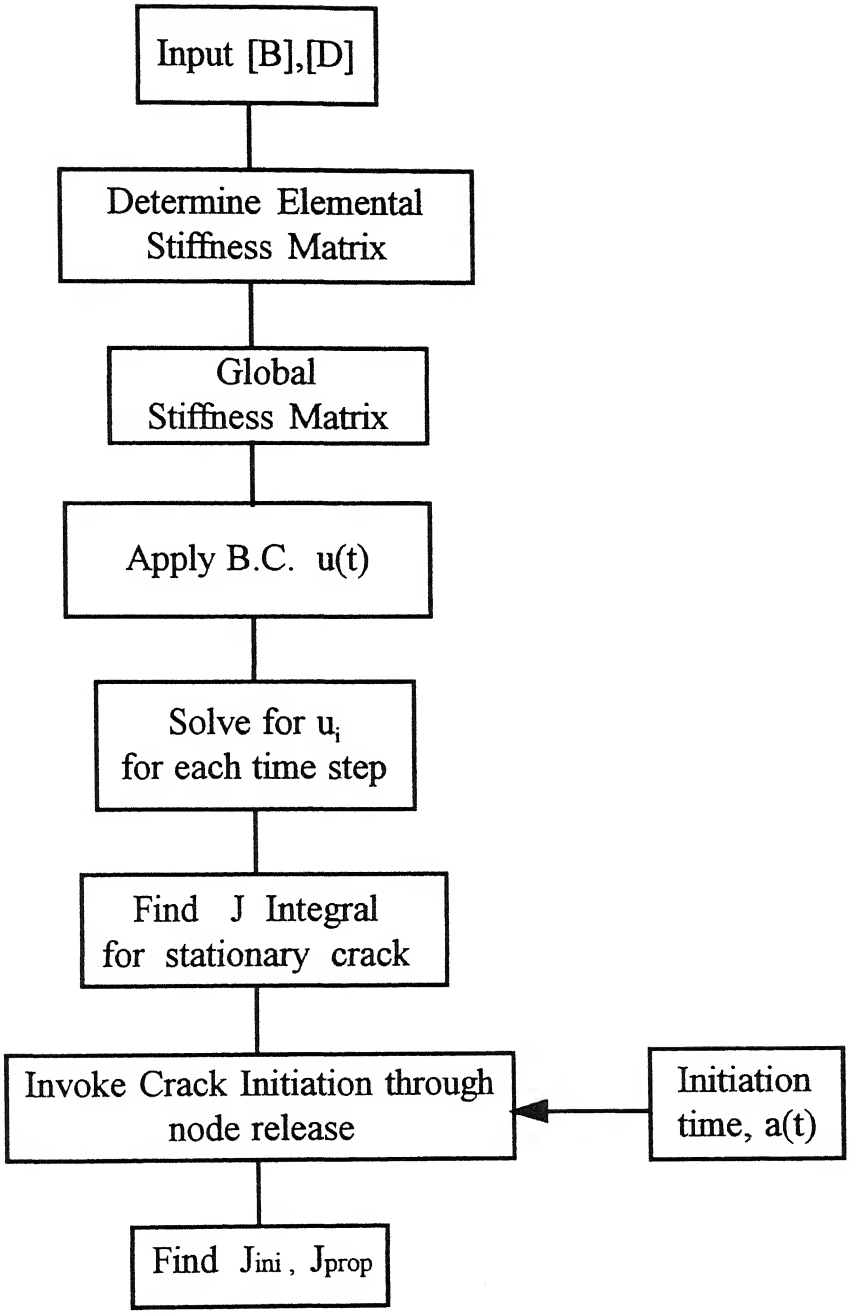

Figure 3.7: Flow chart of the FE code

Chapter 4

Results and Discussion

4.1 Introduction

Experiments are conducted to determine the deflection of the cantilever end, crack velocity and initiation time. These are the inputs to the FE code developed by Verma (1995) along with the material properties. The output of the program is the variation of $\hat{J}$-integral with time in different conditions such as the stationary crack and the propagating crack. This chapter briefly describes the results of initiation toughness, propagation toughness and their comparison with the quasistatic interlaminar toughness and dynamic toughness determined by other investigators.

The precrack length , position of the strain gauges as measured with the travelling microscope are tabulated in Table 4.1.

4.2 Interlaminar Initiation Toughness

Interlaminar initiation toughness of the material is the toughness of the material when the crack is about to initiate. It is the fracture resistance of the material under dynamic loading conditions for a specific crack length and boundary conditions. This section describes the results of the initiation toughness. Experiment 1 is discussed in detail and results of other four experiments are briefly presented highlighting the points when ever necessary.

Table 4.1: Specimen thickness, width, precrack length and strain gauge locations for Expt. 1 to 5.

Expt. No.	Specimen Thickness (mm)	Specimen Width (mm)	Precrack Length (mm)	Strain gauge locations	
				SG1 (mm)	SG2 (mm)
1	3.60	25.5	41.4	43.8	46.4
2	3.20	25.1	39.3	41.6	43.9
3	4.10	25.9	40.1	41.9	44.6
4	4.10	25.8	40.3	42.3	45.1
5	4.04	25	39.6	41.8	44.5

Experiment 1

When specimen of 3.6 mm thickness, and precrack length of 41.4 mm is impacted by a load bar part of the energy is transmitted to the specimen causing the deflection of the cantilever and the remaining energy is reflected back as a tensile pulse. Strain gauges mounted on the load bar monitors the stress pulses and the strain gauges bonded ahead of the crack tip are used to monitor the crack propagation. The response of the load bar strain gauges and and the velocity strain gauges as recorded in the oscilloscope are as shown in Fig 4.1. Channel 1 gives the record of the incident and reflected pulses in the load bar. Channels 2 and 3 give the response of the first and second velocity strain gauges (SG1 and SG2) respectively. The velocity of the load bar end is calculated using the expression (Sec 2.3.5)

$$v_2(t) = \frac{\sigma_3 - \sigma_1}{\rho\, c}$$

where σ_1 is the compressive incident pulse and σ_3 is the tensile reflected pulse in the load bar; ρ, the density of the material and c, the longitudinal wave velocity. The variation of velocity with time is shown in Fig 4.2(a). The end displacement of the load bar is obtained from the following expression, which is obtained by integrating the load bar velocity with respect to time (Sec 2.3.5).

$$u_2(t) = \int_0^t v_2\ dt = \int_0^t \left(\frac{\sigma_3 - \sigma_1}{\rho\, c}\right)$$

Since the specimen is screwed to the load bar the end displacement of the load bar becomes the deflection of the cantilever end. The variation of deflection of the cantilever end with time is as shown in Fig 4.2(b). The loading of the cantilever starts at the time corresponding to mid point of the head of incident pulse and head of reflected pulse. This is denoted as "REFERENCE" in the Fig 4.1.

The response of the velocity strain gauges leads to the determination of crack velocity. When the crack tip passes near a strain gauge the singular strain field gives a strain peak that is recorded in the oscilloscope. Figure 4.3 shows the blown up view of the response of the velocity strain gauges. The crack velocity is determined from the time difference of the peaks of the strain gauges and the distance between the two strain gauges (Sec 2.3.6). The strain gauges are 2.6 mm apart and the difference in the peak response is 5.5 μs. Thus the velocity is found out to be 472 m/s. The initiation time is obtained by extrapolating the crack velocity up to the precrack length (Sec 2.3.7). Figure 4.4 shows the extrapolation to determine initiation time for Expt.1. The first strain gauges in this experiment is located at a distance of 2.4 mm from the precrack. Thus the initiation

time obtained is 50.02 μs.

These experimental data (the deflection of the cantilever end, crack velocity and initiation time) are used as input to the FE code as discussed in chapter 3. The variation of $\hat{J}$ integral in the stationary phase is as shown in the Fig 4.5. The value of $\hat{J}$ builds up and then drops down. The rise of the interlaminar toughness till the initiation is also obtained experimentally by John Lambros and Rosakis A.J (1997a). They investigated the variation of dynamic fracture toughness up to the initiation time on unidirectional graphite/epoxy composite plates with edge notch under impact loading (Fig 4.6). In the present study the experiment is controlled in such a way that the initiation occurs before the $\hat{J}$ reaches the peak value. J_{ini} in this experiment is found out to be 149 J/m^2 (Fig 4.5).

Experiments 2-5

Similar to the Expt 1 four more experiments were carried out to determine the initiation and propagation toughness. The strain gauge peaks, crack velocity initiation time and J_{ini} for various experiments are tabulated in Table 4.2.

Experiment 2 is carried out on a relatively thinner specimen ($3.2mm$) and with a precrack length of 39.3 mm. Figures 4.7-4.9 show the oscilloscope traces, variation of velocity of load bar with time, deflection of cantilever end with time, and the details of extrapolation for this experiment. The crack velocity is 657 m/s and the initiation time is 51.5 μs. Figure 4.10 show the variation of $\hat{J}$ integral with time. The initiation toughness (J_{ini}) is 154 J/m^2.

Experiment 3 is carried out at high crack velocity. The oscilloscope traces and the processed results are shown in Fig 4.11- 4.13. The crack velocity is 900 m/s and the

Table 4.2: Crack velocity, initiation time and J_{ini} for different experiments.

Expt. No.	Precrack Length (mm)	SG1 from Cracktip (mm)	Peak Response		Crack Velocity (m/s)	Initiation Time (μs)	J_{ini} (J/m^2)
			SG1 (μs)	SG2 (μs)			
1	41.4	2.4	54	59.5	472	50.02	149
2	39.3	2.3	55	58.5	657	51.50	154
3	40.1	1.8	52	55.0	900	50.00	357
4	40.3	2.0	51	54.0	933	48.86	322
5	39.6	2.2	55	58.0	900	52.42	141

initiation time is 50 μs. Figure 4.14 shows the variation of $\hat{J}$ with time. The initiation toughness, being 357 J/m^2 is highest among all experiments of this study.

Experiment 4 is very much similar to Expt.3. It is conducted at a velocity of 933 m/s. The initiation time is the lowest among all the experiments. It's value is 48.86 μs. Figures 4.15-4.17 shows the traces and processed data. The variation of $\hat{J}$ integral with time is shown in Fig 4.18. The initiation toughness is 322 J/m^2.

Experiment 5 is also carried out at high crack velocity. But unlike in the case of previous two experiments where the velocity is high and the initiation toughness is also high, the initiation toughness is only 141 J/m^2. Figures 4.19-4.21 shows the oscilloscope traces and processed data. The variation of $\hat{J}$ integral is shown in Fig 4.22.

4.3 Interlaminar Propagation toughness

For determining the interlaminar propagation toughness (J_{prop}) the input to the finite element code consists of the crack propagation history apart from the variation of cantilever end deflection with time. While executing the FE code the crack propagation algorithm is called after the initiation time. Similar to the procedure of the previous section, Expt.1 is discussed in detail and other results are presented briefly.

Experiment 1

As discussed by Verma(1995), once the FE code is executed upto the initiation time, the crack propagation module is called. The location of the crack tip in each iteration is known through the experiment; an appropriate factor is applied to the holding back force for modelling crack propagation (Eqs. 3.5,3.6). A time step of $0.02\mu s$ is chosen in the propagation phase. Using the boundary condition and the crack propagation data the dynamic FE analysis determines the stress/strain field in the specimen in successive time steps. Then the variation of $\hat{J}$ integral with time is obtained as shown in Fig 4.23. In the begining the crack remain stationary upto the initiation time and $\hat{J}$ integral increases. At the initiation time the crack tip starts growing under the known dynamic displacement boundary conditions. Figure 4.24 shows the blown up view of the variation of $\hat{J}$ integral in the crack propagation stage. The $\hat{J}$ integral stabilises after sometime and the stabilised value is treated as the propagation toughness (J_{prop}). The propagation toughness in this case is 70 J/m^2.

The oscillatory behaviour of $\hat{J}$ integral is due to several reasons (Verma (1995)). First and the foremost, the free surfaces of the specimen are very close to the crack tip and, in fact, the propagation time for some stress waves to emanate from the crack tip and to return to the crack tip are as small as 2 - 3μs. The superposition of these waves and their effect on $\hat{J}$ integral will provide ripples. Second, in the finite element modelling the crack

Table 4.3: Values of crack velocity and J_{prop} for different experiments

Expt.No	Crack velocity m/s	Propagation Toughness($\hat{J}_{prop}$) J/m^2
1	472	70
2	657	42
3	900	80
4	933	95
5	900	30

tip is moved from one point to another point in discrete steps by linearly decreasing the holding back force. Thus the FE code may not be simulating the crack propagation behaviour very accurately. The nodal release mechanism can further be modified to smoothly release the crack to rule out its effect on the oscillatory nature of J_{prop}.

Experiments 2-5

Variation of $\hat{J}$ integral with time for the propagating crack for Expt.2 is shown in Fig 4.25. Figure 4.26 shows the blown up view of the $\hat{J}$ variation in the propagation phase. J_{prop} for this experiment is $42 J/m^2$. Table 4.3 gives the values of the J_{prop} for different experiments.

In experiment 3, where the crack velocity and the initiation toughness are high, the propagation toughness is also high. Figure 4.27 shows the variation of $\hat{J}$ of the dynamic crack. The blown up view of the variation of $\hat{J}$ in propagation phase is shown in Fig 4.28.

The response of Expt.4 is similar to Expt.3. The value of J_{prop} here is 95 J/m^2, the highest among all the values. The variation of $\hat{J}$ and its blown up views are shown in Figures 4.29, 4.30 respectively.

Figure 4.31 shows the variation of $\hat{J}$ for Expt.5. The blownup view of the same is shown in Fig 4.32. Even though the velocity is high in this case, the value of J_{prop} is lowest among all the values ($30J/m^2$).

4.4 Comparison of Dynamic interlaminar toughness with quasistatic interlaminar toughness

To compare the dynamic interlaminar toughness with quasi static interlaminar toughness experiments are conducted to determine the quasistatic interlaminar toughness (G_{Ic}) through a standard test (Guedra.D et. al (1987)). The tests involves pulling a DCB specimen in displacement control mode. Load is applied till the crack extends by a small distance (5-10 mm). Then the machine is stopped till the crack becomes stationary and then the specimen is unloaded. The specimen, now with a longer crack length, is loaded again. The compliance of the specimen is determined through the loading curve. The specimen is subjected to several loading-unloading cycles so as to determine the compliance and critical load for several crack lengths. With proper data reduction scheme (Guedra.D et. al (1987)), the critical energy release rate is evaluated. Values of G_{Ic} obtained from the experiments are tabulated in Table 4.4.

It is clear from the Tables 4.2, 4.3, 4.4 that the quasistatic interlaminar toughness is significantly higher than the dynamic interlaminar toughness. Thus it is important to characterize the interlaminar fracture toughness in dynamic conditions.

Table 4.4: Experimentally obtained values of G_{Ic}

Expt.No	Quasistatic interlaminar Toughness (G_{Ic}) J/m^2	Average value
1	1304	
2	1020	1059
3	790	
4	1124	

4.5 Comparison of Results

In this section the values of initiation toughness and propagation toughness are compared with those of Verma (1995), Ramakrishna(1997) and Babu(1998).

The variation of J_{ini} and J_{prop} for the present study is shown in Fig. 4.33. The quasistatic toughness is much higher than the dynamic interlaminar toughness and also initiation toughness is substantially higher than the propagation toughness.

Figure 4.34 shows the variation of initiation and propagation toughness as obtained by Verma (1995) on a specimen made of two steel strips bonded together with epoxy. It is worth noting that J_{prop} decreases with increasing velocity of interlaminar crack. Also it is interesting to observe that unlike the present study, the quasistatic toughness is significantly lower than the initiation and propagation toughness. It may be due to the weak adhesion between epoxy and steel surface. In the present study the resin which binds the plies together is same as the resin of the bulk material, thus heterogeneity is of much smaller degree. Thus micromechanisms of failure are different in nature and

crack growth in steel/epoxy specimen has a threshold level that is much higher than the quasistatic toughness. However, even in steel specimen J_{prop} is substantially lower than the quasistatic toughness.

The variation of $\hat{J}$ with crack velocity as obtained by Ramakrishna (1997) is shown in Fig. 4.35. In his work GFRP laminates used were not as superior as the one used in the present study. The quasistatic toughness (415 J/m^2) is higher than the initiation and propagation toughness. However each of these value is lower than those of the present study.

The results obtained by Babu(1998) are as shown in Fig 4.36. The initiation toughness was 245-600 J/m^2 and the propagation toughness was 45-83 J/m^2. These values are very much comparable to those of the present study, where the initiation toughness is 140-360 J/m^2 and the propagation toughness is 30-95 J/m^2. Figure 4.37 shows the comparison of J_{ini} for the present work with that of Babu's work and Fig 4.38 shows the comparison of J_{prop} for same. The low value of the initiation toughness in the present study may be due to the high crack velocity.

4.6 Closure

The aim of this chapter was to find the initiation toughness and propagation toughness of interlaminar cracks in GFRP laminates. The experimental measurements such as the end deflection of the cantilever, crack velocity and the initiation time are used as the input to the FE code to simulate the dynamic fracture behaviour of the GFRP laminate. The initiation toughness was found to be 140-350 J/m^2 and the propagation toughness is 30-95 J/m^2. To compare the results with the quasi static interlaminar toughness tests are conducted to find the same. It was found that the dynamic interlaminar toughness of the laminate is much smaller than the quasi static interlaminar toughness.

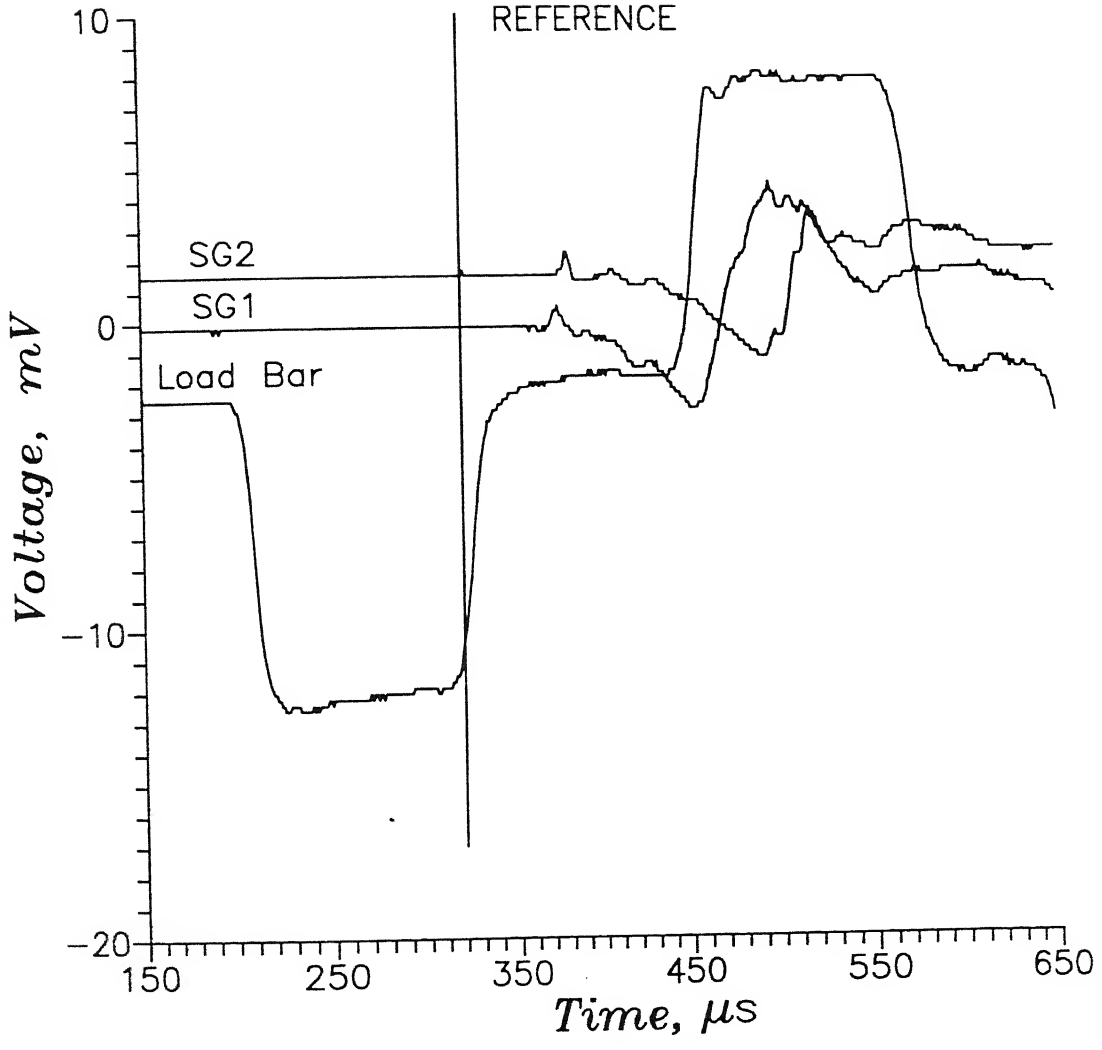

Figure 4.1: Oscilloscope Traces of Expt. 1

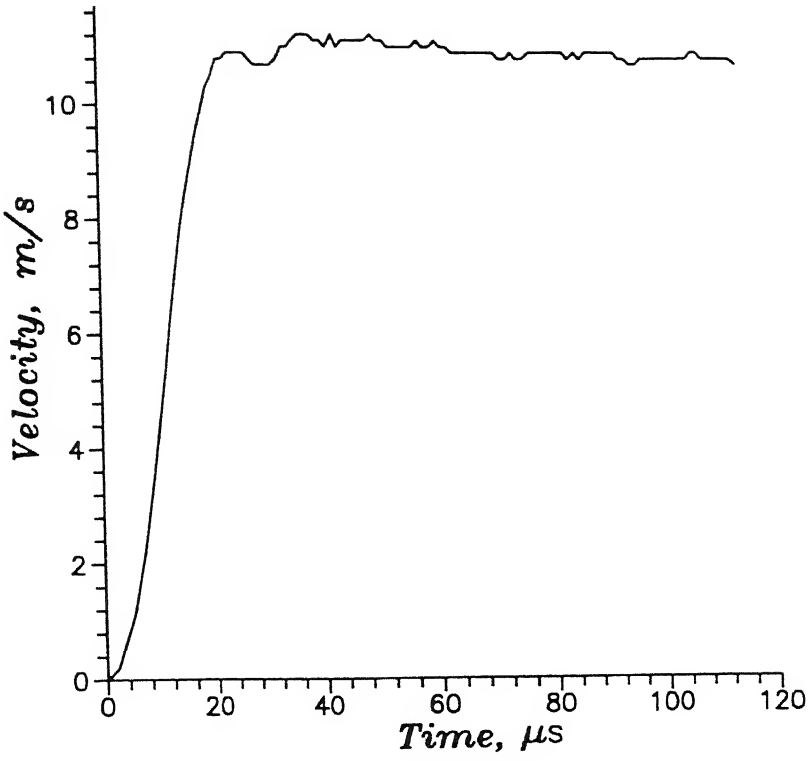

(a)

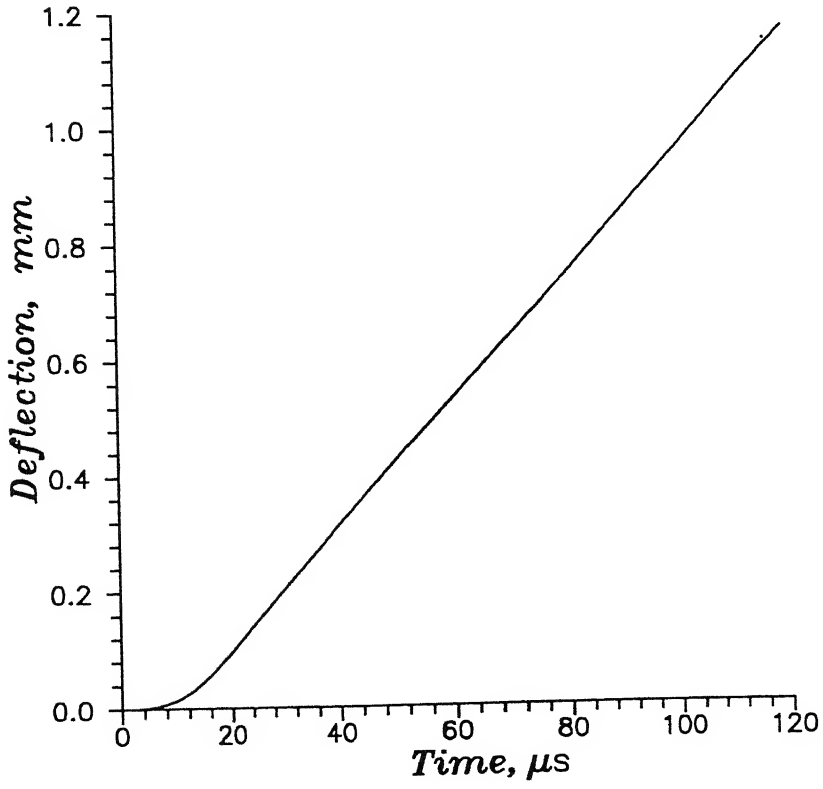

(b)

Figure 4.2: (a)Variation of velocity of load-bar-end with time for Expt. 1, and (b)deflection of cantilever end with time for Expt. 1

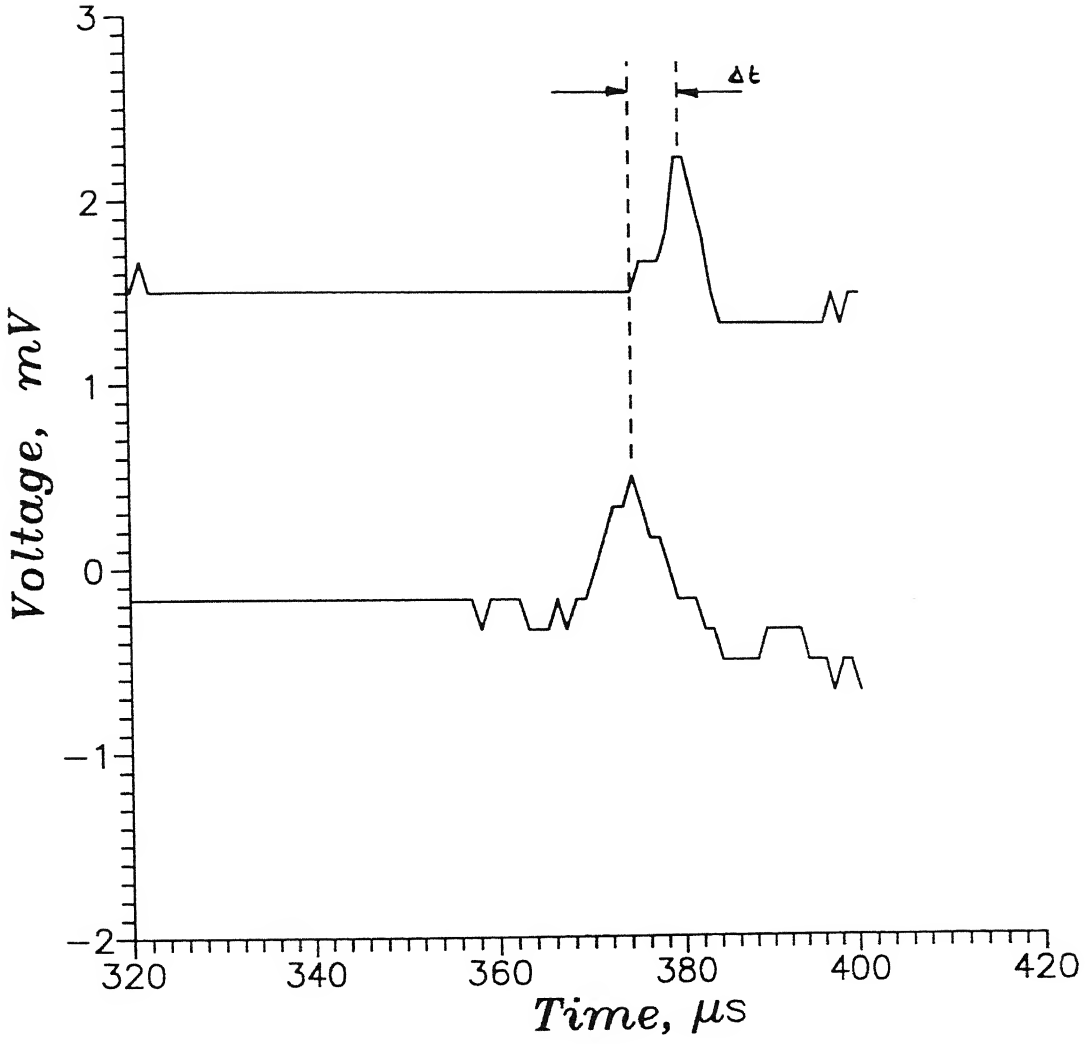

Figure 4.3: Blown up view of responses of Velocity strain gauges(Expt.1)

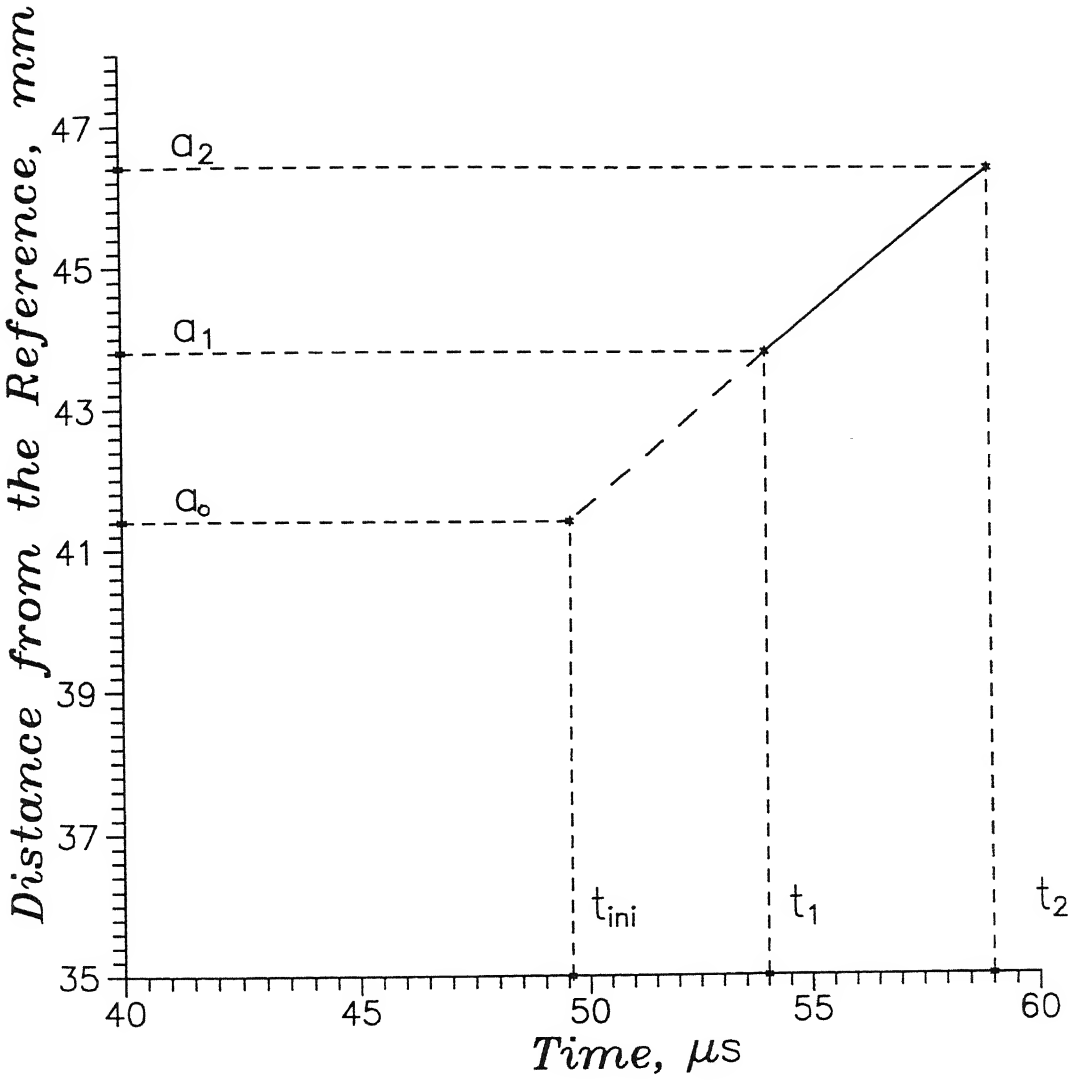

Figure 4.4: Details of extrapolation to find initiation time for Expt. 1

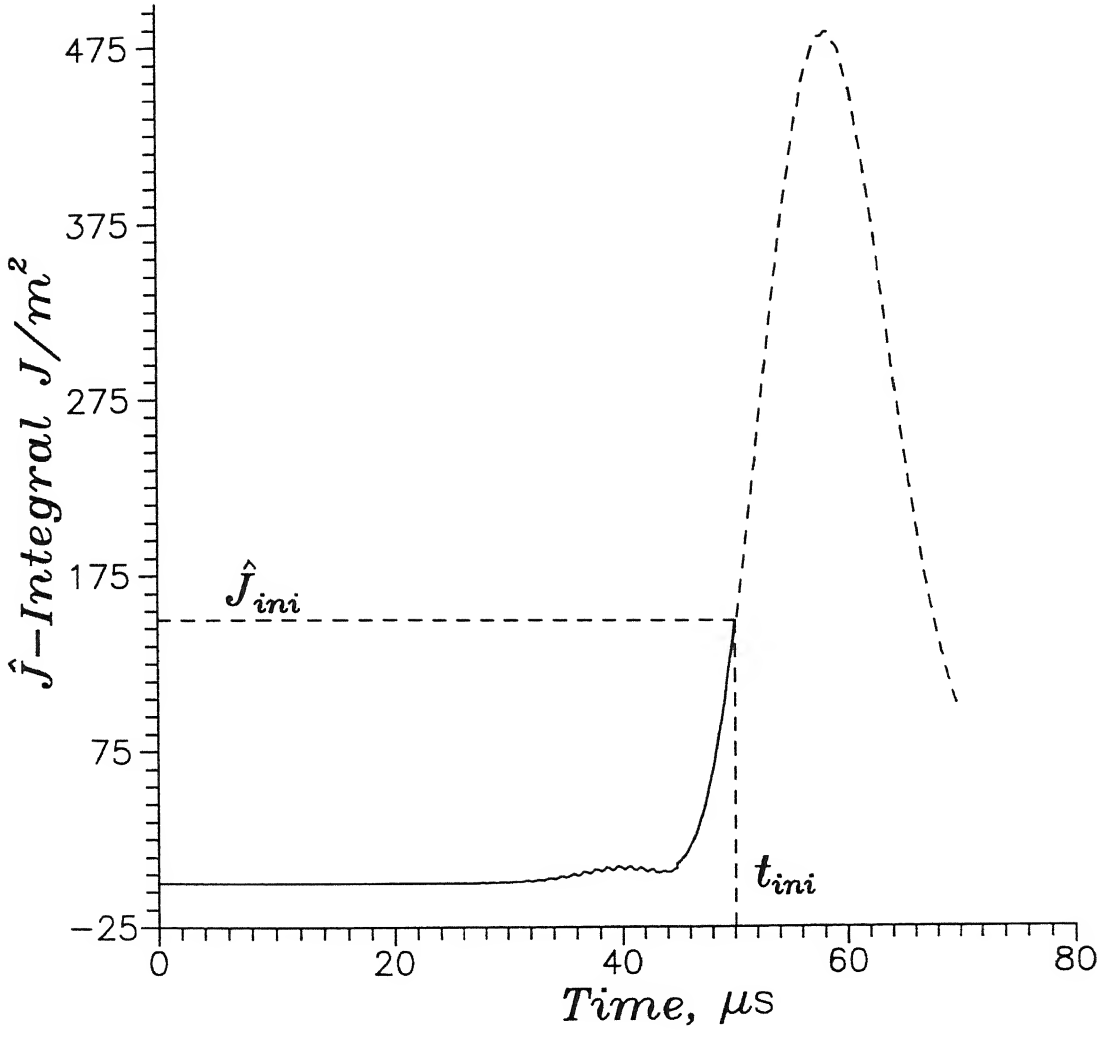

Figure 4.5: Variation of $\hat{J}$ for stationary crack for Expt. 1

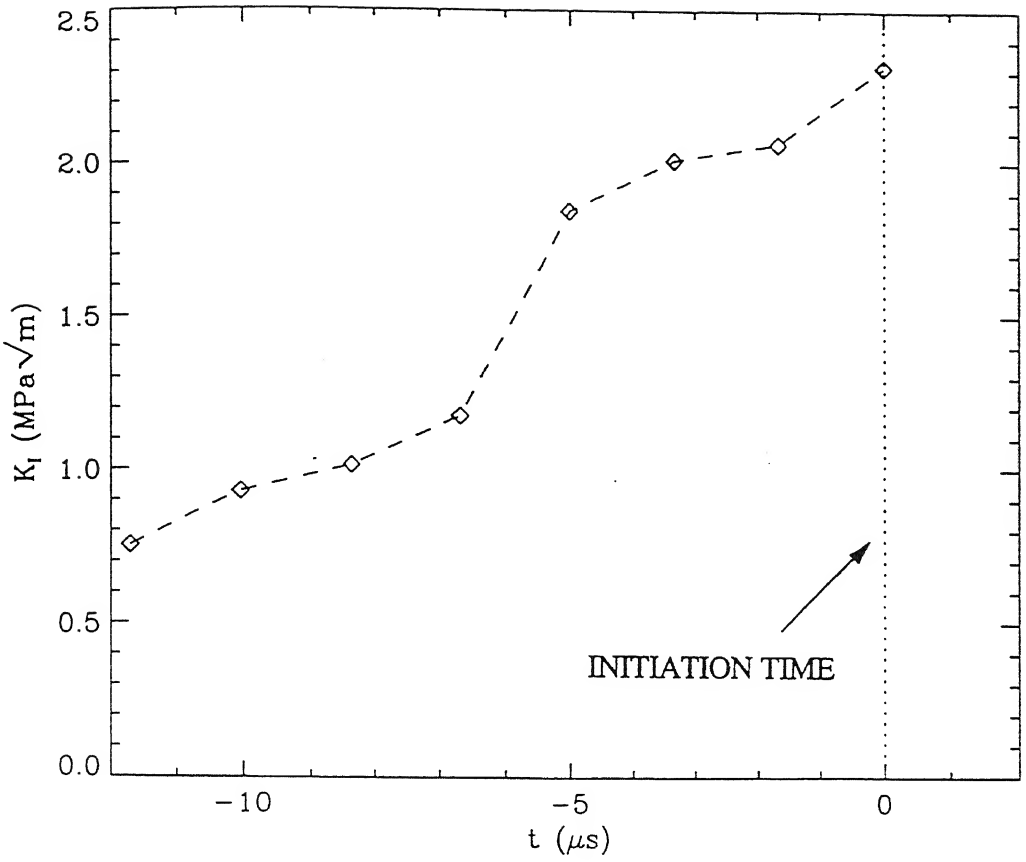

Figure 4.6: Dynamic fracture toughness variation upto initiation time [John L. and Rosakis A.J. (1997a)]

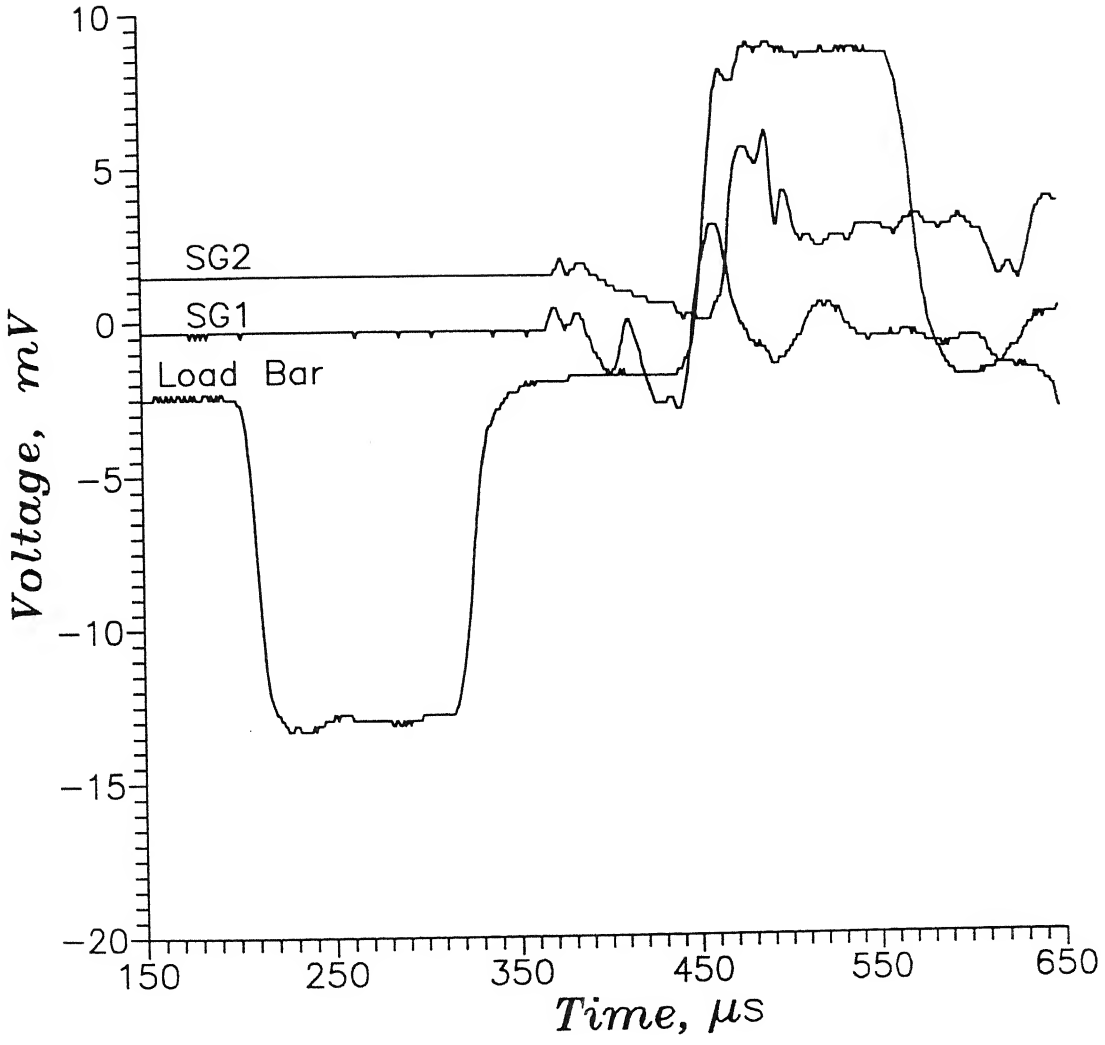

Figure 4.7: Oscilloscope Traces of Expt. 2

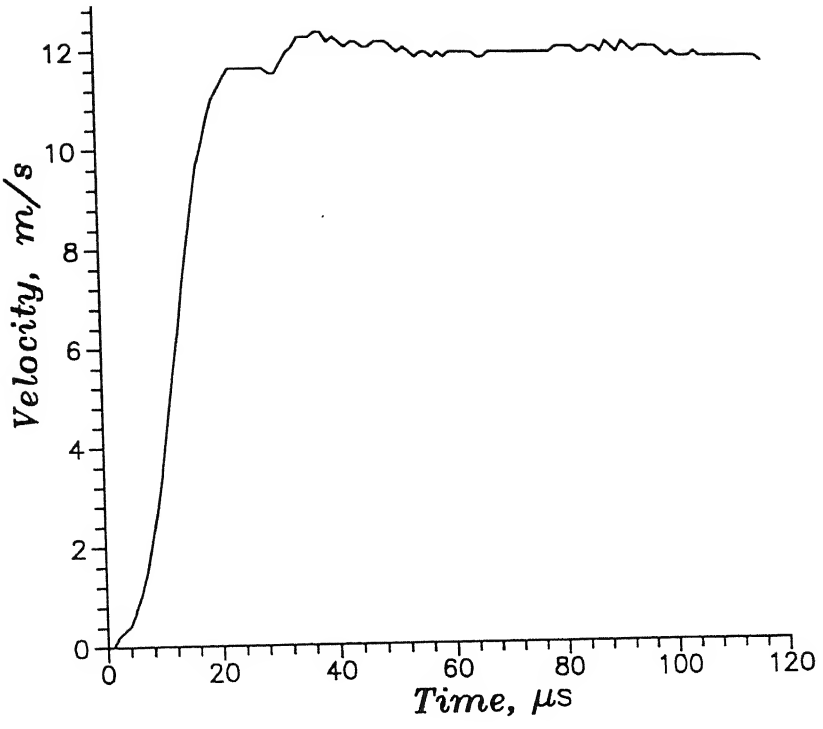

(a)

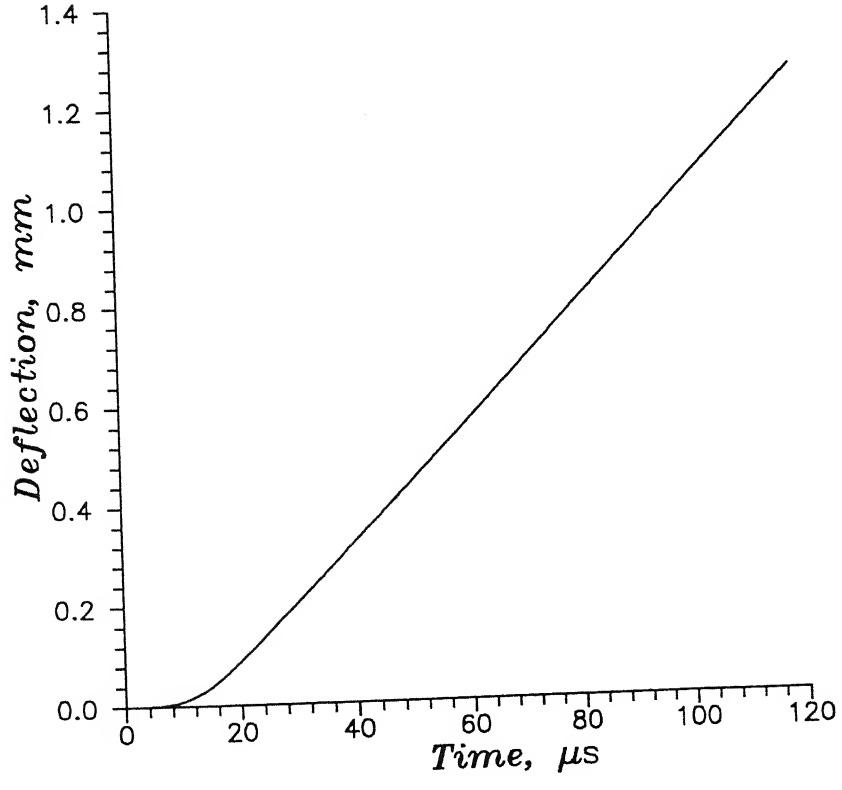

(b)

Figure 4.8: (a)Variation of velocity of load-bar-end with time for Expt. 2, and (b)deflection of cantilever end with time for Expt. 2

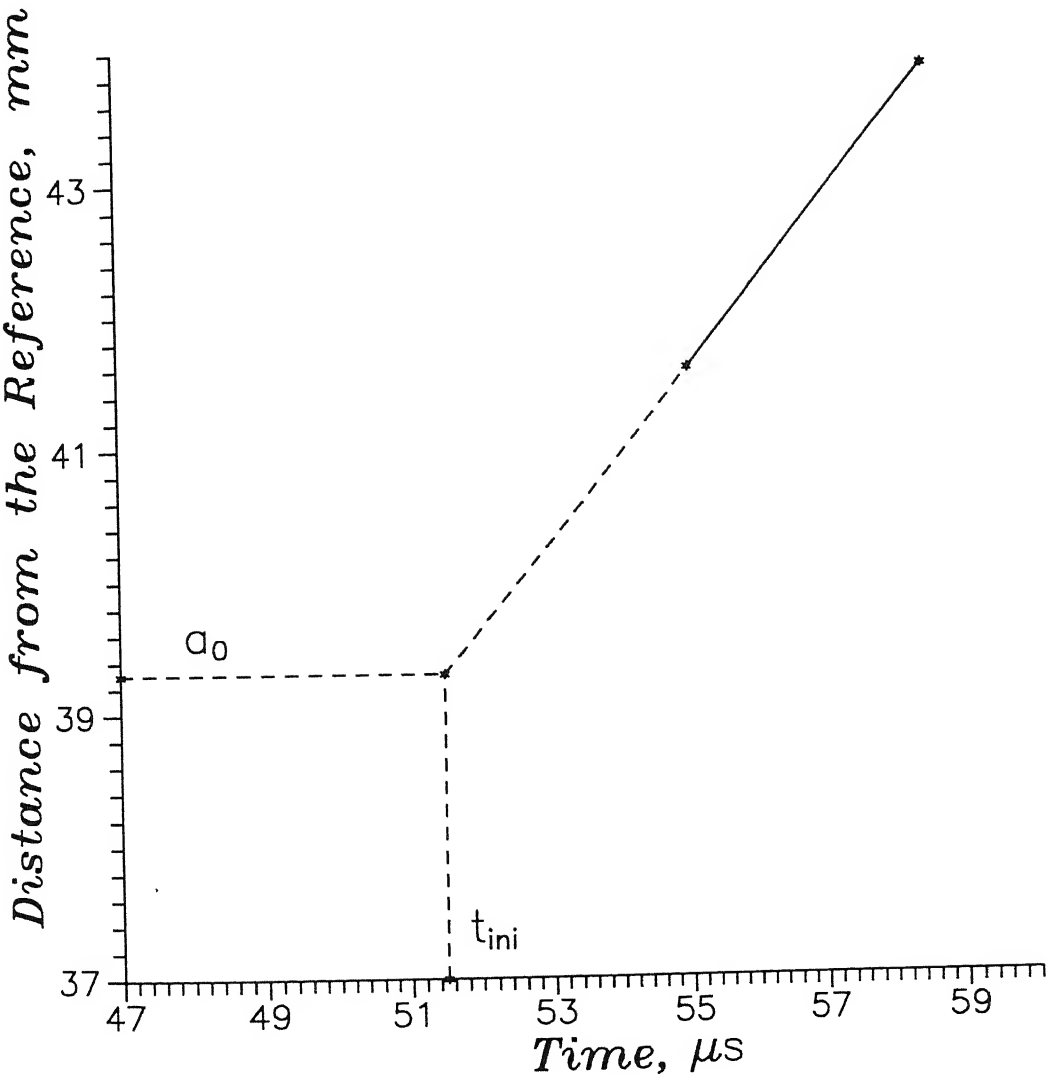

Figure 4.9: Details of extrapolation to find initiation time for Expt. 2

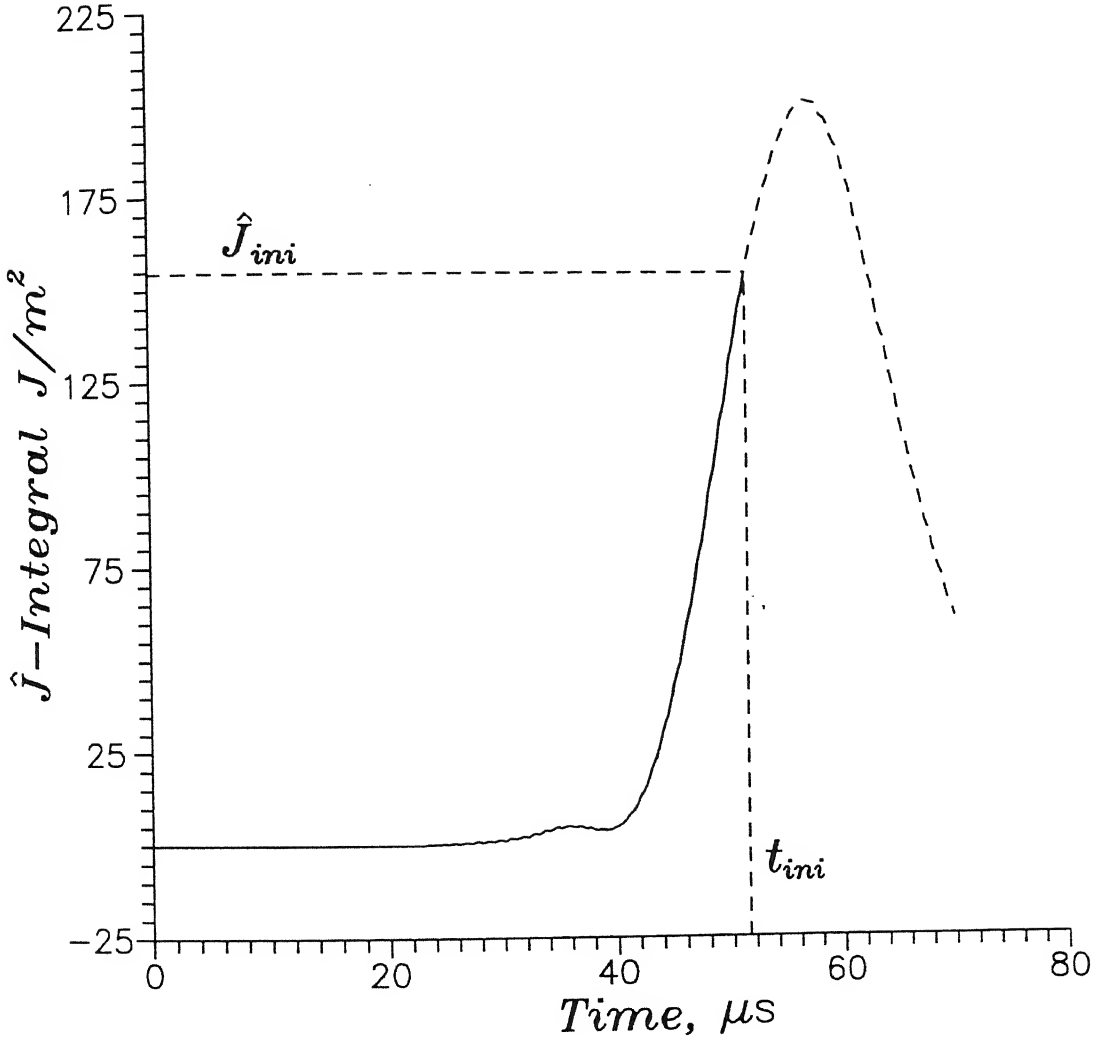

Figure 4.10: Variation of $\hat{J}$ for stationary crack for Expt. 2

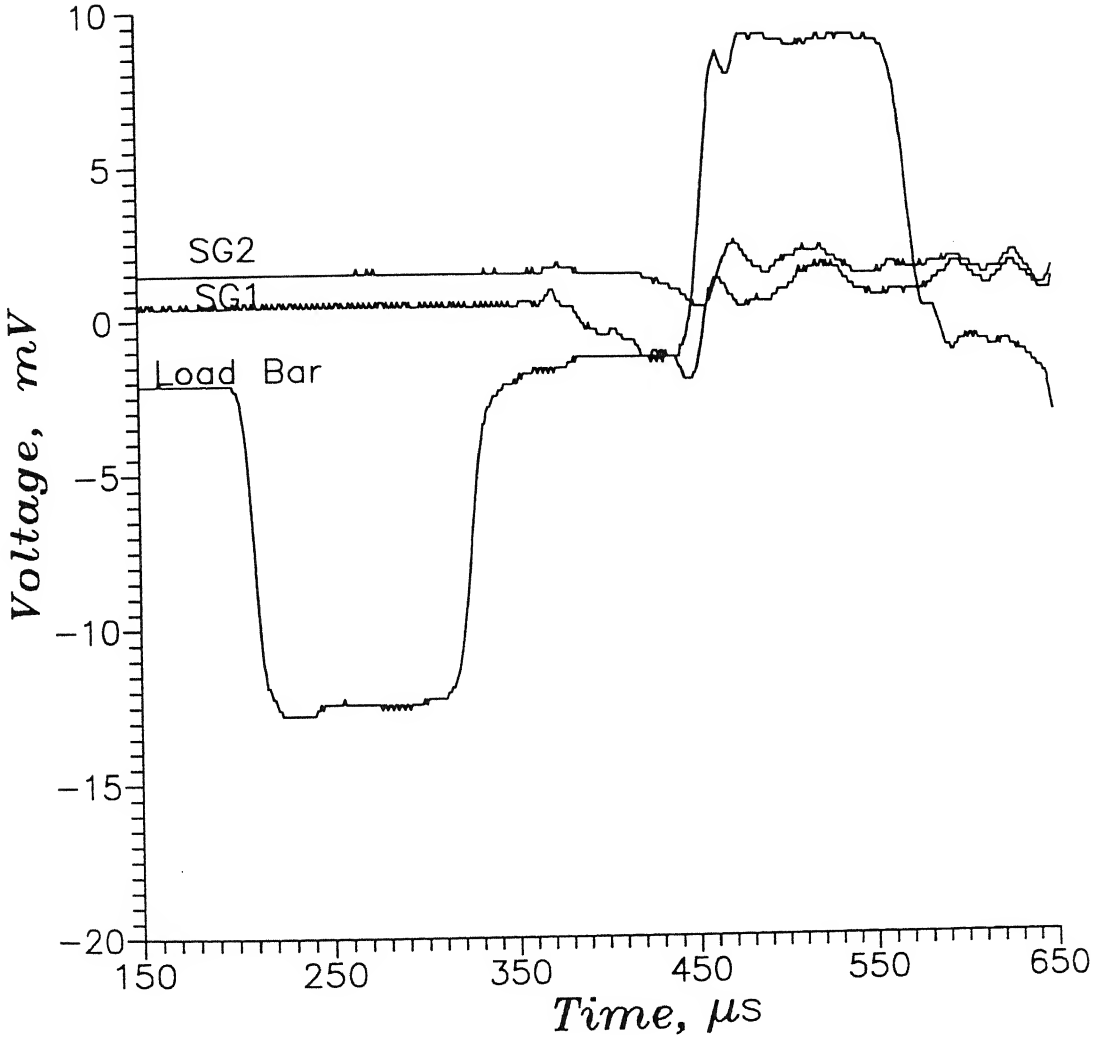

Figure 4.11: Oscilloscope Traces of Expt. 3

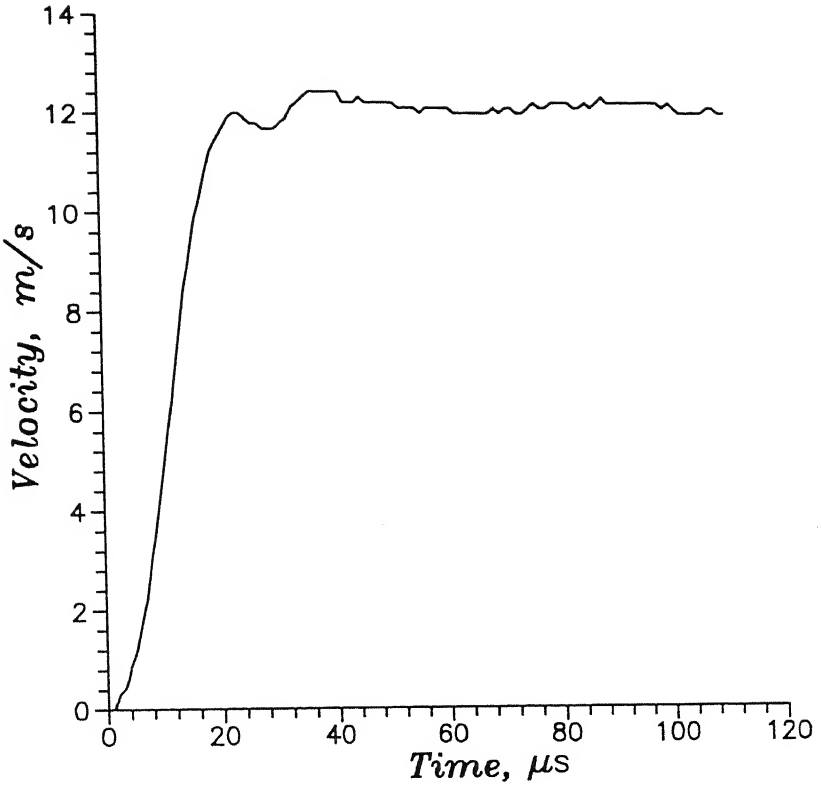

(a)

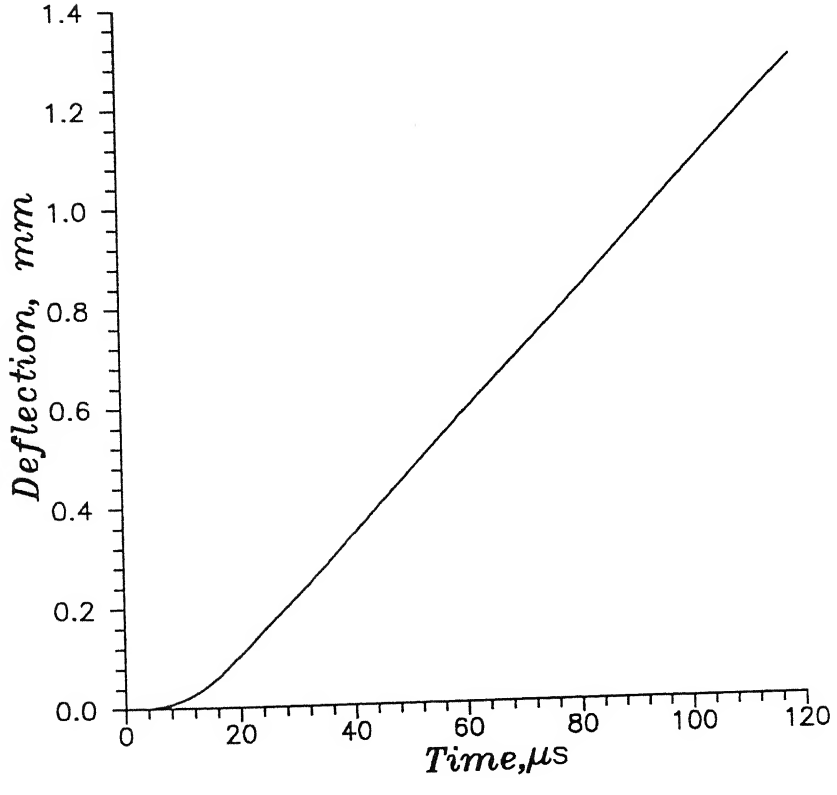

(b)

Figure 4.12: (a)Variation of velocity of load-bar-end with time for Expt. 3, and (b)deflection of cantilever end with time for Expt. 3

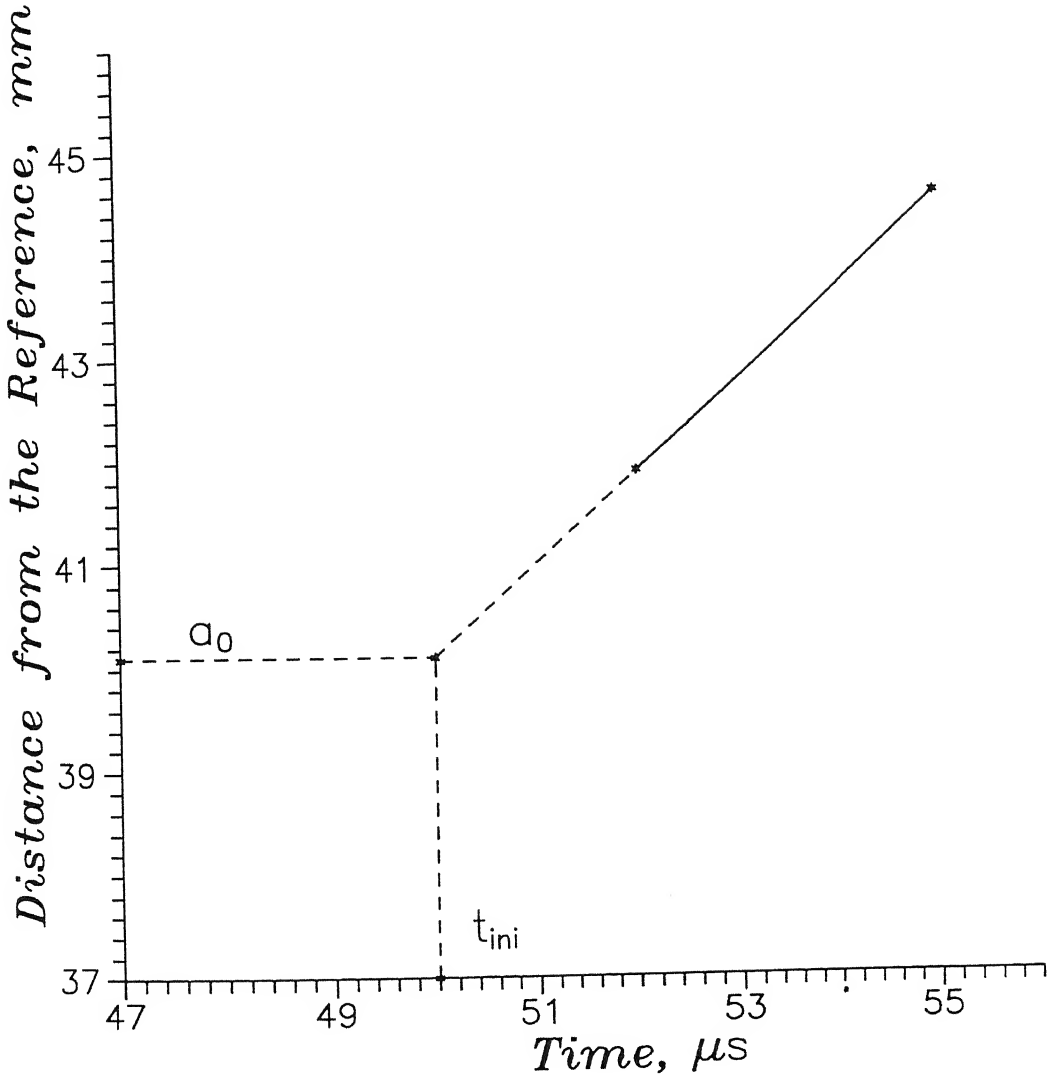

Figure 4.13: Details of extrapolation to find initiation time for Expt. 3

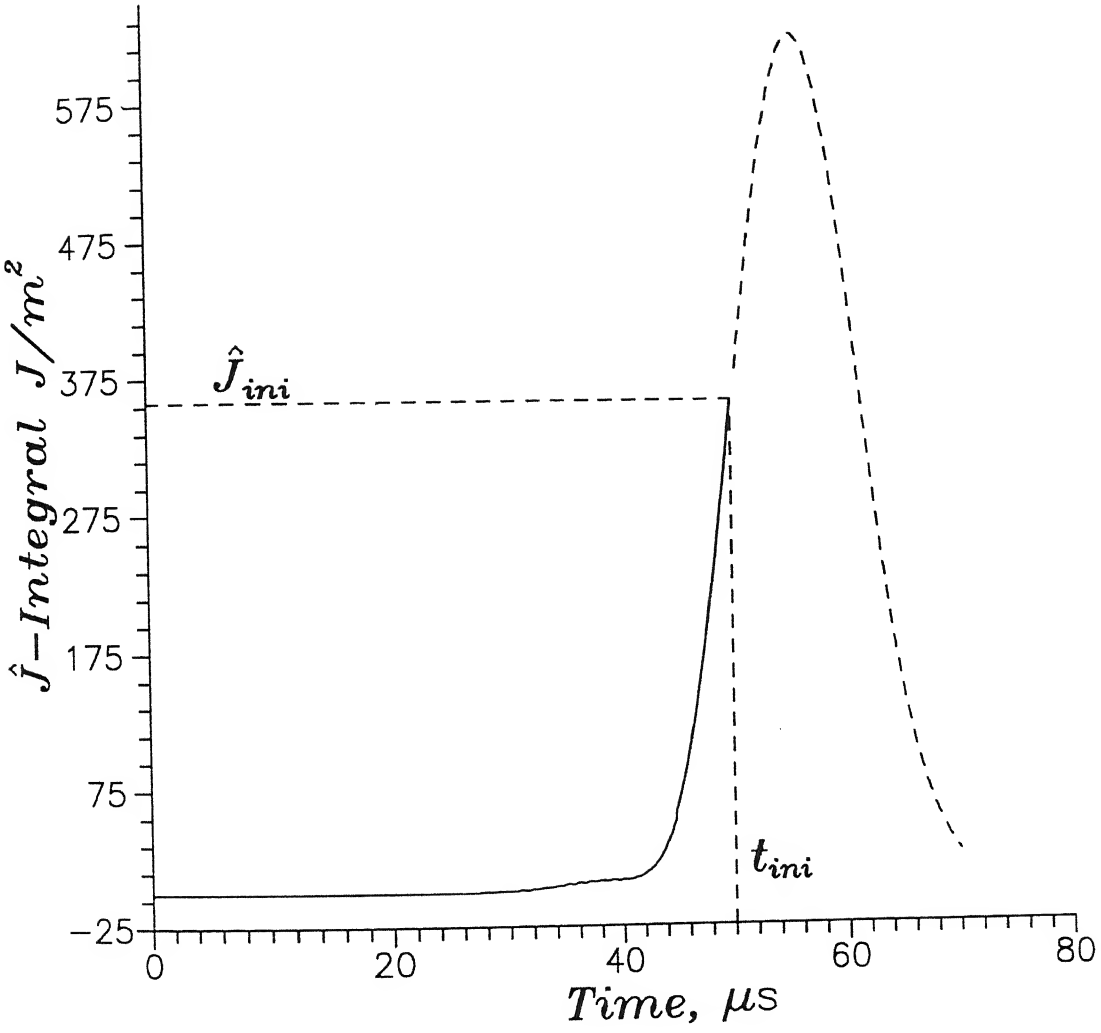

Figure 4.14: Variation of $\hat{J}$ for stationary crack for Expt. 3

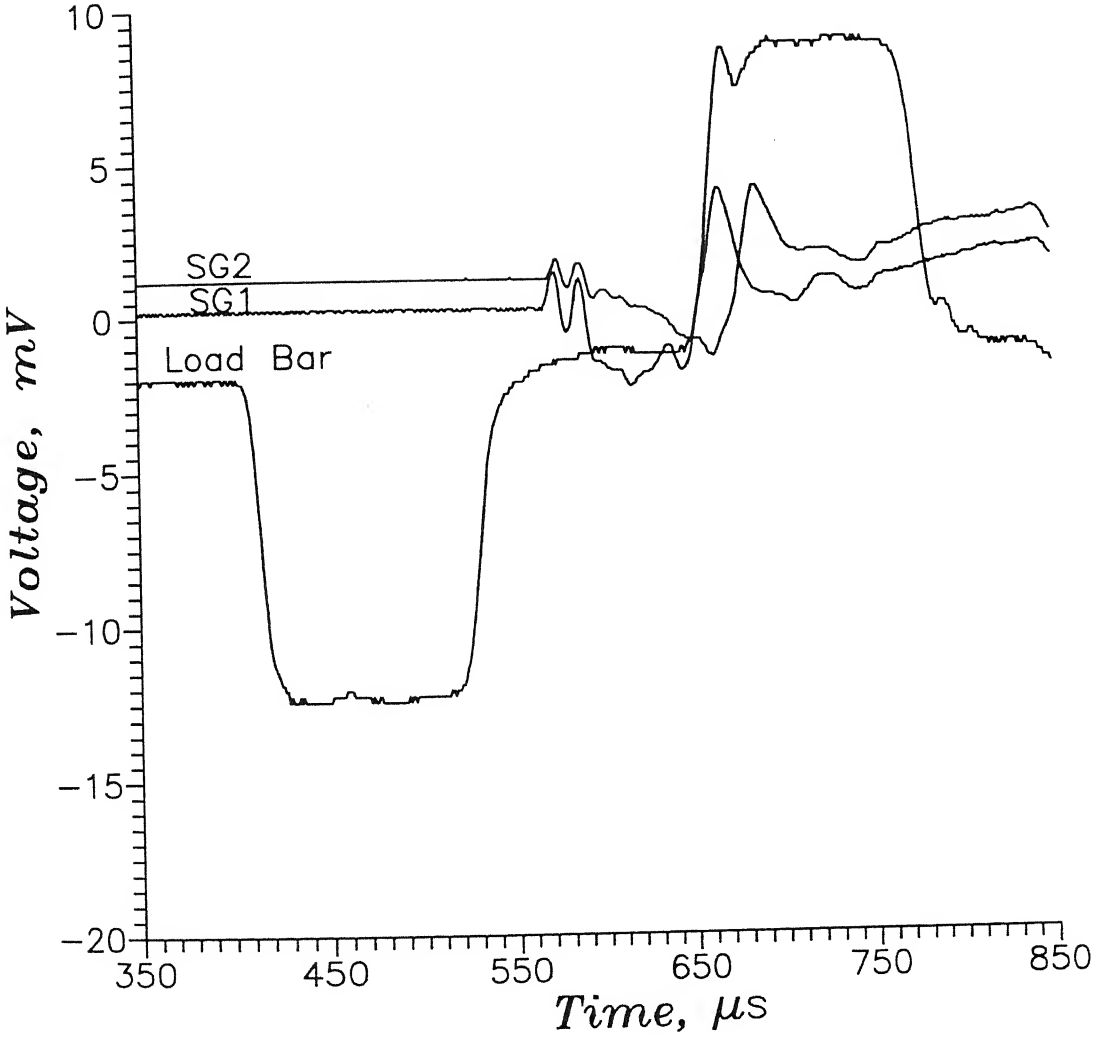

Figure 4.15: Oscilloscope Traces of Expt. 4

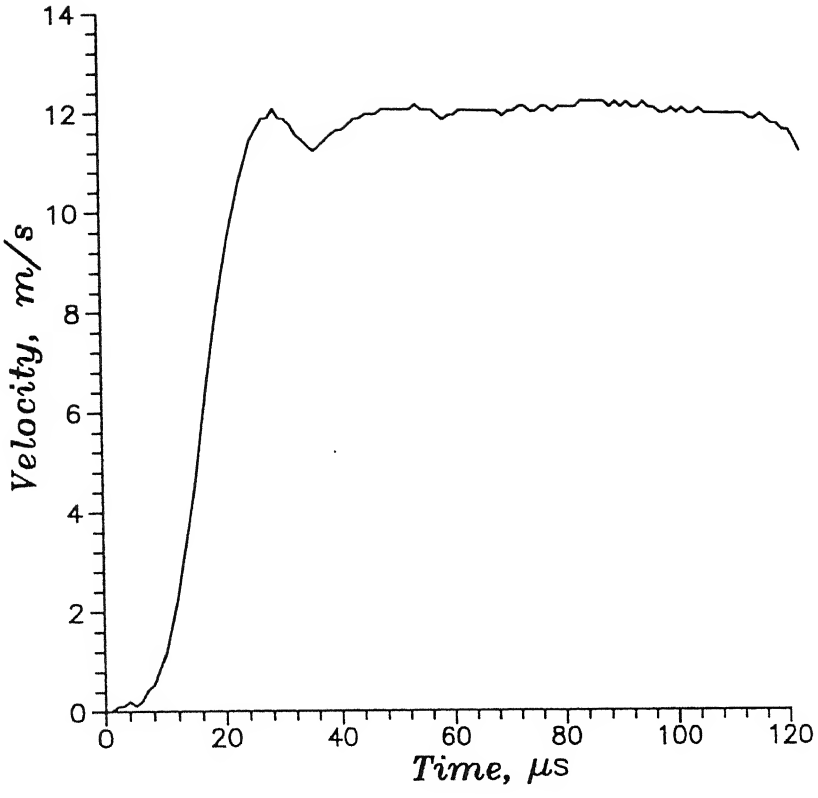

(a)

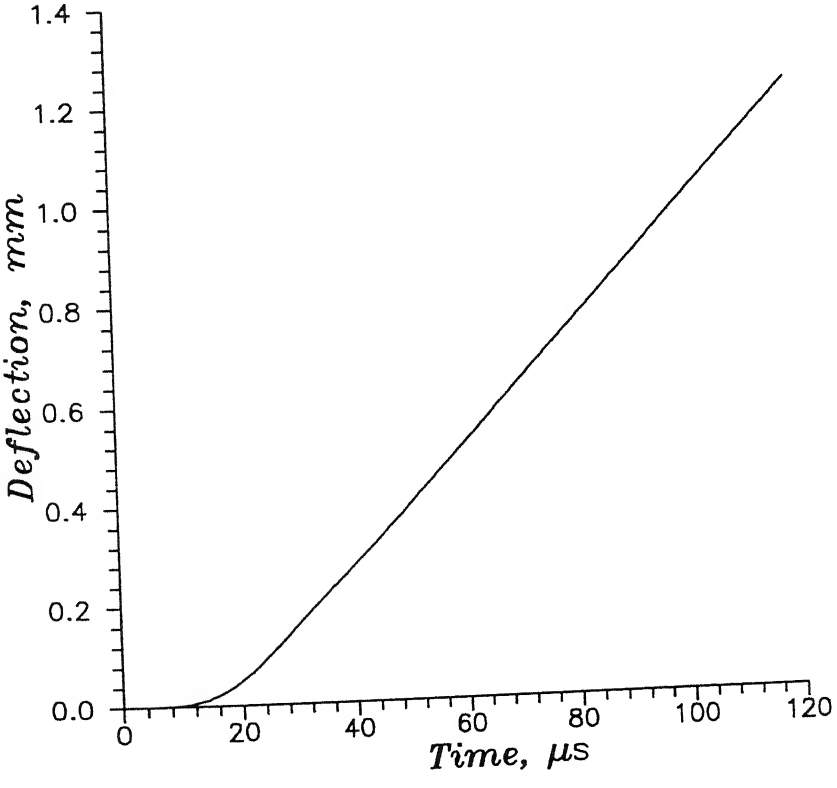

(b)

Figure 4.16: (a)Variation of velocity of load-bar-end with time for Expt. 4, and (b)deflection of cantilever end with time for Expt. 4

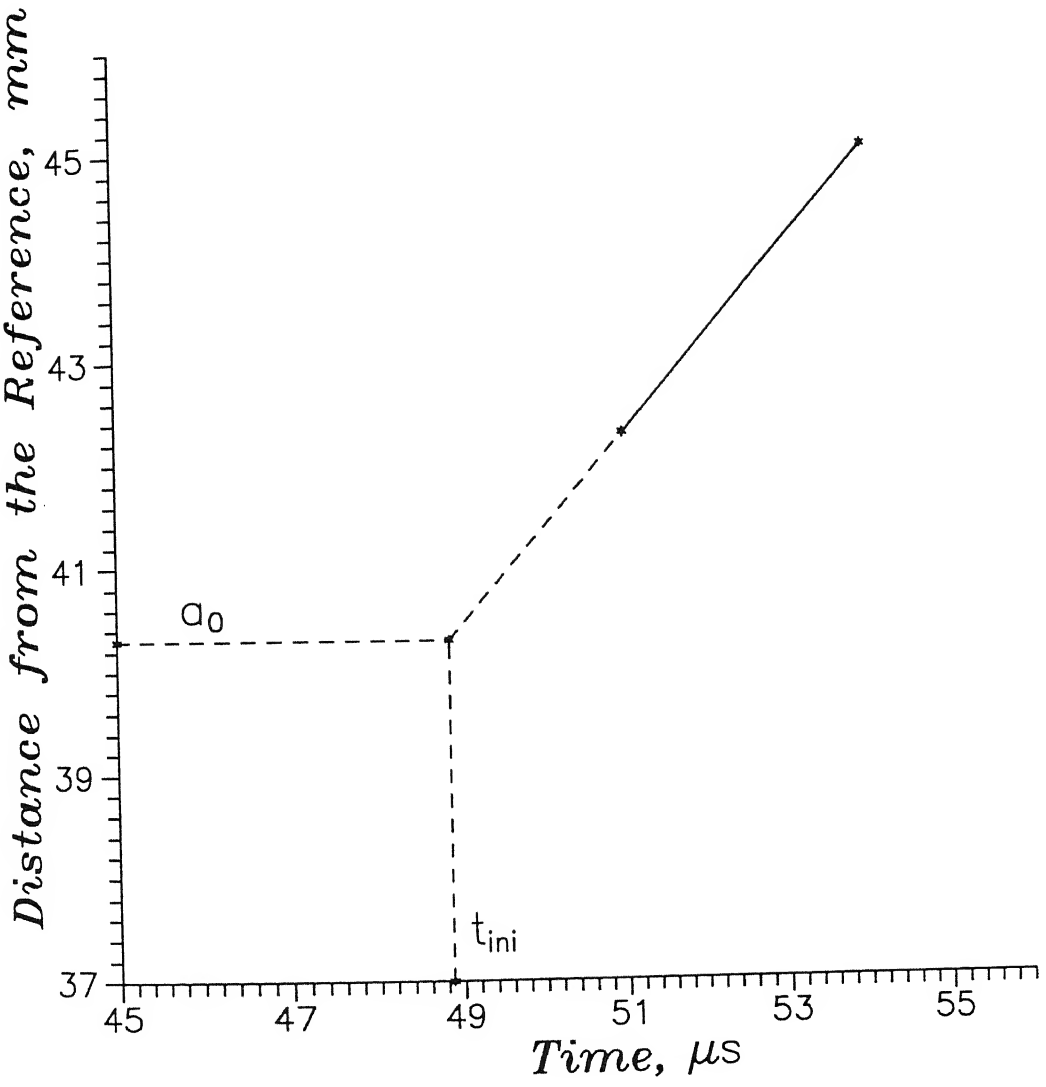

Figure 4.17: Details of extrapolation to find initiation time for Expt. 4

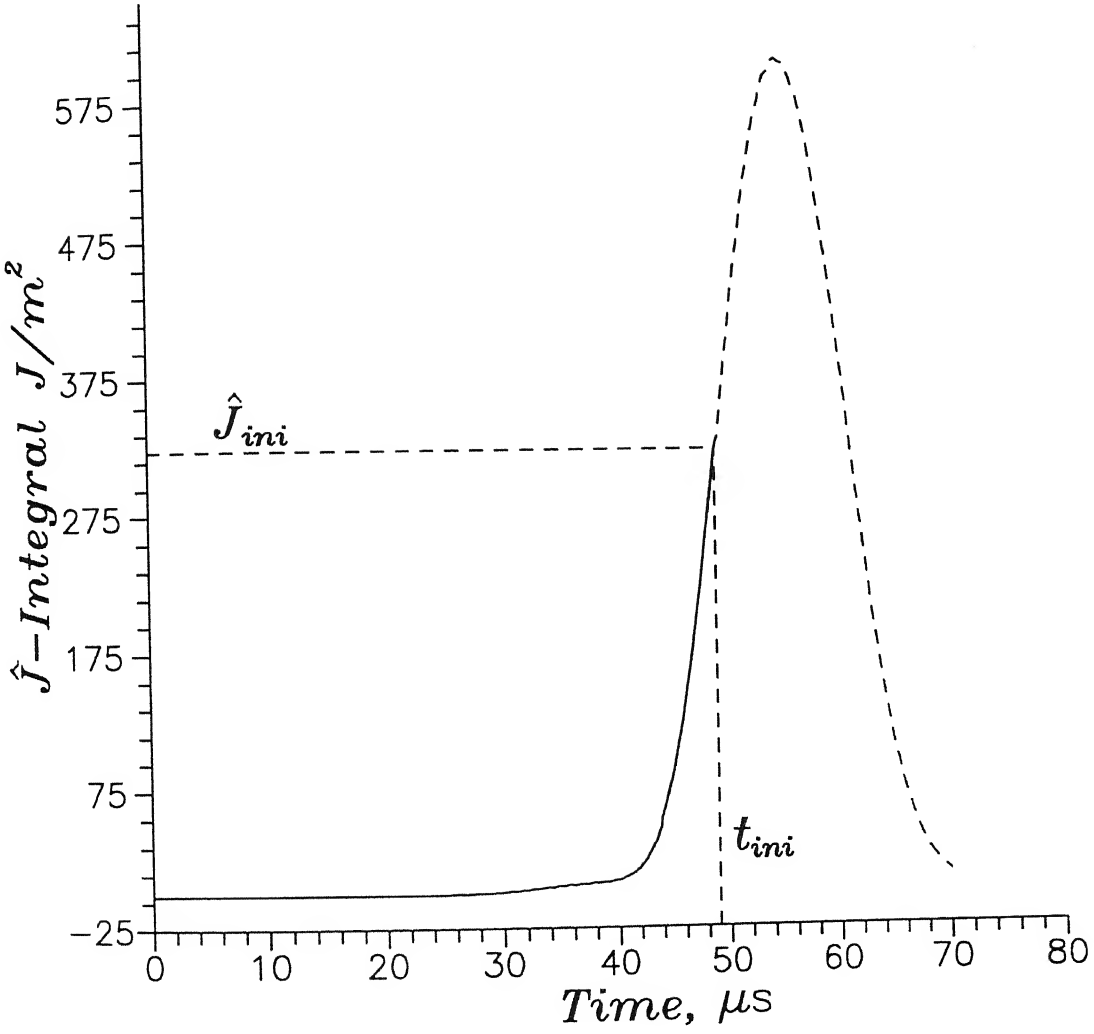

Figure 4.18: Variation of $\hat{J}$ for stationary crack for Expt. 4

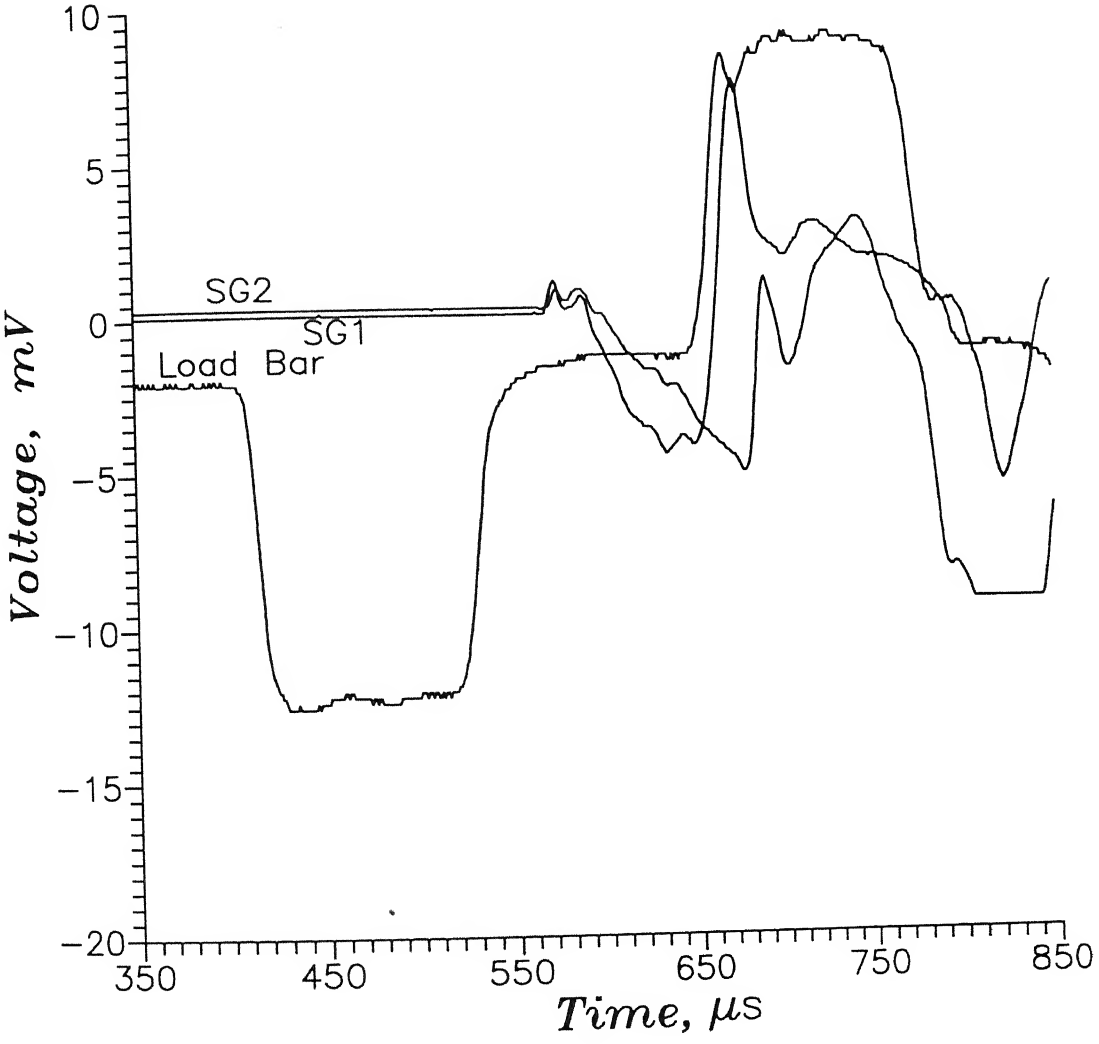

Figure 4.19: Oscilloscope Traces of Expt. 5

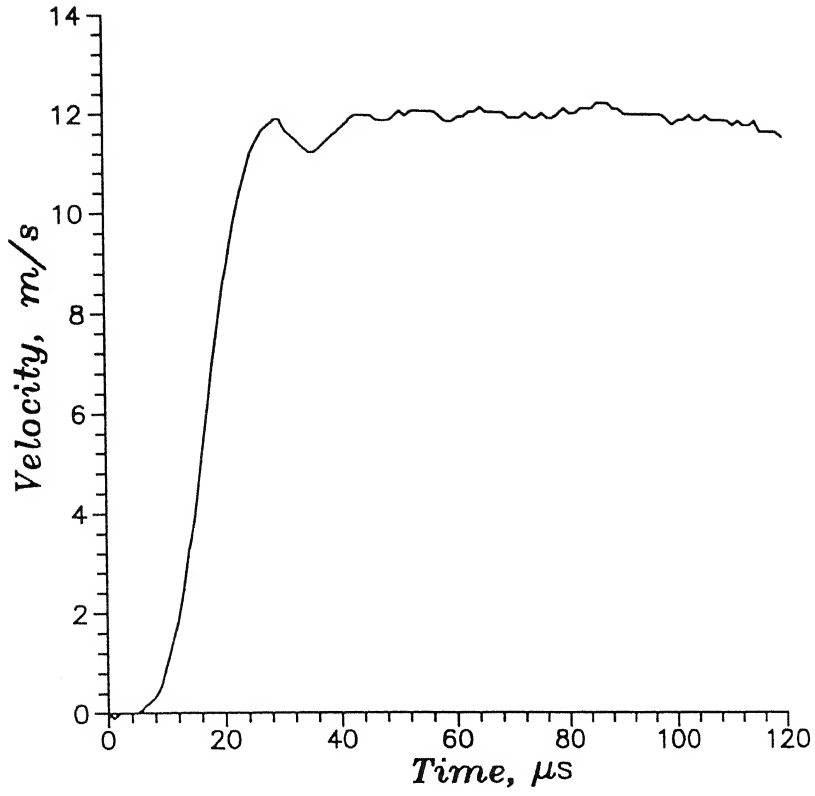

(a)

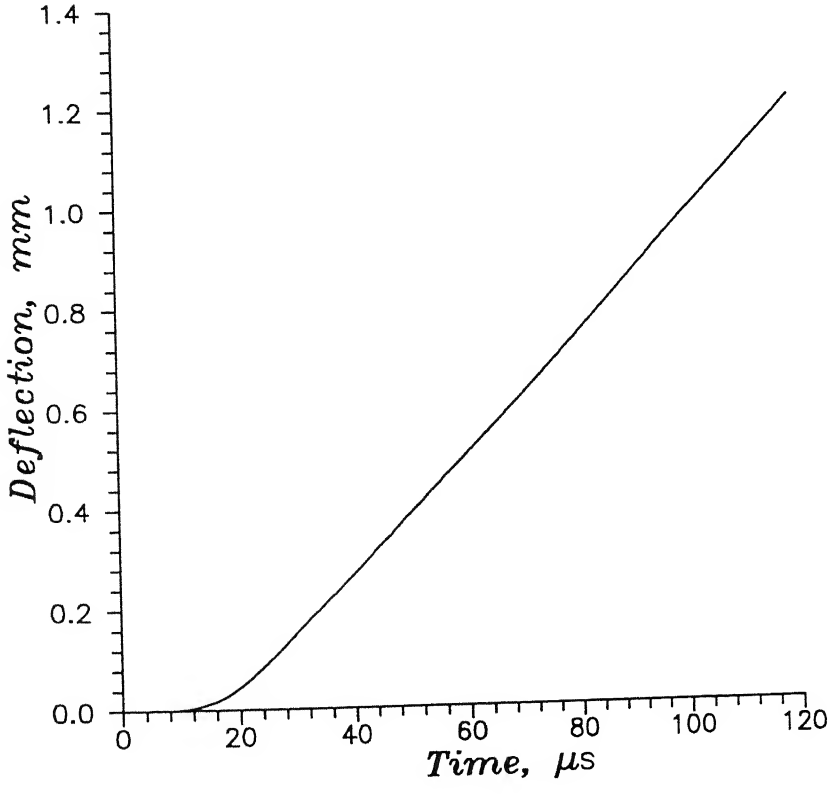

(b)

Figure 4.20: (a)Variation of velocity of load-bar-end with time for Expt. 5, and (b)deflection of cantilever end with time for Expt. 5

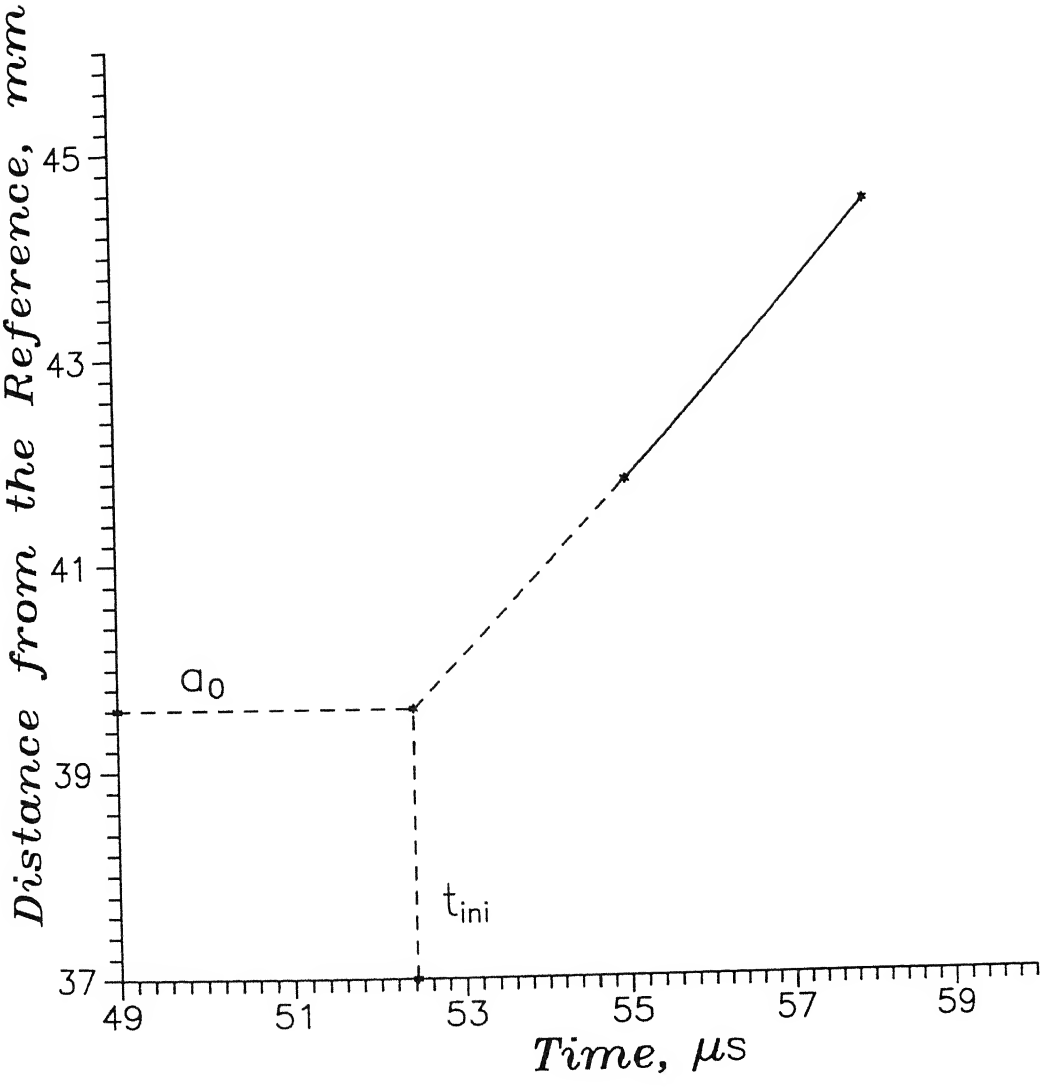

Figure 4.21: Details of extrapolation to find initiation time for Expt. 5

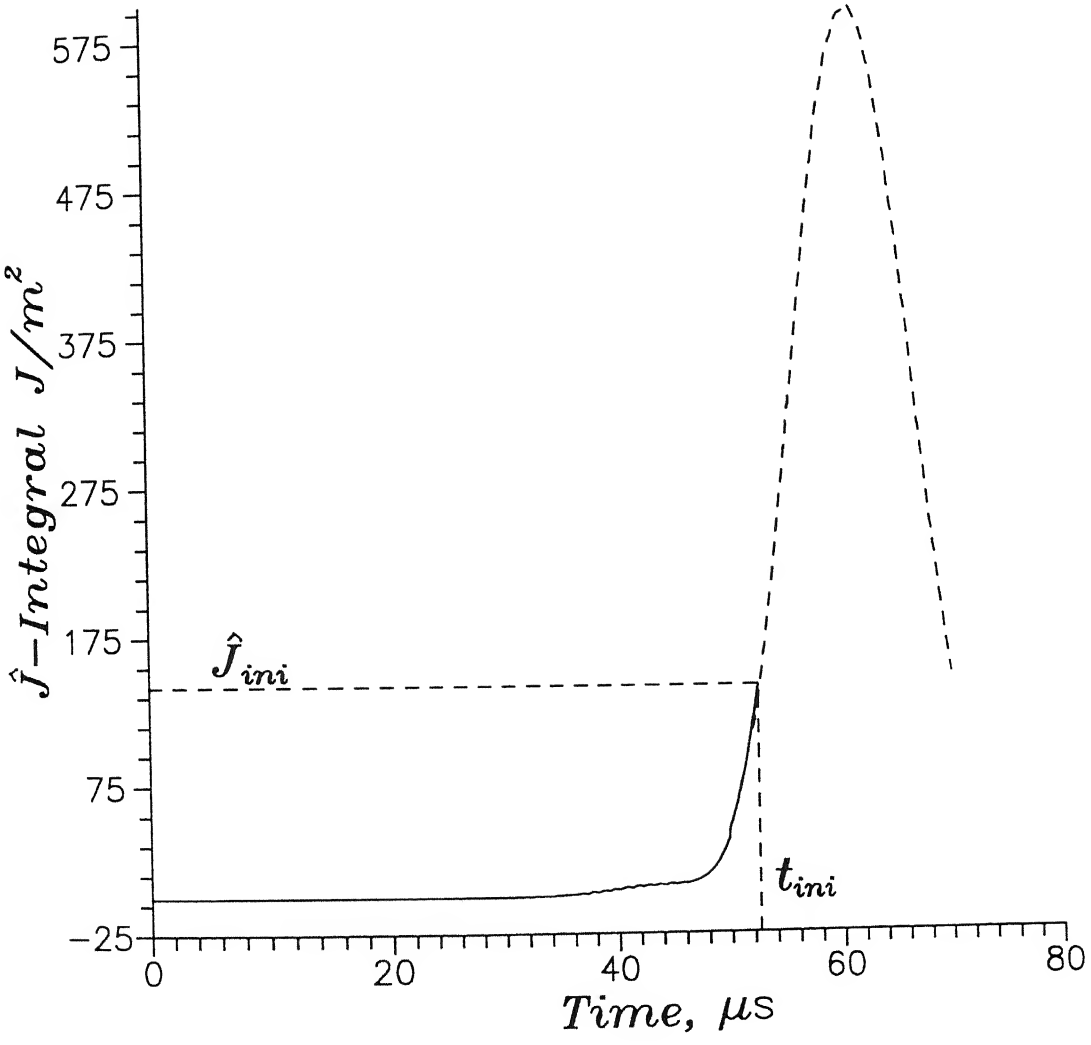

Figure 4.22: Variation of $\hat{J}$ for stationary crack for Expt. 5

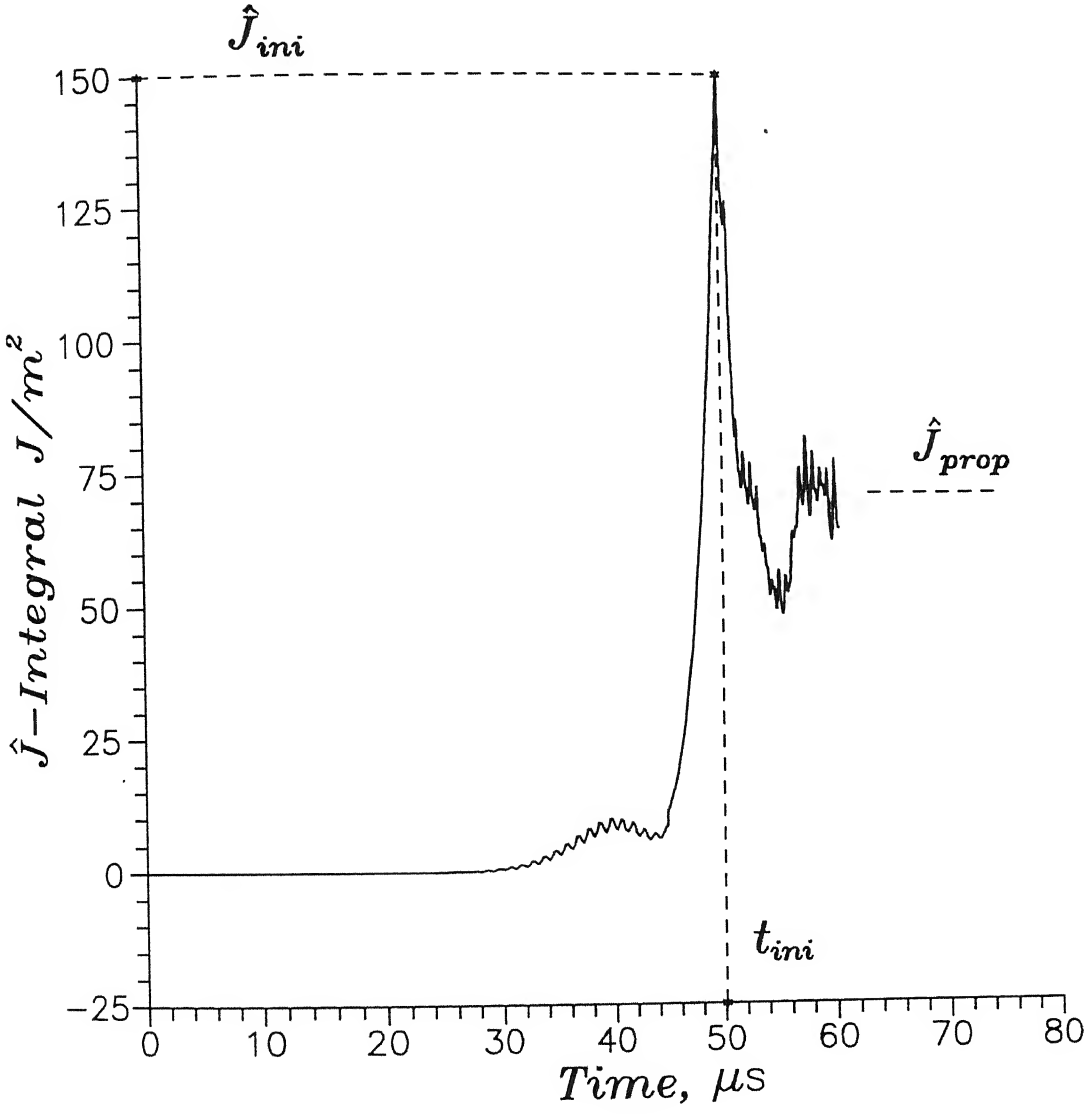

Figure 4.23: Variation of $\hat{J}$-integral for Expt. 1 (Stationary and Propagating phases)

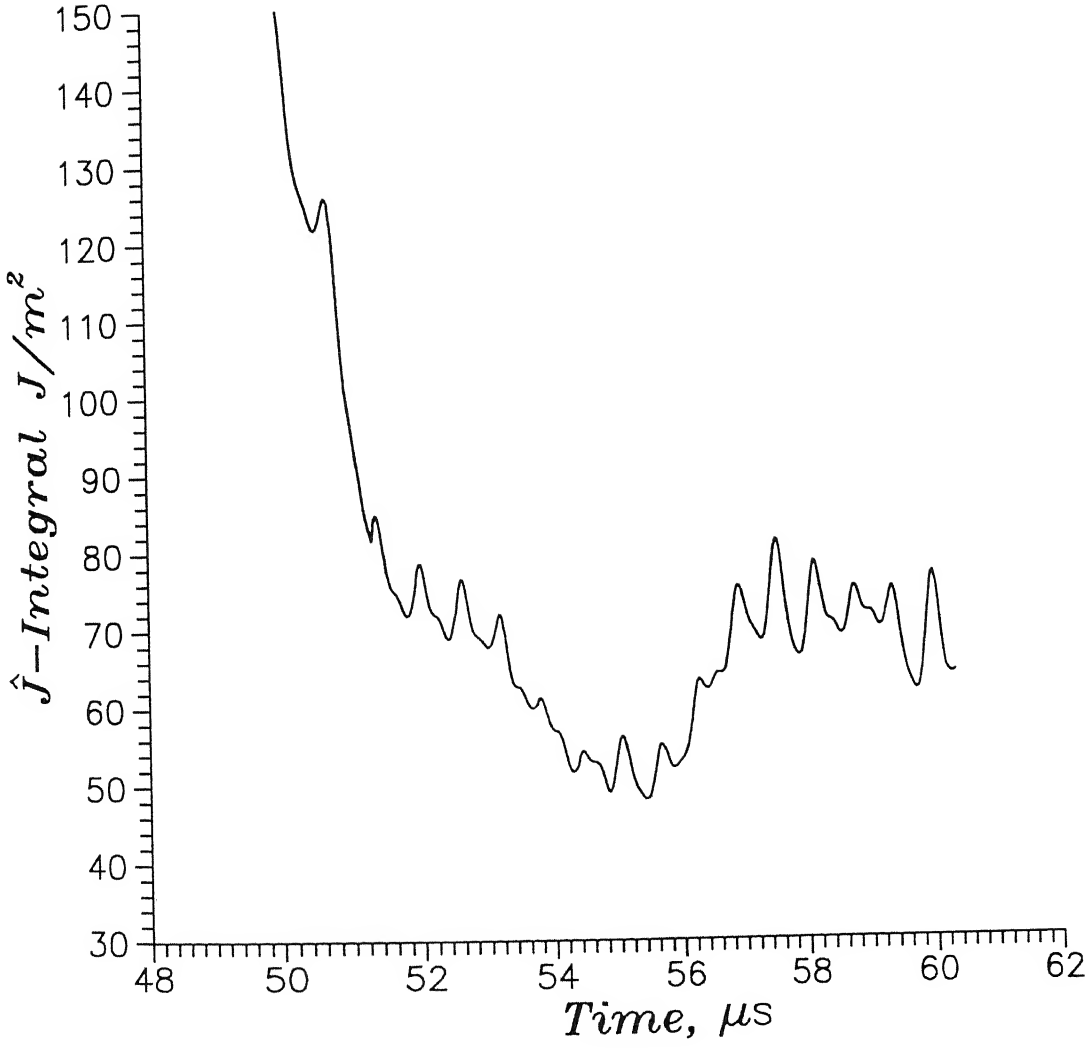

Figure 4.24: Blownup view of variation of $\hat{J}$-integral in propagating phase for Expt. 1

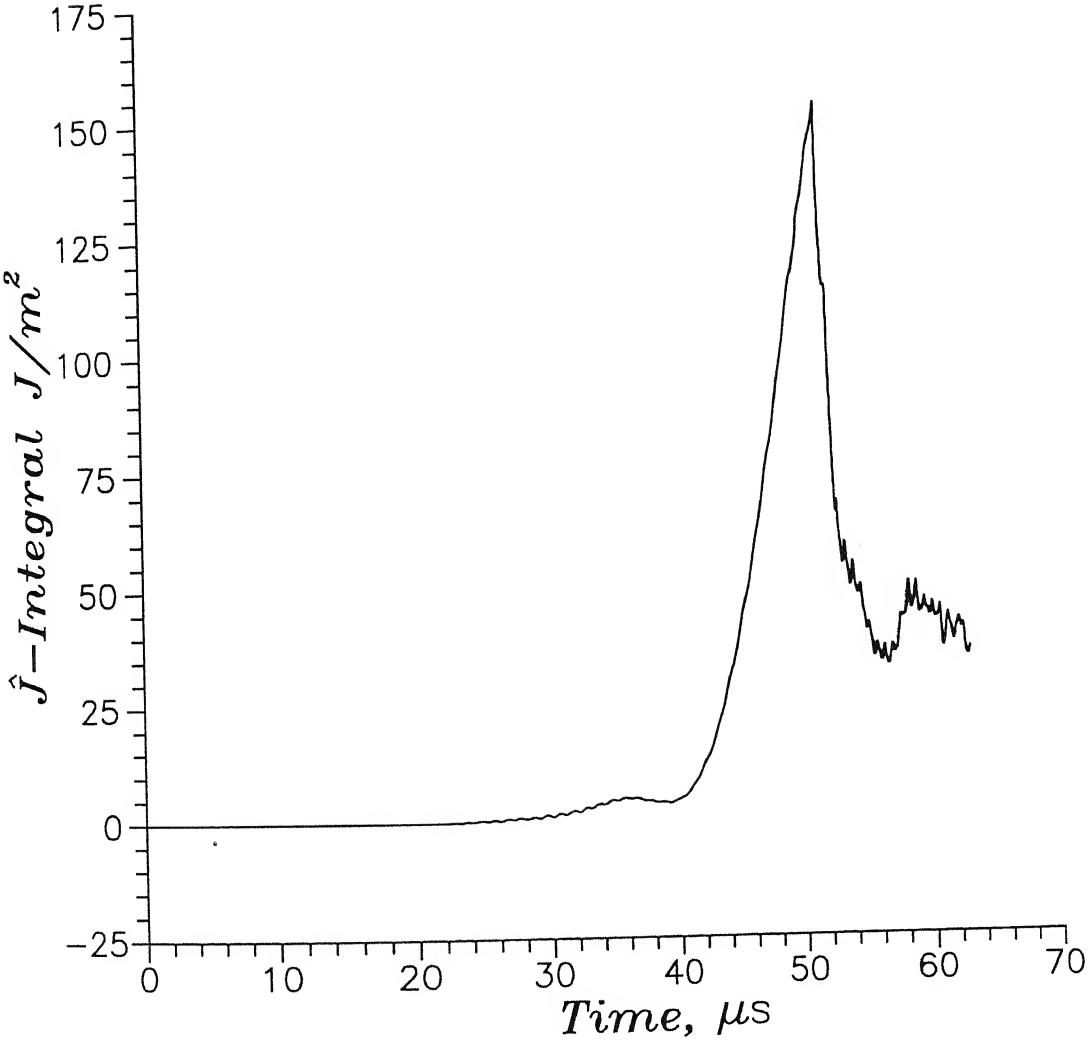

Figure 4.25: Variation of $\hat{J}$-integral for Expt. 2 (Stationary and Propagating phases)

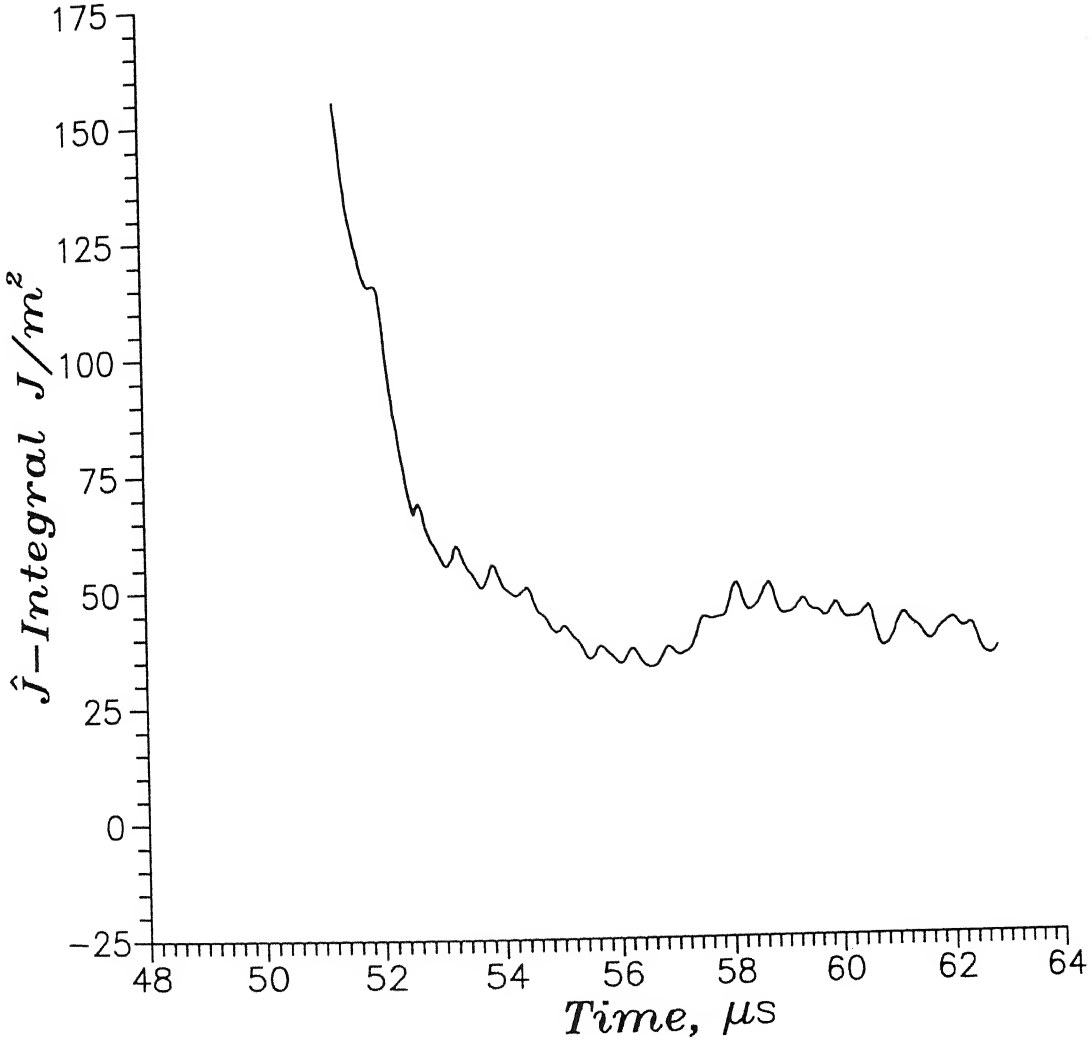

Figure 4.26: Blownup view of variation of $\hat{J}$-integral in propagating phase for Expt. 2

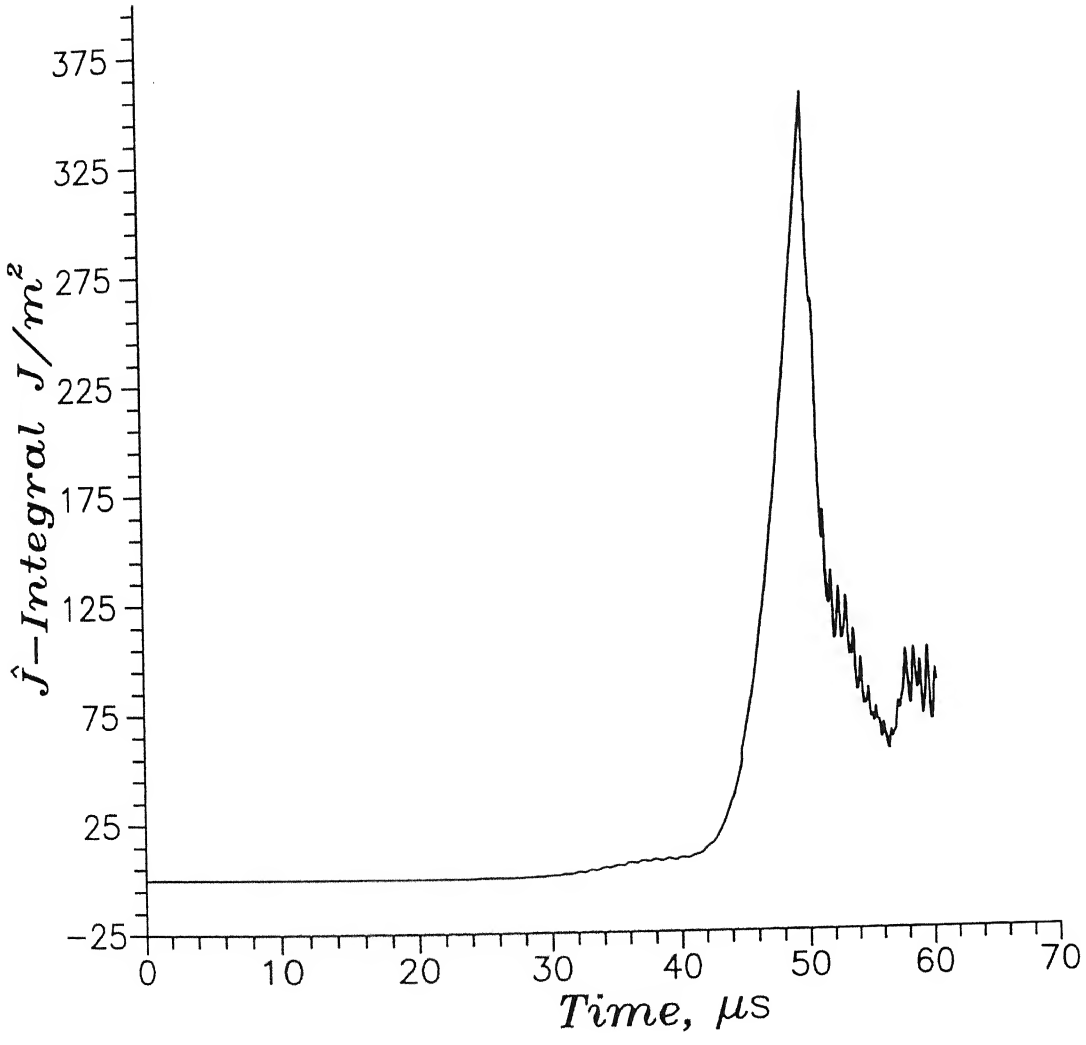

Figure 4.27: Variation of $\hat{J}$-integral for Expt. 3 (Stationary and Propagating phases)

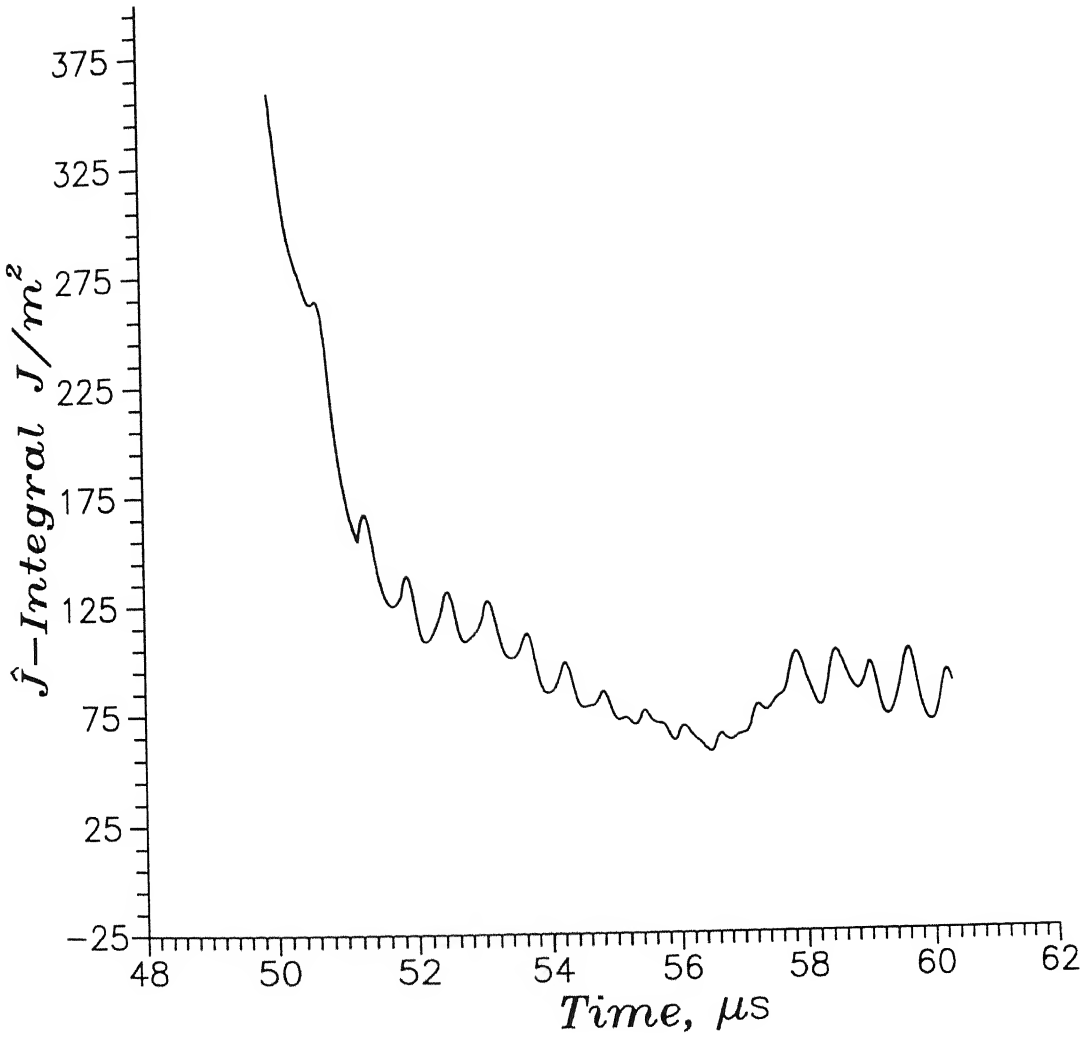

Figure 4.28: Blowup view of variation of $\hat{J}$-integral in propagating phase for Expt. 3

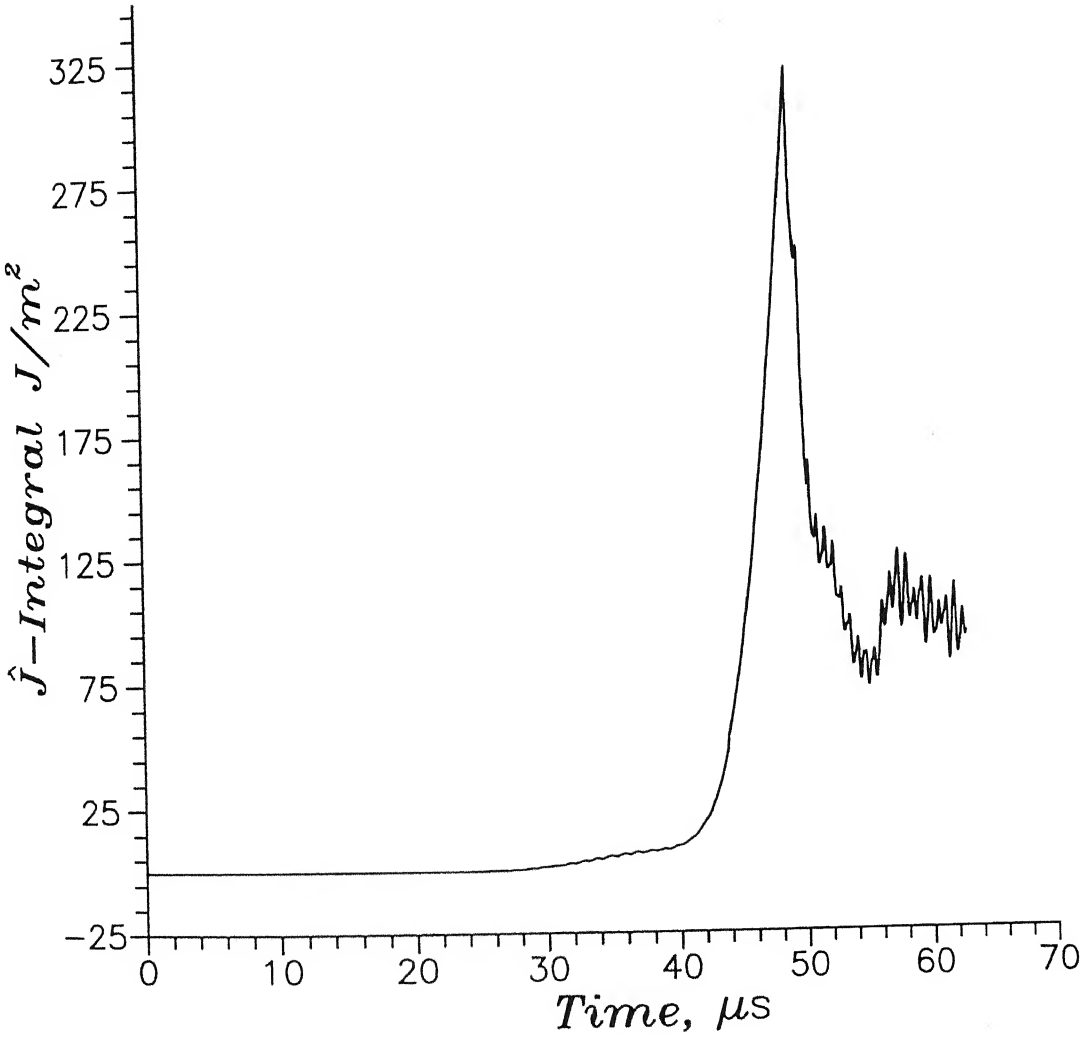

Figure 4.29: Variation of $\hat{J}$-integral for Expt. 4 (Stationary and Propagating phases)

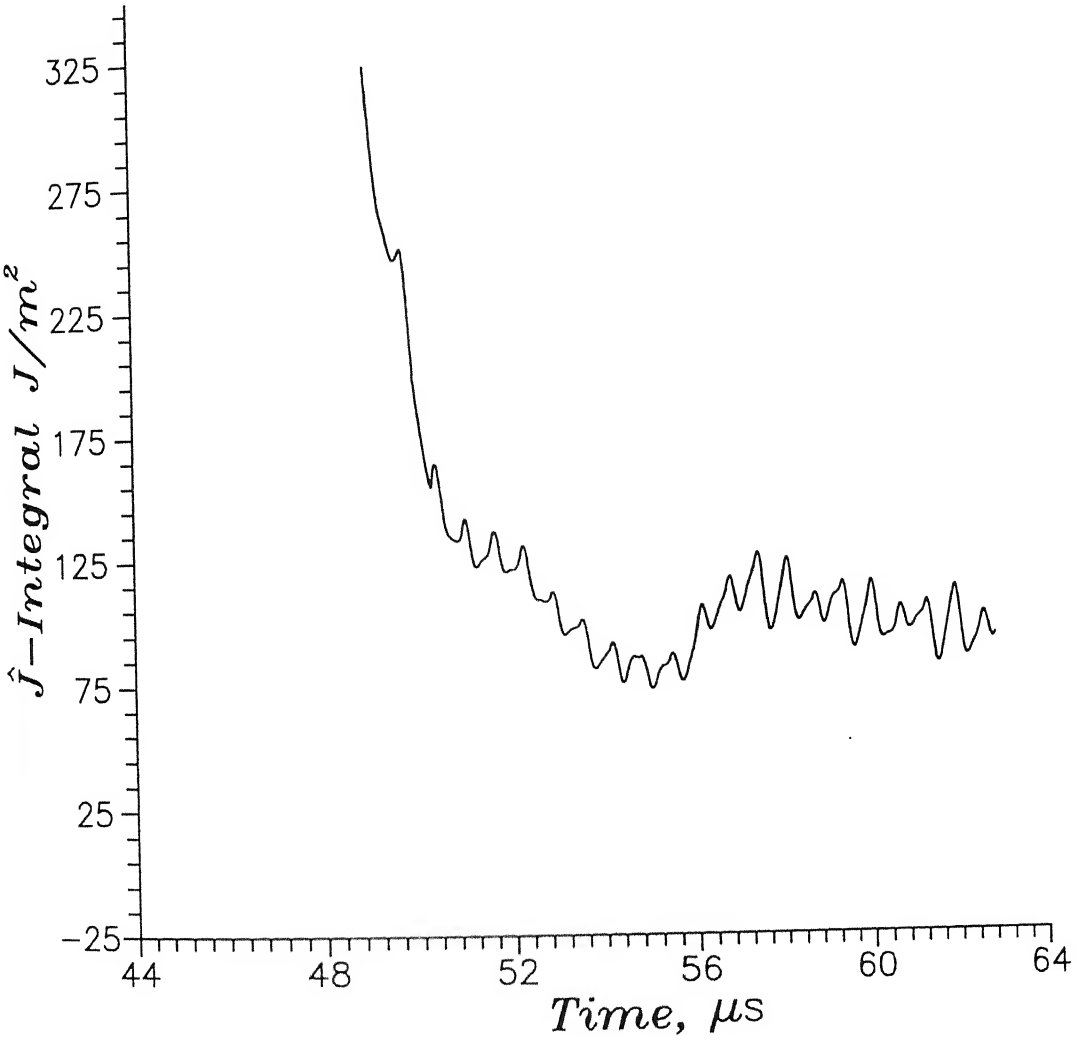

Figure 4.30: Blownup view of variation of $\hat{J}$-integral in propagating phase for Expt. 4

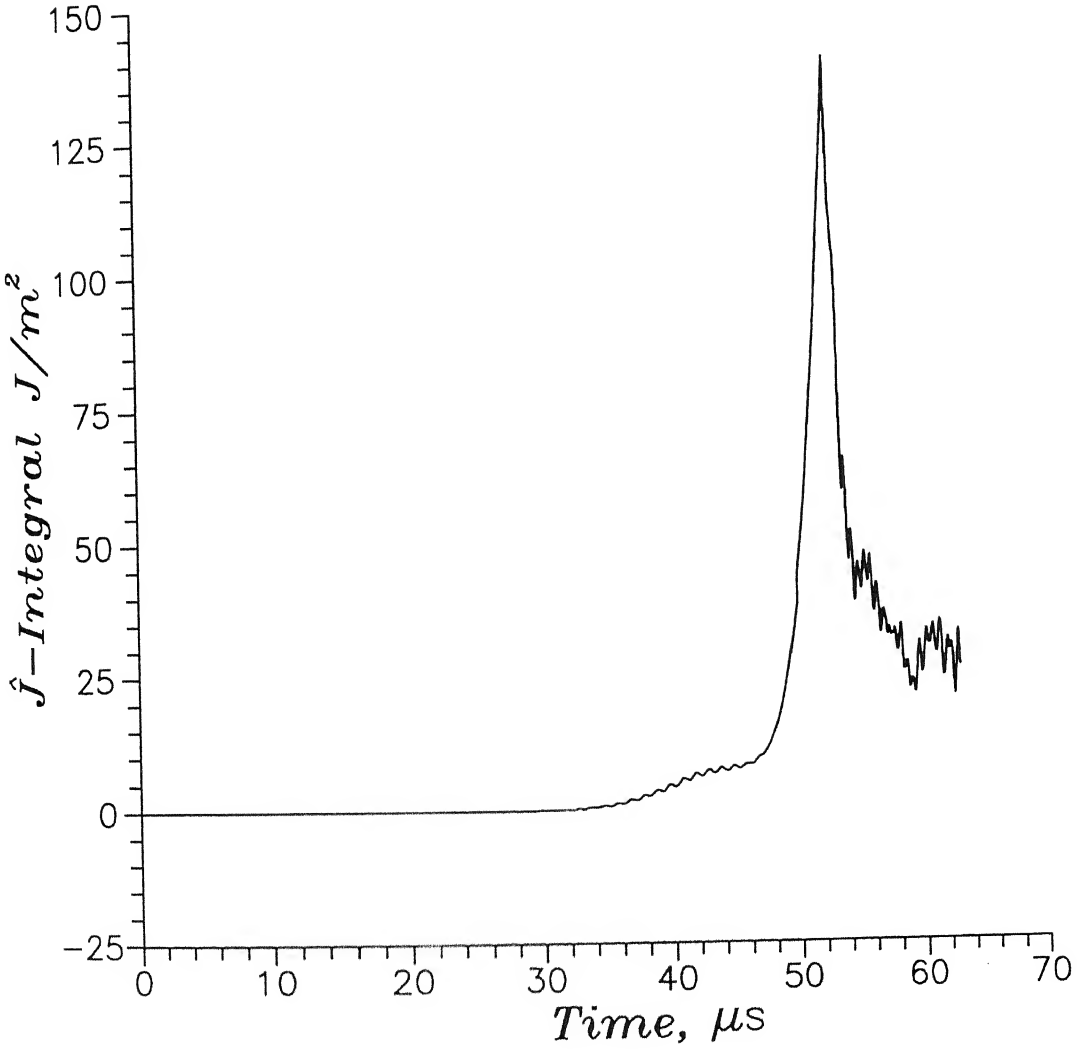

Figure 4.31: Variation of $\hat{J}$-integral for Expt. 5 (Stationary and Propagating phases)

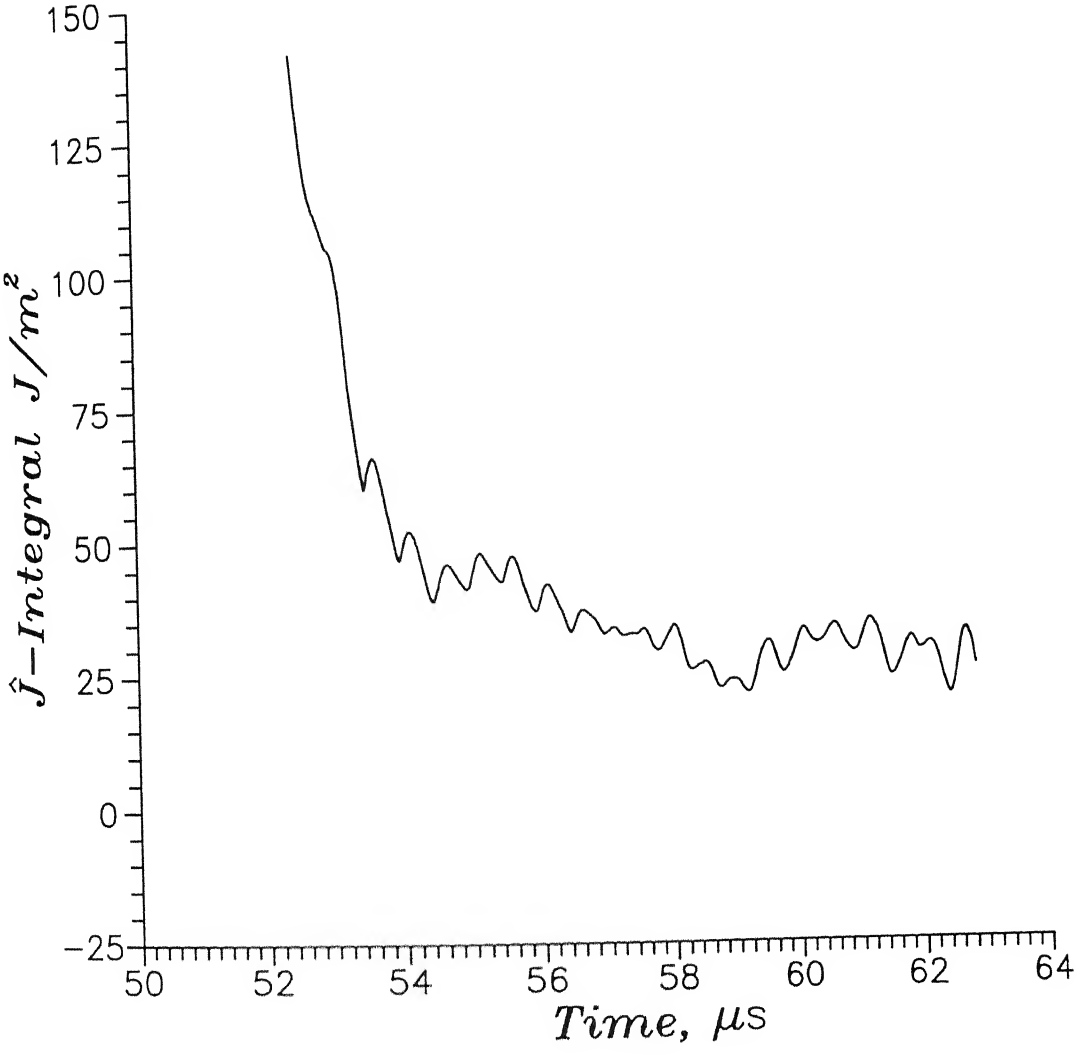

Figure 4.32: Blownup view of variation of $\hat{J}$-integral in propagating phase for Expt. 5

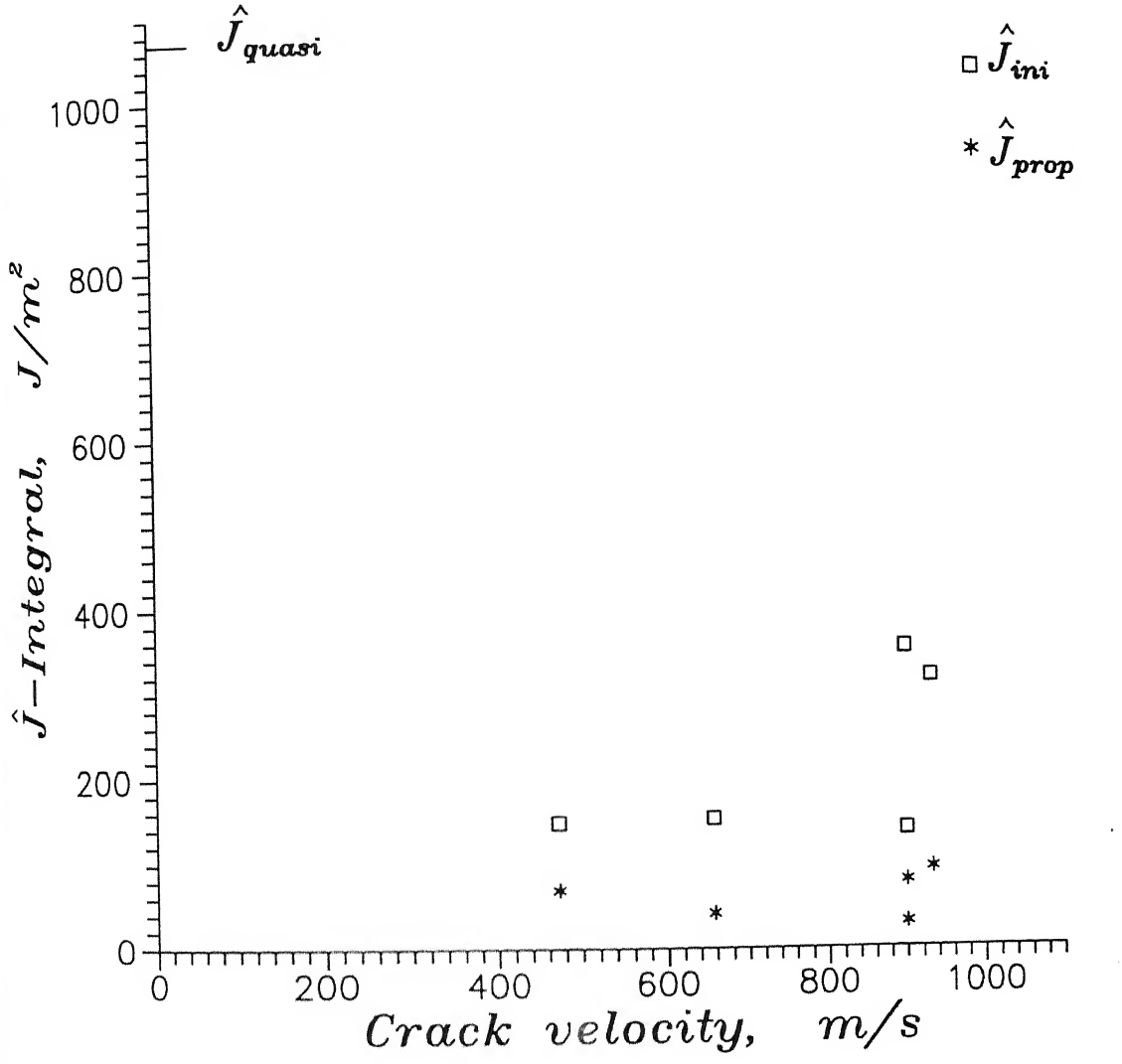

Figure 4.33: Variation of $\hat{J}$ with crack velocity for the present work

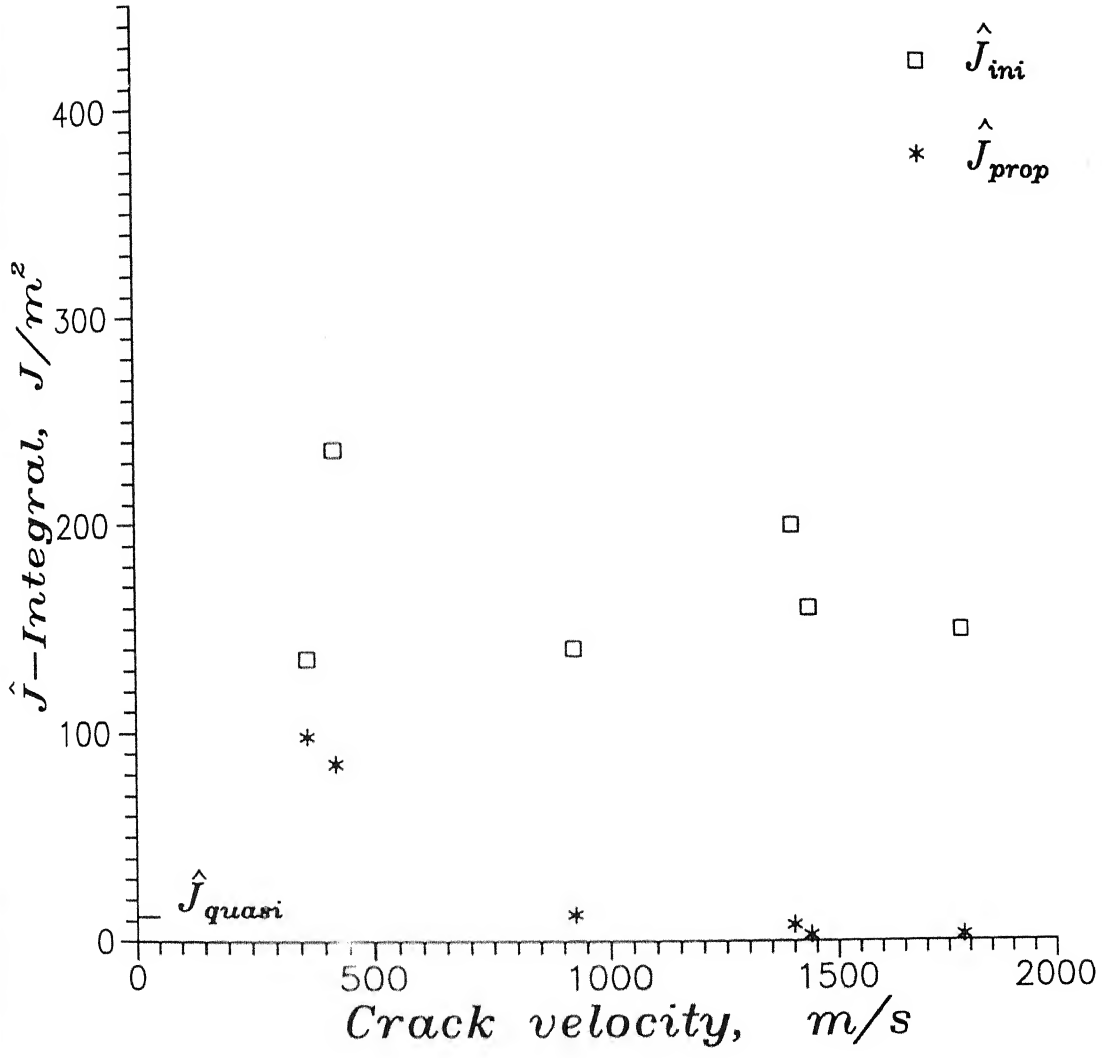

Figure 4.34: Variation of $\hat{J}$ with crack velocity, as obtained by Verma (1995)

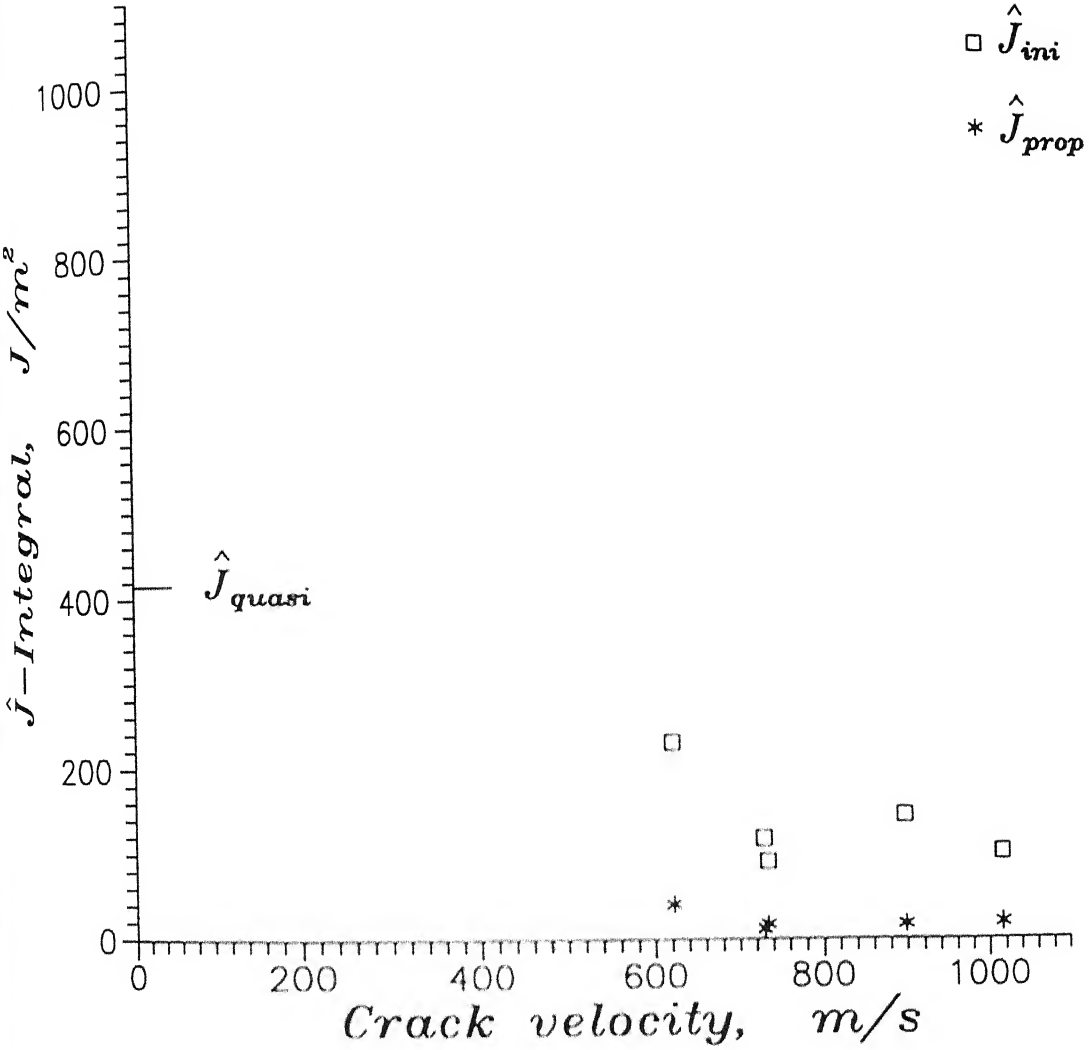

Figure 4.35: Variation of $\hat{J}$ with crack velocity as obtained by Ramakrishna (1997)

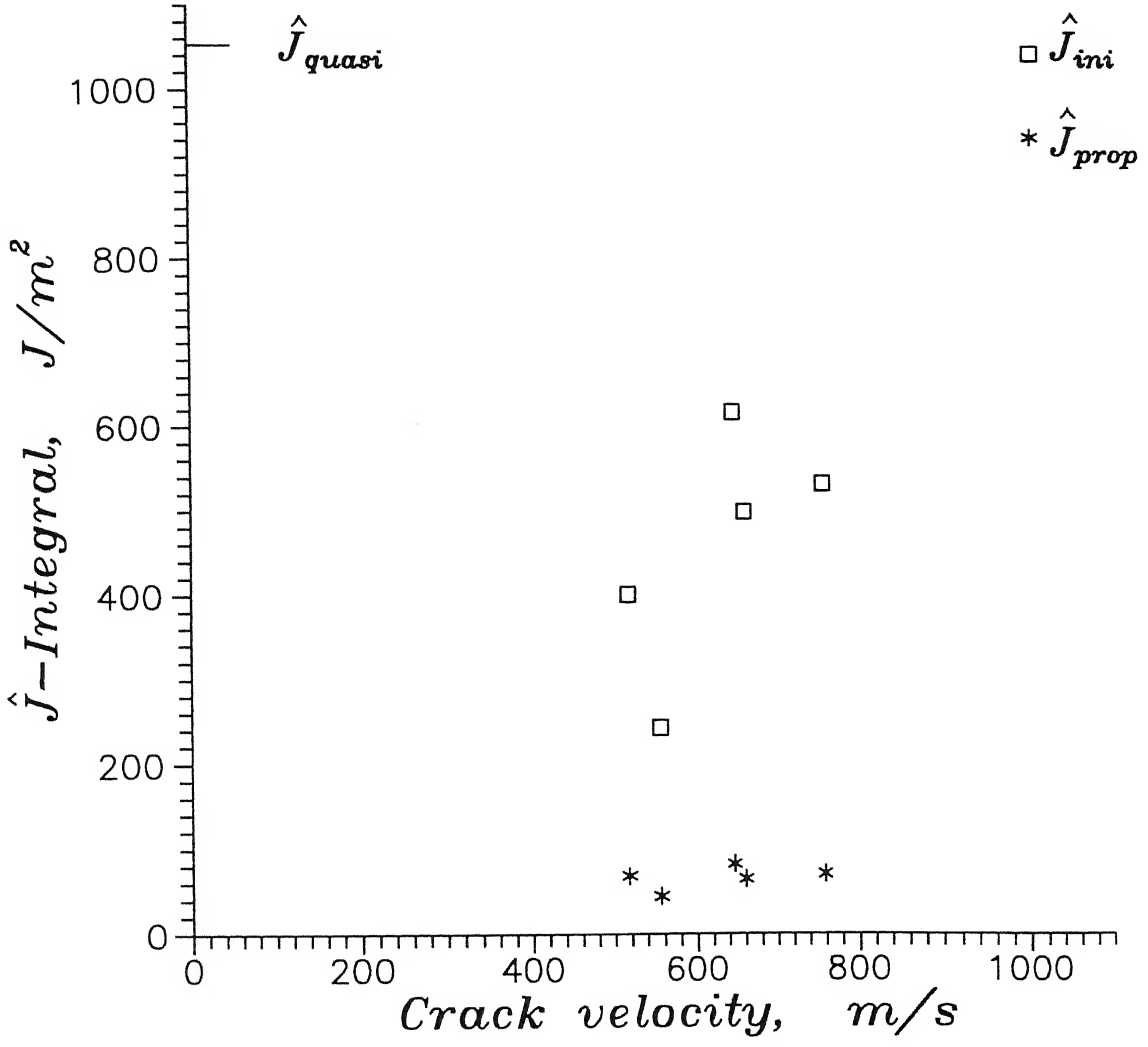

Figure 4.36: Variation of $\hat{J}$ with crack velocity as obtained by Babu (1998)

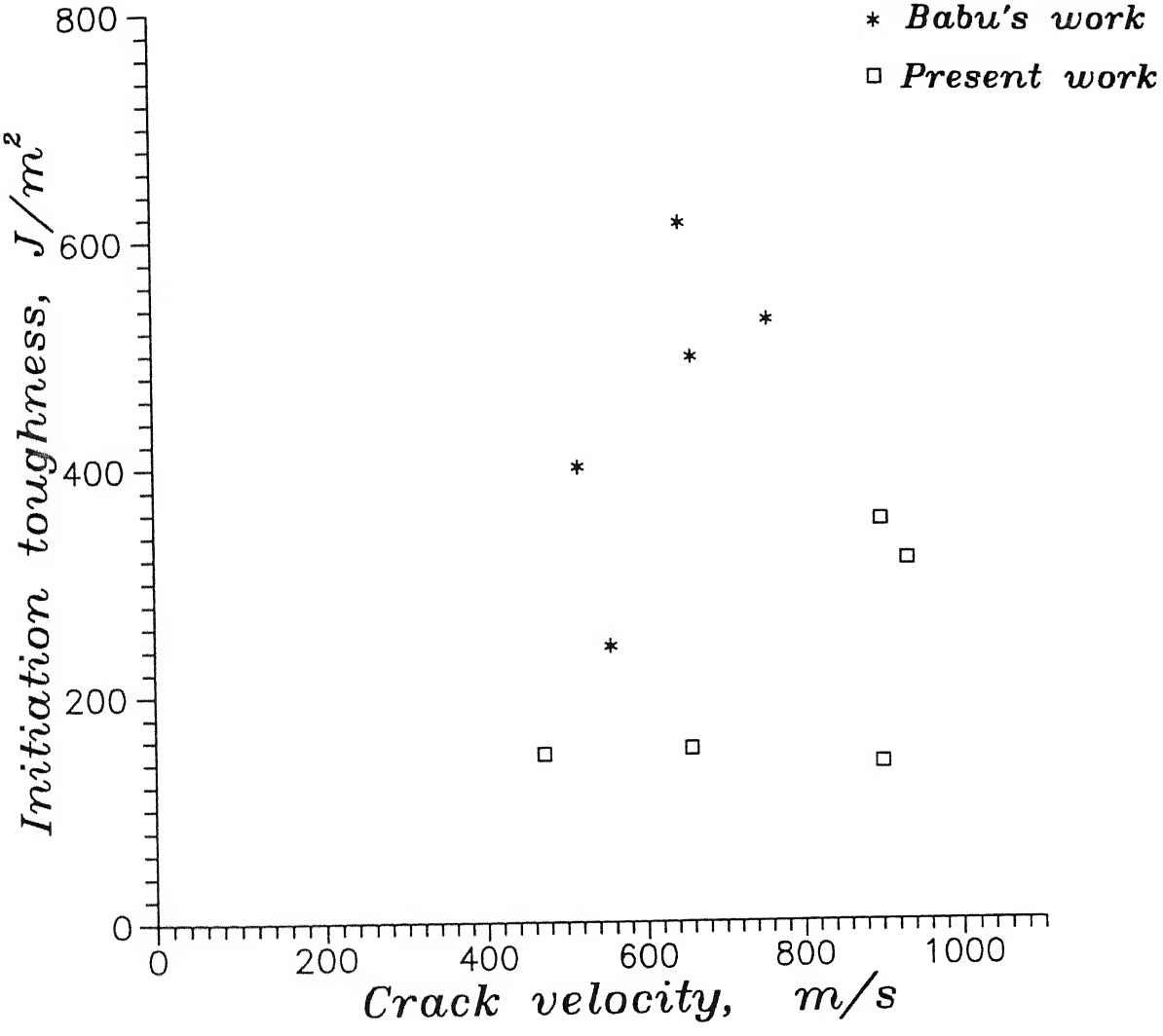

Figure 4.37: Comparision of Initiation toughness with that of Babu(1998)

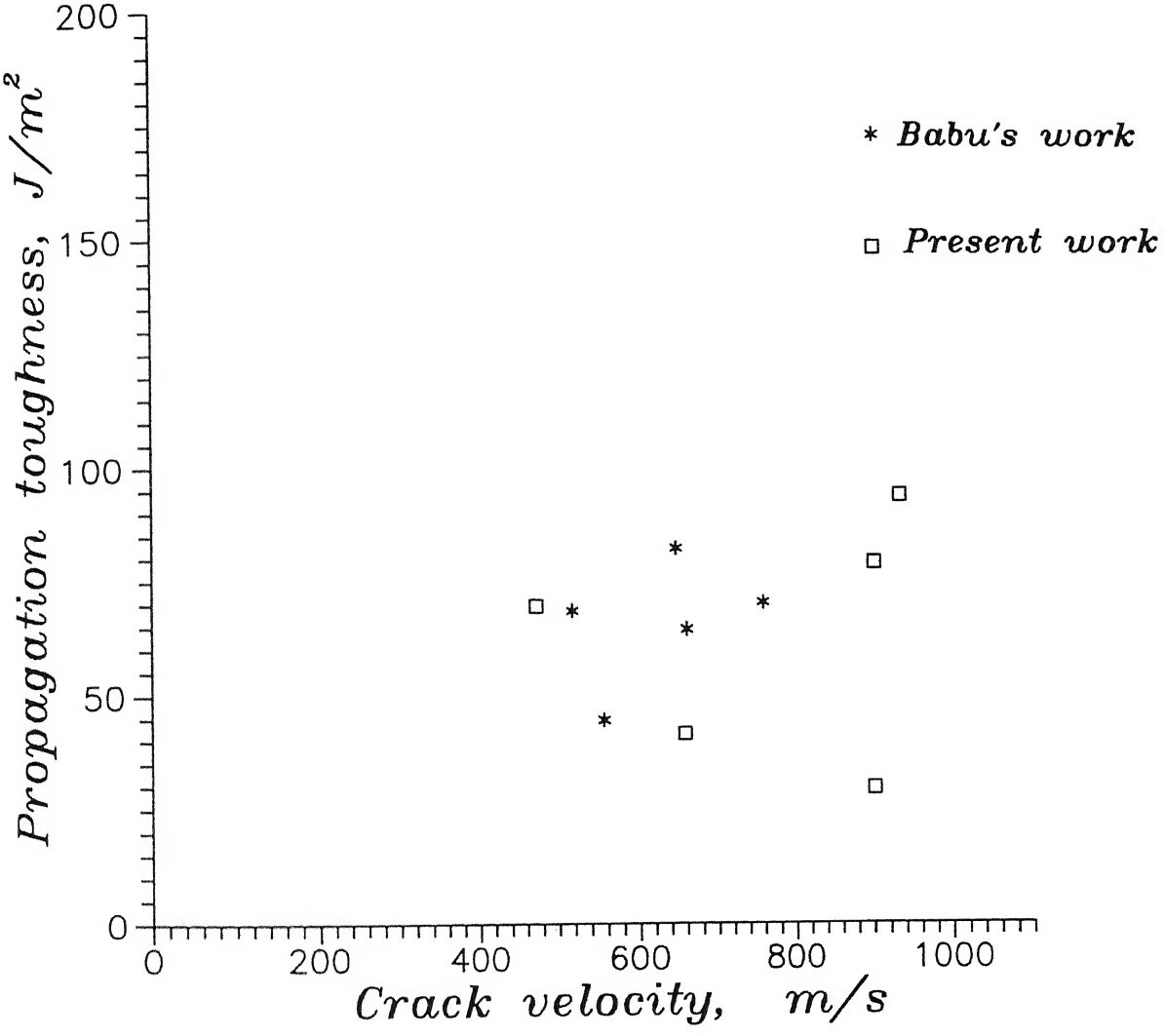

Figure 4.38: Comparision of Propagation toughness with that of Babu(1998)

Chapter 5

Conclusions and scope for further work

5.1 Conclusions

A technique developed by Verma(1995) has been applied to determine the initiation and propagation toughness of fast moving cracks in GFRP laminates. This is a combined experimental and numerical technique.

The experimental technique consists of a specimen; the front face of which is bonded to a rigid block and the cantlever end on the rear is screwed to a load bar. A striker bar impacts the load bar, which in turn impacts the specimen and causes the crack propagation. Two strain gauges bonded on the load bar monitors the stress pulses, which lead to the determination of the end displacement of the load bar. Since the specimen is screwed to the load bar, the end displacement of the load bar becomes the deflection of the cantilever end. Two strain gauges bonded ahead of the crack tip on the specimen monitors the crack propagation. Velocity of the crack is determined from the strain peaks in the response of these strain gauges and the distance between them. It is then extrapolated to the precrack length to determine the crack initiation time.

Thus the experimentation provides the deflection of the cantilever end, crack velocity and the initiation time. These along with the material properties are used as input to the FE code to simulate the fast moving crack. Gradual nodal release method is used to model the crack propagation. The initiation toughness (J_{ini}) was found to be 140-350 J/m^2 and the propagation toughness (J_{prop}) to be 30-95 J/m^2. These results are then compared with quasistatic interlaminar toughness (G_{Ic}). It has been observed that the dynamic interlaminar toughness of the crack is much smaller than the quasistatic interlaminar toughness.

5.2 Scope for further work

- Instead of strain gauges thin conducting strips can be used ahead of the crack tip to monitor the crack velocity
- The precrack length and the thickness of the cantilever can be varied to find their effect on the values of J_{ini} and J_{prop}.
- The work may be extended to angel ply laminates.

REFERENCES

Agarwal B.D. and Broutman L.J. (1980), Analysis and Performance of Fiber composites, *John Wiely & Sons* .

Bathe Klauss-jurgen (1990), Finite element procedure in engineering analysis, *Prentice Hall of India*

Berger J.R. and Dally J.W. (1990a) A spatially overdetermined analysis for propagation toughness using strain gages, *Mechanics Research Communications,* 17, 93-99.

Berger J.R., Dally J.W. and Sanford R.J. (1990b) Determining the dynamic stress intensity factor with strain gages using a crack tip location algorithm, *Engineering Fracture Mechanics*, 36, 145-156.

Brock D. (1984), Elementary Engineering Fracture Mechanics, *Mortinus Nijhoff Publishers*, The Hague.

Freund L.B., (1990) Dynamic Fracture Mechanics, *Cambridge University Press, Newyork.*

Gdoutos E.E. (1993), Fracture Mechanics : An Introduction, *Kluwer Academic Publishers* .

John Lambros and Ares J. Rosakis (1997a), Dynamic crack initiation and growth in thick unidirectional graphite/epoxy plates, *Composites Science and Technology* , 57(1), 55-65.

John Lambros and Ares J. Rosakis (1997b), An Experimental study of Dynamic delamination of thick fiber reinforced polymeric matrix composites, *Journal of Experimental Mechanics* , 37, 360-366.

Kolednik O. (1991), On the physical meaning of the J-a Curves, *Engineering Fracture Mechanics* , 38(6), 403-412.

Lovi R.G. (1993), Experimental investigation of dynamic fracture toughness in DCB specimen. *M.Tech. Thesis, Mech. Engg., I.I.T. Kanpur.*

Nishioka T. and Atluri S.N. (1983), Path independent integrals, Energy Release rate and General solution of Near-tip Fields in Mixed Mode Dynamic Fracture Mechanics, *Engineering Fracture Mechanics* , 18(1), 1-22.

Raman P. Singh, John Lambros, Arun Shukla and Ares J. Rosakis (1997), Investigation of the mechanics of intersonic crack propagation along a bimaterial interface using Coherent Gradient Sensing and Photoelasticity, Department of Aerospace Engineering, California Institute of Technology (submitted for publication).

Ravi Chandar K. and Knauss W.G. (1982) Dynamic crack tip stresses under stress wave loading - A comparison of theory and experiment, *International Journal of Fracture*, 20, 202-222.

Ravi Chandar K. and Knauss W.G. (1984a) An experimental investigation into dynamic fracture : I. Crack initiation and arrest, *International Journal of Fracture,* 25, 247-262.

Ravi Chandar K. and Knauss W.G. (1984b) An experimental investigation into dynamic fracture : II. Microstructural aspects, *International Journal of Fracture,* 26, 65-80.

Ravi Chandar K. and Knauss W.G. (1984c) An experimental investigation into dynamic fracture : III. On steady-state crack propagation and crack branching, *International Journal of Fracture*, 26, 141-154.

Ravi Chandar K. and Knauss W.G. (1984d) An experimental investigation into dynamic fracture : IV. On interaction of stress waves with propagating cracks, *International Journal of Fracture*, 26, 189-200.

Ravichandran G. and Clifton R.J. (1989), Dynamic fracture under plane wave loading, *International Journal of Fracture*, 40, 157-201.

Rosakis A.J., Duffy J. and Freund L.B. (1984) The determination of dynamic fracture toughness of AISI 4340 steel by the shadow spot method, *Journal of the Mechanics and Physics of Solids*, 4, 443-460.

Sun C.T. and Grandy J.E. (1986), Dynamic delamination Fracture Toughness of a Graphite /Epoxy laminate under impact, *Composite Science and Technology*, 31, 55-72.

Takeda N., Sierakowski R.L., Ross C.A. and Malvern L.E. (1982) Delamination crack propagation in ballistically impact glass/epoxy composite laminates, *Experimental Mechanics*, 22, 19-25.

Truss R.W., P.J. Hine and R.A. Duckett (1997), Interlaminar and intralaminar fracture toughness of uniaxial continuous and discontinuous carbon fibre/epoxy composites, *Composites* , 28A, 627-636.

Verma S.K. (1995), Determination of static and Dynamic Interlaminar Fracture Toughness - A Combined Experimental and Finite Element Method, *Ph.D. Thesis, Mech. Engg., I.I.T. Kanpur.*

Verma S.K., Kumar Prashant, Kishore N.N. and Potty P.K.K (1995), Evaluation of critical interlamianar SIF of DCB specimen made of slender cantilever, *Engineering Fracture Mechanics* , 50, 345-353.

Zehnder Alant T. and Rosakis Ares J. (1990) Dynamic fracture initiation and propagation in 4340 steel under impact loading, *International Journal of Fracture,* 43, 271-285.

Narayanan M.D (1988) Energy release rates in delamination of glass fabric reinforced composite materials, *M.Tech Thesis, Mech. Engg I I T Kanpur*

Ramakrishna.A (1997) Initiation and propagation toughness of interlaminar cracks in GFRP laminates under impact loading, *M.Tech Thesis, Mech. Engg I.I.T. kanpur*

Babu. K.N (1998) Dynamic interlaminar toughness of unidirectional GFRP laminates, *M.Tech Thesis, Mech. Engg I.I.T. kanpur*

D.Guedra, D.Lang, J.Rouchon, C.Marris and P.Sigety (1987) Fracture toughness in Mode I : a comparison exercise of various test methods, *VI ICCM* Vol 3, pp 3.347-3.357

D.J.Wilkins, J.R.Eisemann, R.A.Camin, W.S.Margolis and R.A.Benson (1982) Characterising delamination growth in graphite epoxy, damage in Composite materials, *ASTM* STP 775, pp 168-183.

Appendix A

For an orthotropic composite laminate the principal material directions are the longitudinal direction (along the fibres) and transverse direction (across the fibres). Unlike the case of isotropic materials where there are only two independent material constants, in this case there are four independent constants. The constants are the longitudinal madulus (E_L), transverse modulus (E_T), shear modulus (G_{LT}) and the major poissons ratio (ν_{LT}). E_L and E_T are determined by conducting tensile tests on 0^o and 90^o laminates respectively. ν_{LT} can be determined from the tensile test on 0^o laminate by measuring the strain in longitudinal and transverse directions. Figure A.1 shows a sample stress-strain curve for a tensile test on 0^o laminate. Figure A.2 shows the same on 90^o laminate. Tensile test conducted on 45^o laminate yeilds E_{45}. G_{LT} can be found from E_{45} using the formula,

$$\frac{1}{E_{45^o}} = \frac{1}{4}\{\frac{1}{E_L} + \frac{1}{E_T} + \frac{1}{G_{LT}} - \frac{2\nu_{LT}}{E_L}\}$$

Figure A.3 shows a sample stress-strain diagram for tensile test on 45^o laminate.

The tests are conducted on 16 ply laminates. The values of E_L, E_T , G_{LT} and ν_{LT} obtained from the experiments are tabulated in Tables A.1, A.2, A.3, and A.4 respectively.

Table A.1 Experimental values of E_L

S.No	Longitudinal Modulus (E_L) (GPa)
1	46.30
2	35.40
3	43.32
4	37.90
5	42.24
6	40.07
7	38.50

Table A.2 Experimental values of E_T

S.No	Transverse Modulus (E_T) (GPa)
1	6.35
2	8.17
3	7.10
4	5.80
5	7.60
6	7.16
7	7.40
8	7.20
9	6.06

Table A.3 Tabulated values of G_{LT}

S.No	E_{45} (GPa)	Modulus of Rigidity G_{LT} (GPa)
1	8.20	2.997
2	8.02	2.902
3	7.82	2.798
4	7.50	2.673

Table A.4 Tabulated values of ν_{LT}

S.No	Major Poissons ratio (ν_{LT})
1	0.281
2	0.265
3	0.287

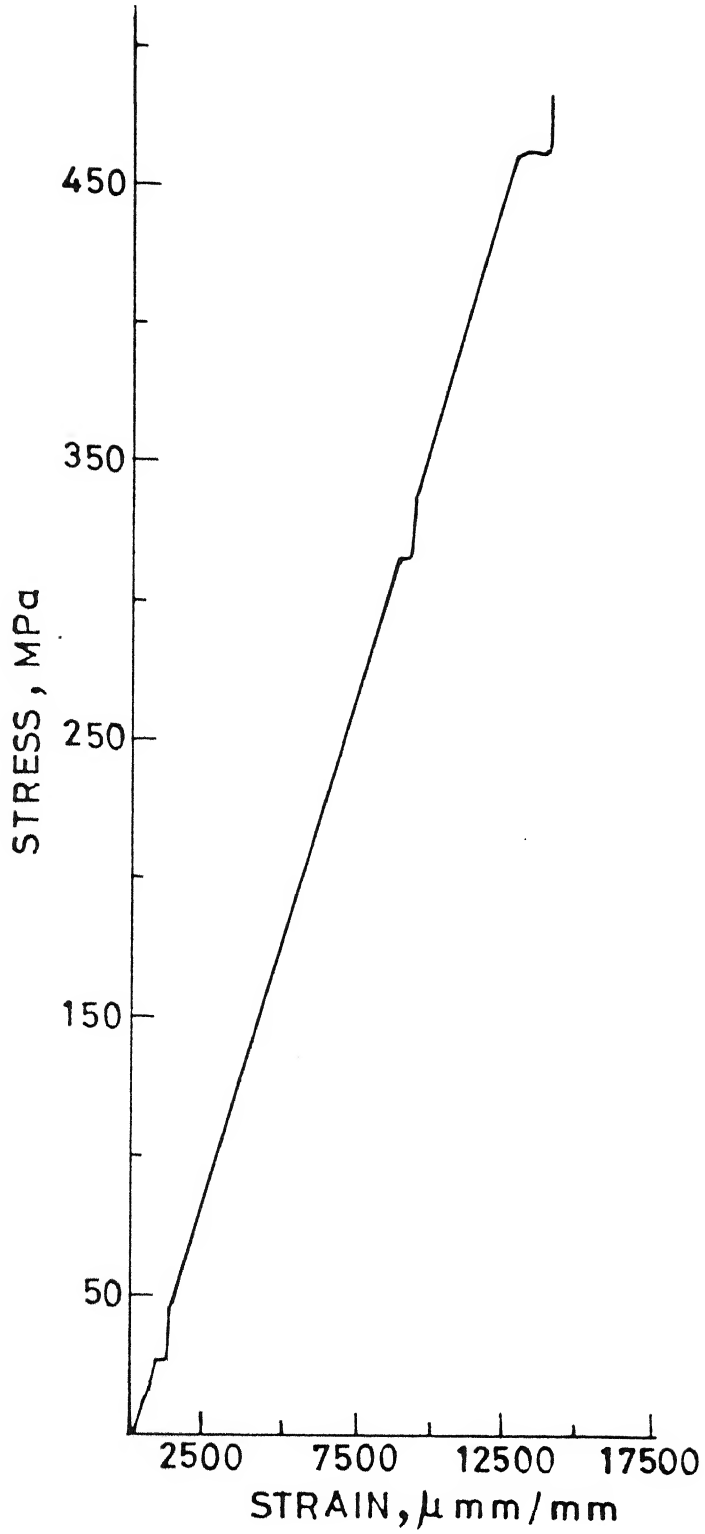

Figure A.1: Stress-strain diagram for tensile test on 0^o laminate

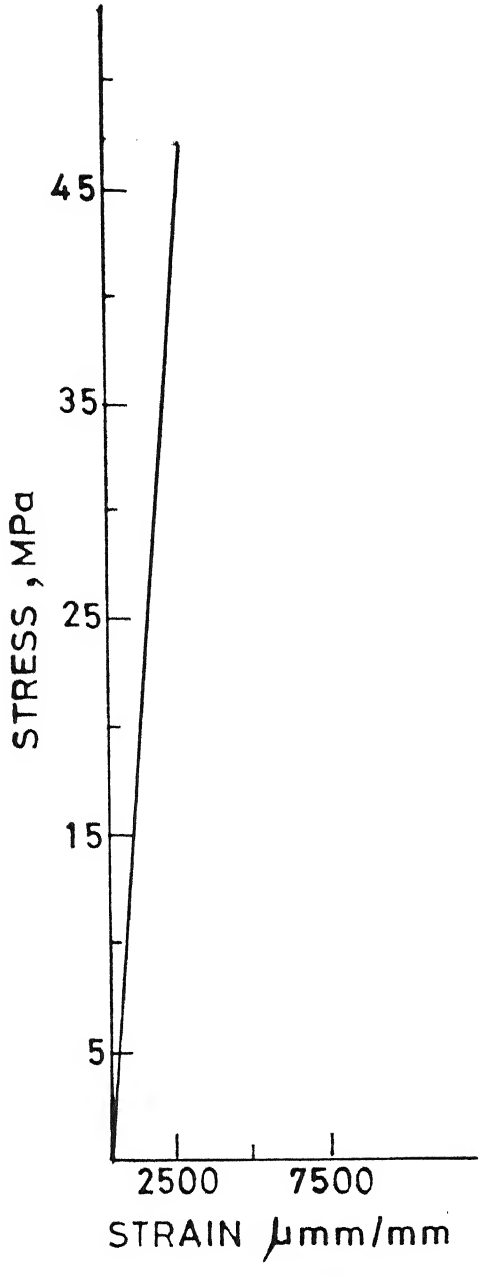

Figure A.2: Stress-strain diagram for tensile test on 90^o laminate

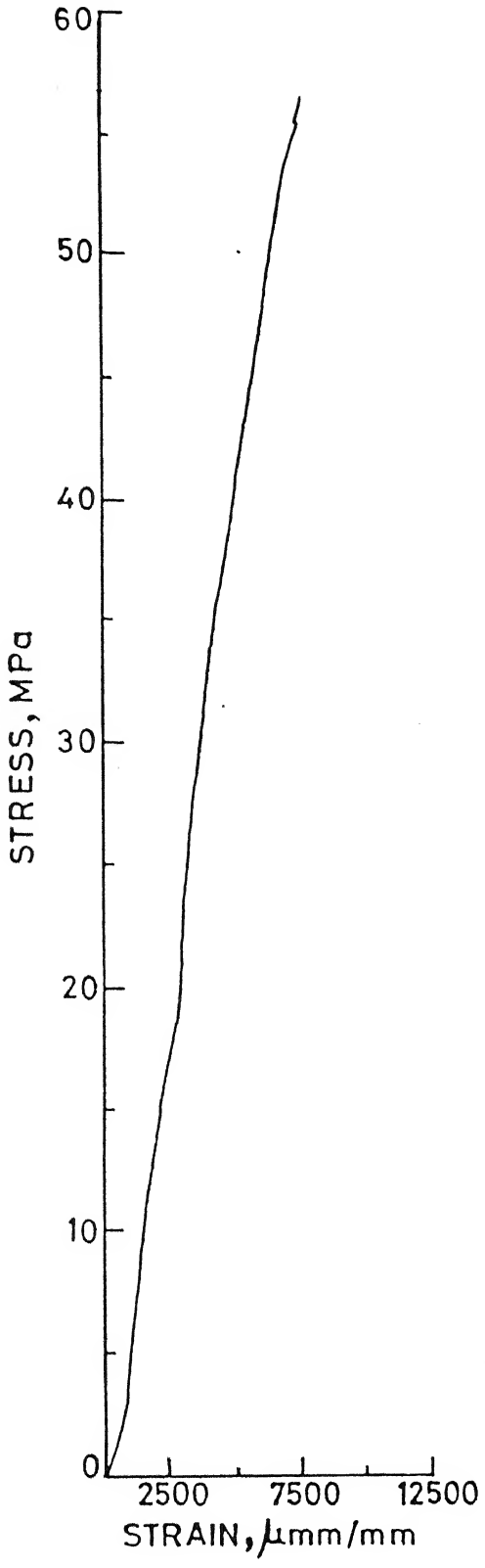

Figure A.3: Stress-strain diagram for tensile test on 45° laminate